MASTER THESIS

Biomimetic Wet Tissue Adhesives for Fetal Surgery

conducted at the Departement of Materials Science and Engineering
at the University of California, Berkeley
under supervision of Prof. Dr. Phillip B. Messersmith
and Dr. Diederik W. R. Balkenende

under co-supervision of Prof. Dr. Miriam M. Unterlass
at the Institute of Materials Chemistry
Technische Universität Wien

conducted by

MIRIAM ZINTL, BSc

born on January 26th, 1995 in Prien am Chiemsee
Koelblgasse 13/18, 1030 Wien

June 18, 2020

Miriam Zintl

"It's more interesting to work on challenges where you don't know the answer. In chemistry, you should enter into an adventure with molecules."

Ben Feringa

Abstract

Surgery on unborn children offers the potential to prevent various congenital anomalies, but is a high-risk intervention. During fetoscopic surgery a small inscission is made in the fragile amniotic sac, which, unlike other human tissue, cannot heal. As the preferred time for this procedure is within the second trimester, the risk of rupture may result in preterm birth with a low survival rate of the fetus. A sealant to close and support the punctured amniotic tissue could prevent preterm labor and substantially increase chances of survival. While a number of medical adhesives are commercially available, after two decades of research they have proven ineffective in fetal surgery.

This diploma thesis deals with the synthesis and characterization of an improved wet tissue adhesive inspired by marine mussels. The *Mytilus edulis* strongly adheres to rocks *via* byssal threads and several sticky interfacial mussel-foot-proteins (mfps). Of those, mfp-5 has been identified as particularly adhesive due to a synergistic relation between high concentrations of dopamine and lysine. In an approach mimicking mfp-5, a methyl methacrylate polymer containing catechol (as a dopamine mimic) and primary amine (as a lysine mimic) motifs has been co-polymerized.

Cohesive strength was then achieved by embedding this sequence macromonomer into an amphiphilic polymer with supramolecular crosslinks (ureido-4-pyrimidone hydrogen bonding dimers). The supramolecular motifs form a cohesive network by reversible crosslinking, resulting in high toughness and flexibility. This approach stands in stark contrast to the majority of tissue adhesive developments, which primarily rely on covalent crosslinking of the adhesive motif to achieve cohesive strength. Using only one motif for adhesive and cohesive strength, such as base catalyzed dopamine crosslinking, restricts the tunability of the polymer.

Through the use of two separate motifs, individually tunable adhesive and cohesive properties were achieved within this project. Furthermore, upon contact with water the amphiphilic matrix provides protection of the water sensitive supramolecular crosslinks by phase separation. Tissue shear adhesion tests showed high adhesion strengths of more than 70 kPa to bovine pericardium compared to about 35 kPa for commercially available sealants such as Cyanoacrylate-based glues, confirming the efficacy of the biomimetic motifs used.

Overall, a mussel-mimetic wet tissue adhesive was developed, that addressed the challenge of strong tissue bond formation under wet, physiological conditions. The material therefore has potential to be used as a general surgical adhesive.

Kurzfassung

Operative Eingriffe am Fetus können eine Vielzahl an angeborenen Anomalien verhindern. Sie sind jedoch mit hohen Risiken verbunden, da bei fetoskopischen Operationen ein kleiner Einschnitt in die Fruchtblase, die entgegen normalem Gewebe nicht heilen kann, gemacht wird. Das Risiko einer Ruptur ist dadurch bedeutend erhöht. Da solche Eingriffe präferiert in den ersten beiden Trimestern durchgeführt werden, kann eine Ruptur der Fruchtblase zu Frühgeburten mit geringen Überlebenschancen für den Fetus führen. Ein Gewebekleber könnte den Einschnitt in der Fruchtblase schließen und das Gewebe stützen. Dadurch könnte eine Frühgeburt verhindert und die Überlebenschancen des Fetus erheblich gesteigert werden. Obwohl einige klinische Gewebekleber kommerziell erhältlich sind, haben diese sich auch nach zwei Jahrzehnten Forschung als ineffizient in der Fetalchirurgie erwiesen.

Im Rahmen dieses Projekts wird die Synthese und Charakterisierung eines von Muscheln inspirierten, optimierten nassen Gewebeklebers behandelt. Der Meeresorganismus *Mytilus edulis* verwendet Haftfäden und adhäsive Proteine um Haftung am Untergrund zu erzielen. Eines dieser Proteine, mfp-5, ist aufgrund von Synergieeffekten zwischen großen Mengen von Dopamin und Lysin besonders adhäsiv. Inspiriert von mfp-5 wurde ein Polymer auf Methyl methacrylat-Basis hergestellt, welches Catechol als Dopamin-Imitat und ein primäres Amin als Lysin-Imitat enthält.

Um Kohäsion im Material zu erzielen wurde dieses Sequenz-Makromonomer anschließend in ein amphiphiles Polymer mit supramolekularen Quervernetzungen (Ureido-4-pyrimidone Wasserstoffbrückenbindungen) eingebettet. Durch reversible Verbindungen bilden die supramolekularen Motive ein kohäsives, zähes und flexibles Netzwerk. Im Unterschied dazu erzielen die meisten Gewebekleber Kohäsion durch kovalente Querverbindungen der adhäsiven Motive (wie bspw. Basen-katalysierte Dopamin-Vernetzungen), was ihre Adjustierbarkeit stark einschränkt.

Durch die Implementierung zweier eigener Motive wurde im Rahmen dieser Diplomarbeit ein Polymer mit individuell adjustierbaren adhäsiven und kohäsiven Eigenschaften entwickelt. Die Wasserempfindlichen supramolekularen Vernetzungen werden hierbei bei Kontakt mit Wasser durch die Phasenseparierung der amphiphilen Matrix geschützt. In Haftkraft Messungen wurden Adhäsionskräfte von mehr als 70 kPa zu bovinem Herzbeutel-Gewebe gemessen. Im Vergleich mit kommerziell erhältlichen Gewebeklebern wie Cyanoacrylat-basierten Klebstoffen (35 kPa) wurde damit die Effizienz der biomimetischen Motive bestätigt.

Insgesamt wurde ein starker Muschel-inspirierter Gewebekleber für die Problemstellung der Haftung unter physiologischen Bedingungen entwickelt. Das Material birgt Potential, auch in anderen Bereichen als chirurgischer Klebstoff verwendet zu werden.

Acknowledgements

Firstly, I want to thank Prof. Phillip Messersmith for enabling me to carry out my thesis in his research group at the University of California, Berkeley, and Dr. Diederik Balkenende for the excellent supervision. Both during my thesis and afterwards, Dirk thoroughly supported me with scientific discussion and advice, and I would like to express my gratitude for the time and the open ear he always had for me.

A special thanks goes to Prof. Miriam Unterlass for urging me to take the opportunity to conduct my thesis abroad and for being my supervisor at TU Wien.

My appreciation also goes to the Marshallplan Foundation for funding my research endeavors.

I would like to thank the entire Messersmith lab at UC Berkeley for welcoming me into their group and providing a cooperative and fun atmosphere throughout all stages of my thesis. My special thanks go to my fellow lab-mates Katarina, Arianna, Sally, Cody and Kelsey for great conversations, collaborations and for refilling the cooling trap with liquid nitrogen when needed.

My Berkeley-family, Ana, Pepe, Jenn and especially Amit deserve my greatest thanks for being there after long work days and providing me with food, sporting activities and necessary distractions. Without them, my time in Berkeley would not have been half as memorable.

I would also like to express gratitude to my friends and fellow students Elli, Patrick, Robert and Michi for the great times we had together cooking in and out of the lab.

I am hugely indebted to my better half Matthias, who endured and supported me these past years. He has always believed in me and constantly found the perfect words to encourage me, motivate me or to remind me to take a break. Thank you for always being there for me.

Finally, I want give my very special thanks to my parents, Annette and Curd, and grandparents Elke and Karlheinz, for raising me to be who I am today, supporting me throughout my life and financially enabling me to follow my path. None of this would have been possible without them.

List of Abbreviations and Symbols

^{1}H NMR	nuclear magnetic resonance	M	molarity [mol/L)]
AcDMA	acetonide protected DMA	M_w	molecular weight [g mol^{-1}]
AEMA	amino ethyl methacrylate	MeOH	methanol
AFM	atomic force microscopy	mfp	mussel foot protein
AIBN	azobisisobutyronitril	mfp-5	mussel foot protein 5
boc	tert-butyloxycarbonyl	MMA	methyl methacrylate
bocAEMA	boc protected AEMA	p-TsOH	p-toluensulfonic acid
$CDCl_3$	deuterated chloroform	PBS	Phosphate-buffered saline
CPBD	2-Cyano-2-propyl benzodithioate	PC	polycarbonate
CTA	chain transfer agent	PEG20MA	poly(ethylene gylcol)20 methacrylate
DBTL	dibutyltin dilaurate	PPROM	premature preterm rupture of membrane
DCM	dichloromethane	Py	pyridine
DMA	3,4-dihydroxyphenylalanine methacrylate	RAFT	reversible addition fragmentation transfer reaction
DMF	dimethylformamide	RDRP	reversible-deactivation radical polymerization
DMSO-d6	deuterated dimethyl sulfoxide	RT	room temperature
dopa	3,4-dihydroxyphenylalanine	SMM	sequence macromonomer
DSC	differential scanning calorimetry	T_g	glass transition temperature [°C]
EA	ethyl acetate	TEA	triethylamine
EHMA	2-ethylhexyl methacrylate	TFA	trifluoroacetic acid
Et_2O	diethylether	THF	tetrahydrofuran
EtOH	ethanol	Tol	toluene
GPC	gel permeation chromatography	Upy	ureido-pyrimidinone
Hex	hexanes	UPyHEMA	UPy hydroxyethyl methacrylate
IUPAC	International Union of Pure and Applied Chemistry		

Contents

Part I

Introduction

Since the first fetal transfusion in 1963, substantial progress has been made in the understanding of fetal development and pathophysiology.[1] Over the last decades, significant advances in surgical tools and imaging methods, such as high-resolution noninvasive fetal imaging, enabled interventions on the fetus itself as a patient.[2]

This allowed for treatment to evolve from high risk open surgery to fetoscopic surgery, a minimally invasive technique. Traditionally, open fetal surgery was performed on a partially exposed fetus after opening the uterus. Due to the associated amniotic fluid loss and preterm labor, it has been mostly replaced by fetoscopic surgery, where the amniotic sac is merely penetrated by a fetoscope.[1,3] In a minimally invasive fetoscopic procedure, one or more small incisions (2.3 - 4 mm) are made in the mother's abdomen in order to access the fetus with instruments or needles. Figure 1 shows a schematic depiction of the procedure, which usually is monitored by real-time ultrasound imaging to guide the surgeon.[1,2,4]

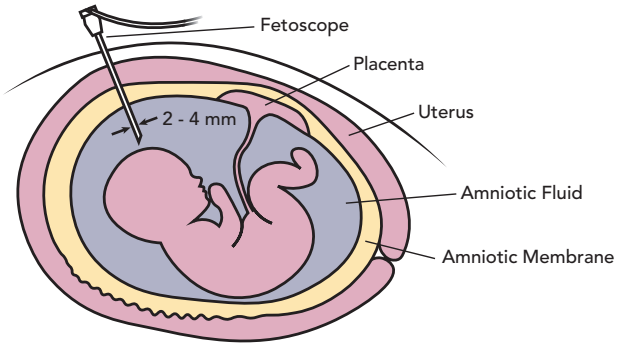

Figure 1: Schematic depiction of fetoscopic surgery on a fetus.

Fetal surgery as an emerging discipline in medicine has saved and improved the lives of numerous mothers and children, as various congenital anomalies can only be prevented by prenatal treatments. Those anomalies include for example the twin-twin transfusion syndrome, a condition that causes delayed organ development in one twin and accumulation of excess fluid in the other twin's organs, and spina bifida (also called myelomeningocele), a defect where the skin does not fully develop around the lower parts of the spinal cord, resulting in malformations and limited lower limb function.[5]

Nowadays, fetoscopic surgery is routinely used to treat those conditions. However, the small defect that is left after surgery still poses a risk to mother and fetus, as the amniotic sac, unlike normal tissue,

is fragile and unable to heal by itself. Hence, the scission induced by the procedure increases the risk of premature preterm rupture of membranes (PPROM) post-surgery.[1,4]

Most fetal surgeries need to be performed between 16 and 26 weeks of gestation, at which premature babies have a low survival rate.[2,6] Figure 2 depicts the survival rate of the fetus in relation to the number of weeks of gestation reported by Ancel and coworkers.[6]

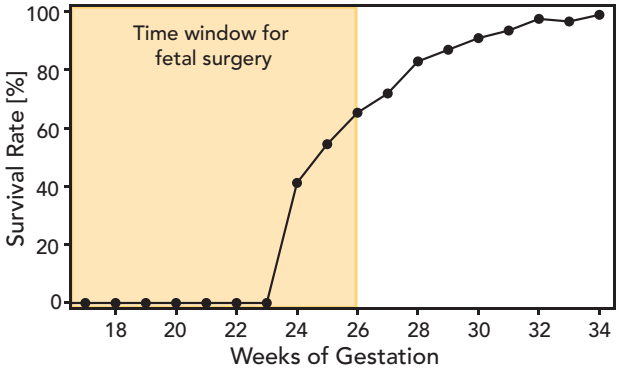

Figure 2: Survival rate of the fetus in relation to the duration of gestation. The time window for fetal surgery is shown in orange.[6]

Providing a sealant for the membrane would prevent the loss of amniotic fluid as well as PPROM and allow for the fetus to remain in the womb for at least 32 of 40 weeks of gestation, therefore drastically increasing its survival rate.[4]

Therefore, researchers are investigating various materials and methods to seal the amniotic sac after fetoscopic surgery. Among others, attempted strategies for sealing or healing the fetal membrane include poly(ethylene glycol)-based biomimetic matrices, hydrogel surgical sealants and amniopatches.[7–10]

However, adhesion to wet tissue is extremely challenging and while there is a number of medical adhesives commercially available, so far none has been accepted as a viable solution for fetal surgery.[4]

The motivation for this diploma thesis was the design and synthesis of such a functional sealant for fetal surgery. In order to achieve strong wet adhesion, the marine mussel and its attachment strategy served as an inspiration for this project. Additionally, the Messersmith lab's recent successful incorporation of supramolecular motifs into mussel inspired sealants provided an advantageous starting point for this work. [11]

This thesis will be focusing on the synthesis, characterization and comparison of the adhesive polymers in four main sections, after discussing the synthesis of the custom-made monomers. The first section will discuss the polymeric adhesive motif on its own, while the two ensuing sections will elucidate two different approaches for the incorporation of the adhesive motif into a supramolecular wet tissue adhesive. The last section will compare the wet tissue adhesives primarily based on their adhesive performance.

Part II

General Background

This chapter will provide a brief overview over the two general themes deployed within this thesis. Initially, bioinspiration and the particular model system will be discussed, followed by theoretical background on polymer chemistry, supramolecular materials and polymerization techniques.

1 Bioinspiration and Biomimetics

The terms *bioinspiration* and *biomimetics* both describe the study of biological mechanisms and biologically produced substances for the purpose of synthesizing similar products by artificial means. Hereby, biomimetics is defined as the direct replication of techniques and processes used in biological systems, whereas bioinspiration covers the broadly defined field of applying concepts found in nature to synthetic settings. However, the formal distinction between both terms can overlap and blur at times.[12] For the purpose of this work, both terms are used interchangeably for the replication of the adhesion mechanism used by the model system.

1.1 Bioinspired Materials

Organisms in nature evolved over billions of years to adapt to unique habitats and specific living conditions. Often, higher-order structuring is used to achieve complex functionality.[13] Hence, in order to overcome specific problems, bioinspiration allows us to skip this evolutionary experimentation and implement natures elegant approaches into our engineered mechanisms and synthetic products.[12]

Biology has inspired a plethora of developments, many of which have been commercialized, in various fields such as organic chemistry, nanocomposites, catalysis and macromolecular science.[14–17]

One of the best known examples of bioinspiration is the so called Lotus effect. This essential phenomenon is used by plants and animals, such as the lotus, water-striding insects and butterflies, to overcome various obstacles. It equips lotus leafs and butterfly wings with the ability of self-cleaning and enables certain insects to walk on water.[18,19] Those capabilities are based on superhydrophobic surfaces, that are nano-structured in a way that provides a very high static water contact angle greater

than 160 °. Therefore, water forms spherical droplets, which solid and organic contaminants easily attach to and which can roll off surfaces even at low inclination angles.[18,20] The reverse-engineering of those properties has inspired surface coatings for various materials, aiming at self-cleaning properties. For instance, windows and solar panels have been outfitted with coatings that mimic self-cleaning properties and facilitating otherwise difficult cleaning processes.[20,21]

Further examples, not all of which have been commercialized yet, include *e.g.* protein elastomers inspired by spider silk and nanostructured photonic materials inspired by natural structural color.[22,23] Natural self-assembly processes such as protein folding or formation of micelles have given rise to numerous biomimetic adaptions, facilitating the formation of synthetic assemblies. Self-assembling hollow bilayer structures *e.g.* were inspired by natural membranes and are investigated as drug delivery systems.[24]

Great interest has also been taken in biology's adhesive strategies, as they comprise an array of unique approaches for different adhesive problems. To overcome diverse obstacles in the development of adhesives and glues, researches have turned toward organisms that are handling comparable problems successfully.

1.2 Bioinspired Adhesion

Especially for adhesives applied under wet or physiological conditions, conventional synthetic approaches often malfunction. Thus, scientists are turning toward marine animals for inspiration. Underwater habitats are confronting organisms with various difficulties, one of which is adhesion to wet surfaces in saline environments and at ambient temperature. Mechanisms, which emerged as a consequence, are particularly of interest as they include the displacement of surface water, as well as the production and curing of the adhesive in a crucially timed manner under wet conditions.[25] Common synthetic adhesives are incapable of displacing layer-bound water, which causes a reduction in non-covalent interactions such as van der Waals forces. This reduction is prompted by the high dielectric constant of water and, in the case of physiological liquids, by the high ionic strength of electrolytes such as salt water.[26,27]

Various animals have evolved highly efficient attachment strategies based on chemical and physical wet adhesion mechanisms.[27] Generally, a differentiation between temporary and permanent adhesion to wet surfaces can be made, each offering inspiration for a separate field of applications.

Temporary adhesion is beneficial especially for reversible and repeated attachment. It is often based on physical wet adhesion strategies, taking the detachment as well as the attachment process into account. Octopi *e.g.* use orifices with dome-shaped protuberances on their tentacles to actuate muscular hydrostatic pressure and adhere to underwater surfaces.[27,28]

Permanent adhesion on the other hand is mainly based on chemical attachment strategies and is found in various marine animals, such as sandcastle worms, barnacles and mussels. The marine worm *P. californica* for instance builds its composite mineral shell by binding together sand grains with proteinaceous glue. This glue appears in form of a microporous water-filled foam, which sets within 30 seconds under cold seawater.[29] Barnacles, too, use a protein-based adhesion strategy to attach to foreign material surfaces. The crustaceans secret a multiprotein complex, so called cement, which shows a significantly different amino acid composition in comparison to underwater adhesives of other organisms (sandcastle worms, mussels).[25,30]

Mimicking and implementing those physical and chemical adhesion strategies has led to the development of various glues. For example, Shao *et al.* mimicked the sandcastle worm glue protein by synthesizing a polyacrylate glue protein analog.[29] The octopus suction cups inspired Baik *et al.* in their development of a wet-tolerant reversibly applicable adhesive patch.[28]

Even though a diverse host of marine animals served as template for such approaches, inarguably the organism that inspired the majority of biomimetic wet adhesives, is the mussel.[27,31] As the model system for the scope of this work, the mussel's adhesion mechanism will be detailed below.

1.3 Biological Model System

As a marine organism inhabiting seashores, the mussel is frequently exposed to high shear forces caused by tidal waves and currents. Its anchoring mechanism to rocks therefore has evolved to withstand elevated mechanical loads caused by its environment.[26,32]

Mussels tether themselves to foreign surfaces *via* bundles of tough byssal threads with adhesive plaques at their distal ends, as depicted for the California mussel in figure 1.1. Threads and plaque are both protein-based and are secreted through different glands in the mussel foot. The change in temperature and/or pH from glands to seawater triggers rapid solidification of the proteins.[33] Waite and coworkers have extensively characterized the plaque and isolated several mussel-foot-proteins (mfp) that contribute to its adhesion chemistry. As many as 20 different proteins constituting the byssal threads are known, of which at least six mfps within the adhesive plaque have been identified.[26,32]

Figure 1.1: California mussel with newly formed byssal threads.

The left part of figure 1.2 shows a scheme of the plaque. While it is constituted of several different mfps, only two, namely mfp-3 and mfp-5, have been implicated as interfacial by MALDI spectrometry.[34] While both highly hydrophilic and polar proteins are suggested to play an important role in interfacial binding, mfp-5 contains the highest amount of 3,4-dihydroxyphenyl-alanine (dopa) among plaque proteins. Dopa is a post-translational modification of tyrosine, which is hypothesized to mediate adhesive strength by forming various types of chemical interactions.[32,33] The amino acid sequence of mfp-5 is depicted in the right part of figure 1.2.

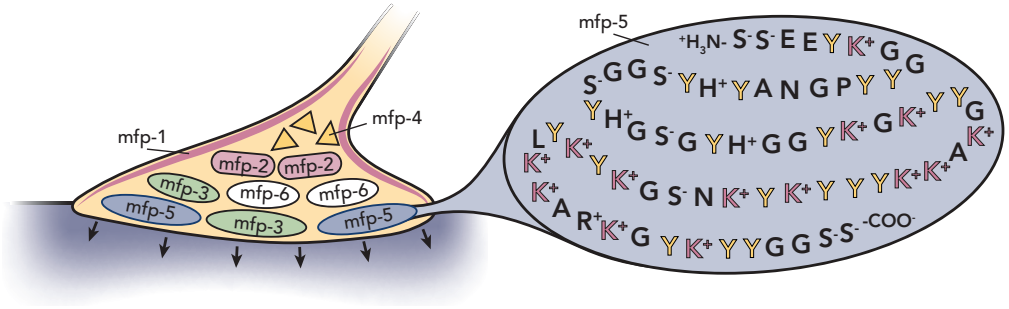

Figure 1.2: Left part: Scheme of the plaque and its mussel foot proteins. Right part: Amino acid sequence of mfp-5 with dopa (Y) and lysine (K+) highlighted.

The high binding strength of dopa, shown by atomic force microscopy measurements by Lee and coworkers, arises from several types of non-covalent and covalent interactions with various surface types.[35] Hydrogen bonding of the dihydroxy functionalities of catechol *e.g.* enables absorption to hydroxyapatite surfaces and mucosal tissue. π-π and π-cation interactions of the benzene ring improve cohesion and promote attachment to aromatic surfaces. Metal-oxygen coordination allows for binding to inorganic substrates such as metals and metal-oxides, whilst adhesion to organic surfaces is accomplished covalently.[32] In alkaline seawater, the catechol residue of dopa **(1)** is in equilibrium with its reactive oxidized form, an o-quinone side chain **(2)**. The o-quinone is postulated to form covalent bonds either with further catechol residues (crosslinking for in-situ solidification), or by reaction with nucleophilic functional groups *via* different pathways. Proposed mechanisms are depicted in figure 1.3 and include Michael-type addition to lysine residues (**A**), Schiff base formation with lysine residues (**B**) and cross-linking with cystein residues (**C**).[32,35–37]

In order for dopa to provide the mussel with strong and durable adhesive interactions, mussel foot proteins need to overcome hydration barriers to form an intimate interface with the substrate for bonding. This obstacle is managed by the cationic amino acid lysine, which often flanks dopa within mfps, and displaces interfacial hydrated salt ions.[27,38] The synergy between catechol and lysine is thought responsible for the mussel's outstanding wet adhesion properties and it reasons the high content of dopa and lysine in the surface priming proteins mfp-5 and mpf-3.[38] Among the plaque proteins, mfp-5 contains the highest amounts of dopa and lysine residues with 30 %mol and 20 %mol respectively, followed

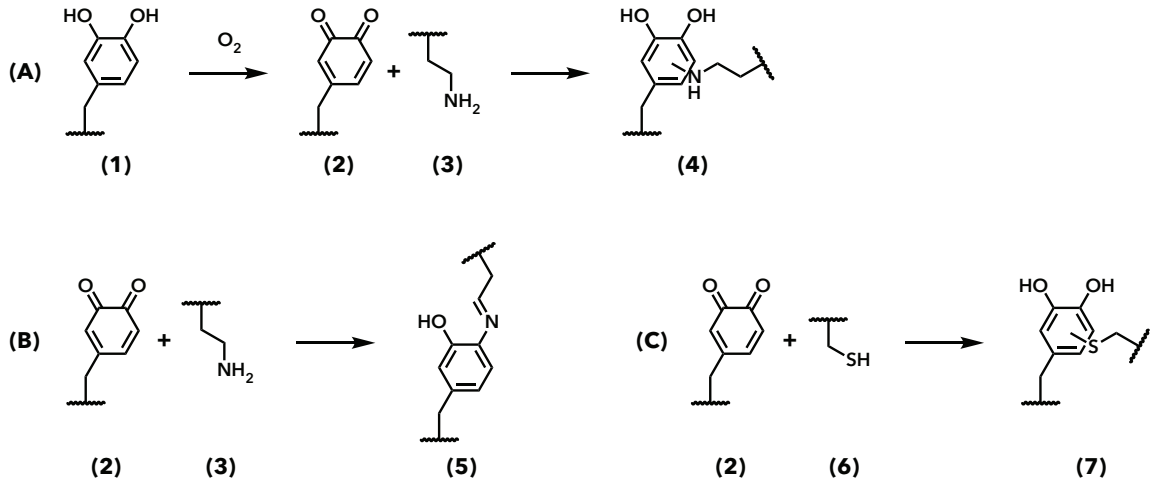

Figure 1.3: Scheme of reaction pathways of dopa: **(A)** Pendant dopa-chain **(1)** oxidizes to o-quinone **(2)** and links to lysine residue **(3)** *via* Michael-type addition. **(B)** O-quinone **(2)** links to lysine residue **(3)** *via* Schiff base formation. **(C)** O-quinone **(2)** links to cystein residue **(6)** *via* Michael-type addition.

by mfp-3 with 19 %mol dopa and 15 %mol lysine residues.[32] Rapp and coworkers recently showed that this synergy is greatest if catechol and amine are within the same molecule.[38]

The mussel's exceptional adhesive strength to wet surfaces gives rise to implement the synergy between dopa and amines into a synthetic wet tissue adhesive to improve adhesion properties. The synthesis of a macromonomer mimicking mfp-5, and its incorporation into a supramolecular polymer was approached in this work by use of polymer chemistry.

2 Mimicking Nature's Sticky Proteins - Polymer Chemistry

According to the International Union of Pure and Applied Chemistry (IUPAC), a polymer is "*a substance composed of macromolecules*", with a macromolecule being "*a molecule of high relative molecular mass, the structure of which essentially comprises the multiple repetition of units derived, actually or conceptually, from molecules of low relative molecular mass*".[39] The structure, composition and constitution of the polymer, as well as the chemical nature of the low molecular weight molecules it is built from, define its properties.[40] The variety of different monomer units available for polymerization and various polymerization techniques allow for tailoring polymer properties to numerous applications and their demands. By designing composition and constitution *e.g.* according to the melting point, density and tensile properties, polymers can function as porous, light materials like Styropor®, as high performance electrical insulators like Kapton®or as soft hydrogels for contact lenses.[41,42]

Narrowing on polymeric materials used for clinical applications, this class of macromolecules is

generally designed to match the mechanical properties of the host tissue. Surgical adhesives additionally need to exhibit high adhesive strengths to the tissue. While fibrin, gelatin and polyethylene gylcol (PEG) based materials, among others, are already commercialized as sealants, they each raise different concerns regarding their composition and applicability.[43]

Furthermore, their use in fetal surgery is limited by many technical and biological obstacles.[44] Mussel inspired tissue adhesive polymers, such as catechol modified branched amphiphilic poly(propylene oxide)-poly(ethylene oxide) block co-polymers, provide a promising direction for applicable fetal membrane sealants.[44] Further research and development of such a polymeric tissue sealant for punctures in the amniotic sac is suggested to take the following properties into consideration: be bio-compatible, show mechanical properties similar to the substrate, be fluid impenetrable, exert strong adhesion strength and maintain those properties for an appropriate duration to prolong gestation time for several weeks.[4]

To address those qualities, the polymerization techniques deployed need to ensure control over molecular composition and molecular weight M_W. This is especially true for polymers mimicking biological systems. Here, Reversible Addition-Fragmentation Chain Transfer (RAFT) polymerization offers a convenient method to exert control over the polymer.

The first section below will discuss supramolecular chemistry and the use of self-assembling motifs. In the second section, the theory of synthetic polymerization techniques applied within this research project will be explained for further reference. In order to provide a solid understanding of the materials constitution, the motifs used for the development and enhancement of the polymeric wet tissue adhesive are elucidated in a third section. A fourth section will detail the state-of-the-art-polymer developed by Balkenende and coworkers.[11]

2.1 Supramolecular Materials

Supramolecular chemistry is a field of materials science, in which molecules or polymers are held together by non-covalent interactions, such as hydrogen bonds, ionic interactions or metal-ligand coordination. A so called supermolecule is formed when a large number of building blocks assembles by spontaneous association into a specific phase.[45–47] Numerous biological systems as well as synthesized materials, many of which are of polymeric nature, make use of those principles.[27,45,48,49] Generally, supramolecular polymers can be divided into two broad categories. The first comprises one-dimensional assemblies of monomers engaging in entanglements and molecular stacking, the second includes noncovalent crosslinks between specific recognition motifs on polymeric precursors.[50,51]

Crosslinking polymeric precursors, such as hydrogel materials, with physical bonds opens up a variety of properties unavailable to covalently crosslinked materials.[11,50] Dynamic supramolecular

crosslinks afford a more precise control over a material's mechanical properties like tunable biological and chemical properties and tailored viscoelasticity, and bear the potential for self healing and stimuli-responsive properties.[10,11,47,51]

Supramolecular polymers are well suited for biomaterials, as they efficiently couple the orthogonality of supramolecular chemistry with the beneficial properties of the polymer itself.[50,51]

A number of specific, directional supramolecular moities has been developed for orthogonal design approaches.[51] Of special interest to this thesis is the hydrogen-bonding motif ureido-4-pyrimidinone (UPy) **(8)** established by Meijer *et al.*.[52]

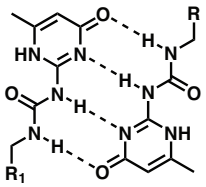

(8)

Figure 2.1: Scheme of the hydrogen-bonding dimer ureido-pyrimidinone.

UPy, as depicted in figure 2.1, is capable of self-complementary quadruple hydrogen bonding upon dimerization.[45] The fraction of bound UPys as well as their interaction strength within a material depend on the choice and molar ratios of co-monomers, temperature, pH, hydrophobicity and presence of water rather than the absolute content of the supramolecular motif.[11,53] UPy forms inherently dynamic crosslinks, what makes its use in biomaterials highly desirable.[50,51,54,55]

2.2 Polymerization Techniques

Generally, polymerization techniques can be divided into two groups, one comprising step-growth polymerizations like polycondensation and polyaddition, and a second group including chain-growth polymerizations like free radical polymerization and ionic polymerization.[40] According to IUPAC, chain-growth polymerizations are defined as follows: "*A chain reaction in which the growth of a polymer [ ] chain [ ] proceeds exclusively by reaction(s) between monomer(s) [ ] and reactive site(s) on the polymer chain with regeneration of the reactive site(s) at the end of each growth step.*"[39]

Chain-growth techniques such as free radical polymerization are well suited for monomers based on methacrylate, as they comprise a terminal double bond -$C(CH_3)$=CH_2, which is comparably unobstructed and can easily be targeted by radicals.[56] As the control over polymer growth and M_W exerted by free radical polymerization is limited, a modified living radical polymerization, namely RAFT polymerization, emerged in 1998 and has grown in appeal ever since.[57,58]

Within the scope of this thesis the two chain-growth techniques free radical polymerization and

RAFT polymerization were employed. Their mechanisms will be elucidated below.

2.2.1 Free Radical Polymerization

Free radical polymerization is the most used chain polymerization and is employed to produce a wide variety of polymers. It is started by a free radical adding to a monomer, followed by successive addition of monomer blocks in order to grow the polymer chain. Depending on the number of species of monomers used in the polymerization, a homopolymer (only one monomer species is used) or a copolymer (at least two monomer species are used) can be generated.[39,40,42] A scheme of the mechanism is shown in figure 2.2. While for easier understanding, the reactions **A-E** are discussed successively, they all take place simultaneously.[59]

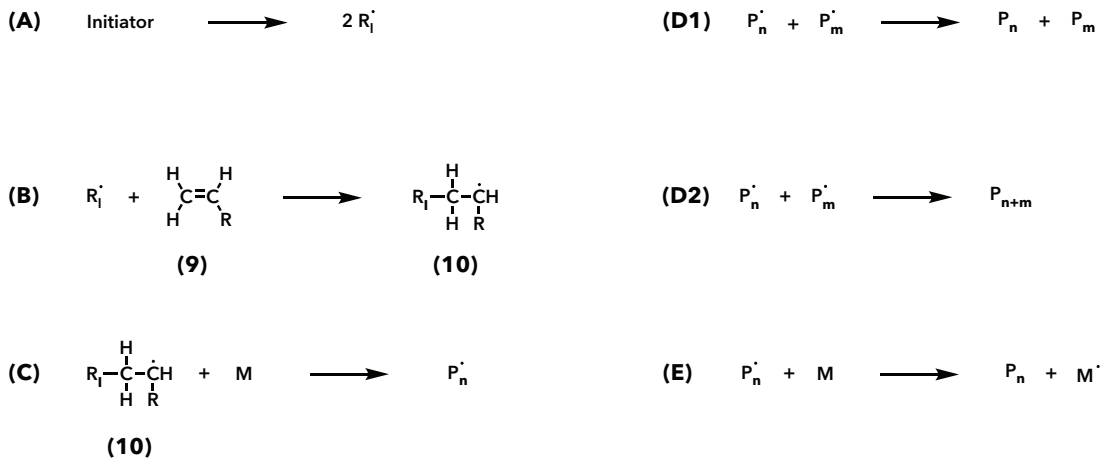

Figure 2.2: Scheme of the mechanism of a free radical polymerization with initiation **(A-B)**, propagation **(C)**, termination **(D1-D2)** and side reaction **(E)**.

First, a radical is usually produced by thermal decomposition, irradiation or a redox reaction of an initiator, such as a peroxide or azo compound **(A)**. A commonly employed thermal initiator used as radical starter is azobis(isobutyronitrile) (AIBN). A significant part of the primary radicals $\mathbf{R_I\cdot}$ undergoes immediate recombination. This occurs due to a reasonable probability for the fastest possible reaction to take place, which is with the radical's nearest neighbor, another primary radical. The reaction is then initiated by the radical $\mathbf{R_I\cdot}$ adding to the double bond of a monomer unit **(9)** and generating a new, longer monomer radical **(10)**. This second step **(B)** usually is much faster than the rate of initiator decomposition, making step **(A)** the rate-determining step. Subsequent addition of the generated new monomer radical **(10)** to further monomers **M** yields a growing polymer chain with a radical active center $\mathbf{P_n\cdot}$. The process of monomer addition is called chain propagation **(C)** and continues until the active radical is terminated. Commonly, the monomer conversion rate increases over time as longer polymer chains are formed and viscosity increases. This is accounted for by limited diffusion and hindered primary radical recombination, resulting in higher radical concentrations. Chain termination **(D)** can take place

by either disproportionation of two polymer radicals $\mathbf{P_n}\cdot$ and $\mathbf{P_m}\cdot$ **(D1)** or by their combination **(D2)**. Which of these reactions is more likely to occur depends on monomer type and temperature. For methyl methacrylate monomers *e.g.* disproportionation is favored at high temperatures. This affects the M_W, as combination of two polymer chains raises the average M_W, while for disproportionation, the average M_W remains the same. Another elementary reaction occurring in free radical polymerization is a chain transfer reaction **(E)**. This side reaction describes the transfer of the radical from a polymer chain $\mathbf{P_n}\cdot$ or macromonomer to another molecule. The radical can be transferred to solvent molecules, to monomer units **M**, to initiator molecules or to other polymer chains $\mathbf{P_m}$.[40,42,59]

As all four reaction steps and side reactions **(A-E)** happen simultaneously, at any point of time during the reaction polymer chains of different length are present. This results in a broad molecular mass distribution upon chain termination.[59]

2.2.2 RAFT Polymerization

RAFT polymerization allows for the synthesis of controlled molecular weight polymers while offering much of the versatility of normal free radical polymerizations. Ever since it was established, it has been widely used for the production of high M_W polymers with very narrow polydispersities in research and science. A wide range of monomers is accessible to RAFT polymerization, including methyl methacrylates.[57,58]

RAFT polymerization belongs to the group of controlled/living radical polymerizations, where a living polymerization is defined as a chain polymerization from which chain transfer and chain termination are absent.[39,59] Practically, a living polymerization is considered as such, if the polymer's end groups remain prone to growth at least for the duration of reaction completion. Since termination reactions are inevitable for free radical polymerizations, a reaction, such as a RAFT polymerization, can be regarded as pseudo-living polymerization if a large portion of polymer chains is dormant and they all have the same potential to grow further.[59]

Particularly, RAFT is a reversible-deactivation radical polymerization (RDRP), meaning it is based on a dynamic equilibrium of dormant and active species. RAFT operates on the principle of degenerative chain transfer, utilizing a so called chain transfer agent (CTA).[59,60] Thiocarbonyl thio compounds are used as CTAs due to their very high transfer constants, granting the polymerization a living character. Figure 2.3 depicts the general structure of a CTA **(11)** as well as example compounds **(12)-(14)**. The precise compound deployed as CTA needs to be adapted for the monomer species to ensure fast transfer reactions. In general, **Z** should activate the **C=S** bond toward radical addition and **R** needs to be a good free radical leaving group. As a radical, $\mathbf{R}\cdot$ should effectively reinitiate a free radical polymerization.[57,58]

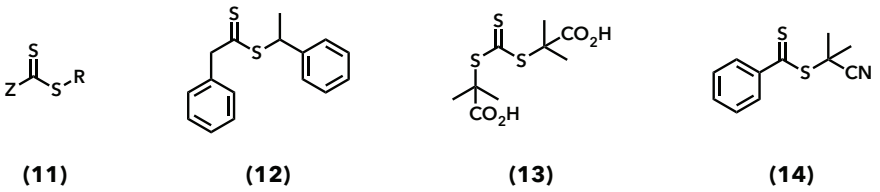

Figure 2.3: Scheme of the CTAs general structure **(11)** and exemplary compounds: 1-phenylethyl phenylethanedithioate **(12)**, 2,2'-(carbonothioyldisulfandiyl)bis(2-methylpropanoic acid) **(13)** and 2-cyano-2-propyl benzodithioate (CPBD) **(14)**.
[61]

The detailed mechanism of a RAFT polymerization is shown in scheme 2.4 and discussed hereafter.

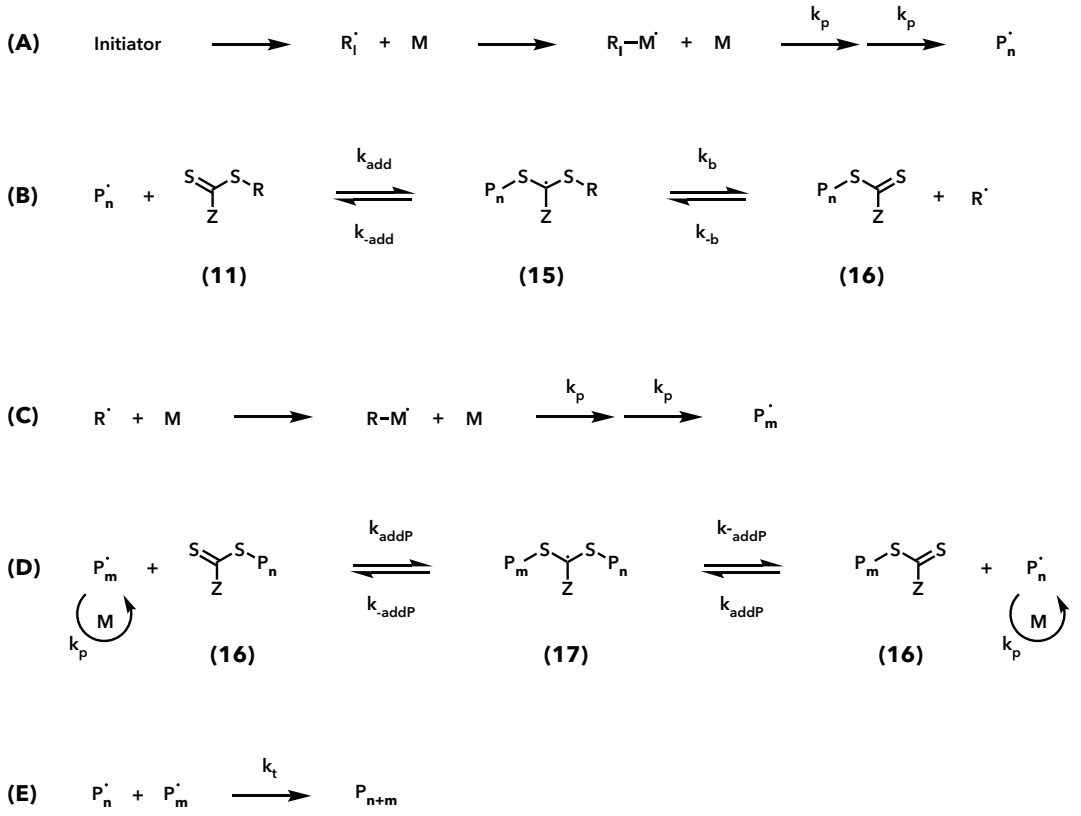

Figure 2.4: Scheme of the mechanism of a RAFT polymerization with initiation **(A)**, degenerative transfer **(B)**, reinitiation **(C)**, chain equilibration and propagation **(D)** and termination **(E)**.

The reaction is started by a radical initiator such as the usual azo or peroxy initator, which is triggered thermally or by irradiation. As for free radical polymerization, a very common initiator is AIBN. The newly formed radical $\mathbf{R_I}\cdot$ then adds to monomer units **M** to form a polymeric radical $\mathbf{P_n}\cdot$ **(A)**. This polymeric radical $\mathbf{P_n}\cdot$ subsequently undergoes a degenerative transfer step, in which the active center, the radical, is transferred from the polymeric chain to the fragmented CTA **(B)**. In detail, the polymeric radical $\mathbf{P_n}\cdot$ adds to the thiocarbonyl thio compound **(11)** to form an intermediate radical **(15)**. The intermediate radical **(15)** decomposes into a dormant polymeric chain **(16)** and a new radical $\mathbf{R}\cdot$. The radical $\mathbf{R}\cdot$ can then reinitiate polymerization by reacting with a new monomer **M** to a polymeric radical $\mathbf{P_m}\cdot$ **(C)** or react with the newly formed dormant polymeric chain **(16)** to activate it again. Once the initially

added CTA is consumed, the chain propagation is based on rapid equilibria between active propagating polymer chains ($\mathbf{P_n}$ or $\mathbf{P_m}$) and dormant polymer chains (**16**) **(D)**. These rapid equilibria provide equal probability for each chain to grow. Termination of the reaction can occur by bimolecular termination **(E)** where two active polymeric radicals $\mathbf{P_n}\cdot$ and $\mathbf{P_m}\cdot$ combine. After completion or stopping of the reaction, the main part of the polymer chains retains the CTA thiocarbonyl thio endgroup.[57–61]

As long as the number of active and dormant polymeric chains N is large enough, the living character of the polymerization is sustained and can be observed by linear molecular weight conversion and narrow polydispersion.[57,59] Due to the linear M_W and the rapid equilibria, which afford all monomer units the same probability of growth, it is possible to plan and predict the M_W. Additionally, it can be calculated at any point of conversion from the ratio of CTA to monomer consumed.[57,61] Similar to free radical polymerizations, the reactivity of the propagating polymer chain and the probability of monomer addition in RAFT can be affected by the monomer species.[59]

As the thiocarbonyl thio endgroup is retained at the end of the reaction, a convenient option for end group functionalizations is given, either by choice of the CTA or by post-polymerization functionalization.[57]

While the advantages of RAFT polymerization are apparent, shortcomings do exist. The reaction needs external initiators, which might lead to radical termination events. Furthermore extended polymerization times are required for full polymerizations.[59,60]

2.3 Monomers of Interest

Building on the state-of-the-art-system developed by the Messersmith lab (discussed in section 2.4), the implementation of lysine is hypothesized to strengthen adhesion and delay the effect of detachment over time. Within this project, lysine is incorporated in the form of amino ethyl methacrylate into a sequence macromonomer (SMM) with dopa methacrylate and methyl methacrylate. The components of the SMM, as well as the motifs of the supramolecular matrix all contribute differently to the properties of the polymers developed within this thesis, which are based on an orthogonal chemistry approach.

Following motifs, depicted in figure 2.5, are discussed in regard to their functionality:

- 3,4-dihydroxyphenylalanine methacrylate (DMA) (**18**)
- amino ethyl methacrylate (AEMA) (**19**)
- methyl methacrylate (MMA) (**20**)
- ureido-4-pyrimidinone hydroxyethyl methacrylate (UPyHEMA) (**21**)

- p(ethylene glycol)20 methacrylate (PEG20MA) (**22**)
- ethyl hexyl methacrylate (EHMA) (**23**)

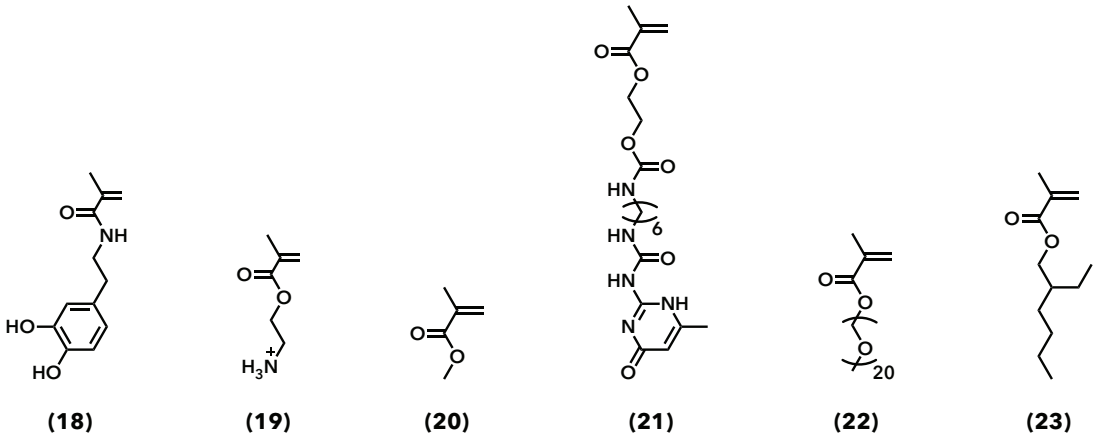

Figure 2.5: Scheme of the motifs DMA (**18**), AEMA (**19**), MMA (**20**), UPyHEMA (**21**), PEG20MA (**22**) and EHMA (**23**).

DMA contains the biomimetic adhesive motive dopa and contributes by providing an adhesive interface, while AEMA improves the adhesion by synergistic effects with DMA. MMA is used as a spacer for DMA and AEMA in order to form a mfp-5 mimetic SMM. UPyHEMA provides cohesive strength and PEG20MA and EHMA are building blocks for an amphiphilic matrix. The methacrylate group of each motif is needed for the synthesis by radical polymerization and constitutes the methacrylate backbone of the SMM as well as of the target polymers.

3,4-Dihydroxyphenylalanine methacrylate (DMA)

The mussel-mimetic motif DMA (**18**) is incorporated as an adhesive motif to provide strong covalent bonds to wet tissue. As depicted in figure 1.3, dopa (auto)oxidizes to dopa-quinone (**2**). In the case of tissue sealants, this reaction is hypothesized to be promoted by physiological liquid. The subsequent cross linking reactions *via* Michael addition or Schiff base formation can then form covalent bonds between the dopa-quinone and tissue pendant amine and cystein residues.[27,37] Even though the precise reaction mechanisms and pathways are still being investigated, it has been shown time and again that dopa binds covalently to nucleophilic substrates and holds great potential for adhesive applications.[27,32,62,63]

Amino ethyl methacrylate (AEMA)

AEMA (**19**) serves as a methacrylic motif mimicking lysine, an amino acid often found in close proximity to dopa within the model protein mfp-5 (see section 1.3). Lysine was shown to mediate surface priming to wet mineral surfaces through synergistic interaction with dopa in model siderophores, promoting

adhesion to the wet surface.[38] To make use of this beneficial synergy, the design of a mfp-5 mimetic SMM containing DMA as well as AEMA was targeted in this thesis.

In detail, under physiological conditions, AEMA is present in its cationic form, which is expected to displace and dissipate hydrated salt ions from the tissue surface. Therefore it allows for dopa to cohesively bind to amino acid residues on the now dry tissue substrate.[64,65] This suggests that lysine can augment the initial adhesion strength of dopa as well as adhesive behavior over time.

Methyl methacrylate (MMA)

MMA (**20**) is used as a spacer in the sequence macromonomer for two reasons. Firstly, in order to mimic the dopa and lysine content in the mfp-5, MMA serves as a filler and substitutes any further amino acids naturally occuring in the mfp-5. Furthermore the implementation of multiple small MMA units between DMA and AEMA motifs is hypothesized to increase the chain flexibility of the SMM. This facilitates the orientation of the adhesive motifs in the SMM toward the hydrophilic phase, therefore aiding the DMA and AEMA motifs in their orientation toward the substrate.

2-Ureido-4-pyrimidinone hydroxyethyl methacrylate (UPyHEMA)

UPyHEMA (**21**) motifs provide cohesive strength by developing strong noncovalent interactions. They dimerize by means of a self-complementary donor-donor-acceptor-acceptor array of four hydrogen bonds (see figure 2.1 in section 2.1) and can therefore build supramolecular polymers.

UPy provides the target polymers with excellent compression molding processability and even healing capabilities to a certain degree (temperatures above physiological conditions are needed), due to the reversibility of supramolecular interactions.[52,66]

Poly(ethylene glycol)20 methacrylate (PEG20MA) and Ethyl hexyl methacrylate (EHMA)

PEG20MA (**22**) and EHMA (**23**) are implemented into the target polymers to create an amphiphilic matrix for the cohesive and adhesive motifs. The PEG20MA-EHMA system exhibits a self-assembling, phase-separated morphology, that forms a hydrophilic PEG20MA phase and a hydrophobic EHMA phase.[67] Contact with water is thought to accelerate the phase separation, thus causing the hydrophilic phase to turn outwards upon swelling of the polymer.

The EHMA phase serves as hydrophobic spacer for the cohesive units of UPyHEMA by shielding the -NH groups from hydration by water. This allows for effective dimerization by H-bonding of the UPyHEMA -NH units and increased crosslink density.[11,50,54]

The hydrophilic phase, consisting of PEG20MA, is hypothesized to contain the adhesive motifs DMA and AEMA within the SMM. As this phase is turned outwards upon swelling, this design allows for the

adhesive motifs to form a strong interface with the tissue substrate.

2.4 State of the Art

To address the qualities needed in a polymeric tissue sealant (discussed at the beginning of chapter 2), Balkenende and coworkers used an orthogonal approach to include cohesive supramolecular motifs into an adhesive polymer. This contribution afforded cohesive interactions within the material and adhesive strength toward wet tissue, which were tunable independent of each other.[11]

Specifically, the referenced system is the random co-polymer p(p(ethylene glycol)20 methacrylate-ethyl hexyl methacrylate-ureido-4-pyrimidinone hydroxyethyl methacrylate-dopa methacrylate), abbreviated (p(PEG20MA-EHMA-UPyHEMA-DMA)) **(24)**. Within this polymer, which is shown in figure 2.6, the H-bonding motif UPy was incorporated for the first time into otherwise methacrylic and p(ethylene glycol) based mussel inspired adhesives.[11,63,68]

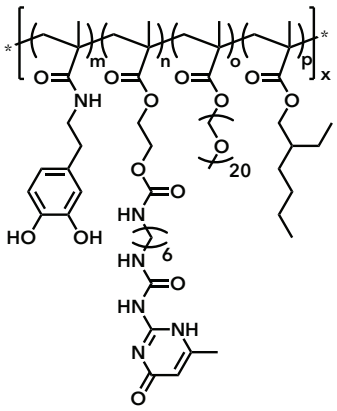

(24)

Figure 2.6: Scheme of the random co-polymer p(PEG20MA-EHMA-UPyHEMA-DMA) synthesized by the Messersmith lab.[11]

The contributions of the orthogonal adhesive and cohesive motifs DMA and UPyHEMA were tested separately and it was confirmed that both monomers were essential for achieving high tissue adhesion strength. Additionally, the necessity of hydrophilic and hydrophobic motifs was proven by experiments with either one of the phases lacking. The amphiphilic matrix was hypothesized to form a phase separated morphology upon contact with physiological liquid. This assumption was confirmed by atomic force microscopy (AFM) images and differential scanning calorimetry (DSC) measurements. Phase separation resulted in high adhesion strength, hypothesized to be achieved by two effects. Firstly, by shielding UPyHEMA from water, the dynamic equilibrium was shifted to the bound state, thus inducing high cohesive interactions. Secondly, by allowing DMA to get in close contact with the tissue surface, interfacial bonds were formed.[11]

Multiple combinations of hydrophilic and hydrophobic monomers of different length were tested to find the ideal combination and ratios leading to optimal cohesive interactions and superior tissue adhesion. The resulting polymer contained 11.3 %mol DMA, 10.5 %mol UPyHEMA, 23.3 %mol PEG20MA and 54.9 %mol EHMA. The polymer p(PEG20MA-EHMA-UPyHEMA-DMA) was shown to exhibit adhesive and cohesive strength superior to commercially available tissue adhesives. However, the adhesive strength of the polymer decreased rapidly with time. Severe swelling with an equilibrium of 266 ± 4 %w was hypothesized to induce strain to the polymer-substrate interface, resulting in the material's detachment from the tissue surface.

Tests investigating the failure mechanism revealed adhesive failure, indicating that the polymer's cohesive contribution exceeded the adhesive interfacial strength.

Further optimization of the material should therefore focus on the development of more reactive adhesive motifs.[11]

Part III

Aims and Motivation

The overall motivation of this project was to prepare a strongly adherent, biocompatible polymeric material as a **tissue adhesive for fetal surgery**, with potential to use as a general wet tissue adhesive.

The project was aimed at initially synthesizing a **mfp-5 mimetic sequence macromonomer** with controlled molecular composition by use of RAFT polymerization. In an orthogonal approach, this SMM was to be **incorporated in a supramolecular, amphiphilic matrix** *via* two different synthetic pathways. Tissue adhesion experiments would then allow conclusions about the distribution of monomer and the potential of the mfp-5 mimetic SMM in tissue adhesives.

In detail, the dopa and lysine mimetic monomers DMA and EHMA in their protected states (acetonide-protected DMA (AcDMA) and boc-protected AEMA (bocAEMA)) were chosen for the polymerization with MMA to yield the SMM **(25)** (see figure 2.7), as synergistic effects promoting wet adhesion were reported for them.[38] The obtained sequence macromonomer p(AcDMA-bocAEMA-MMA) was analyzed *via* ^{1}H nuclear magnetic resonance (^{1}H NMR), gel permeation chromatography (GPC) and differential scanning calorimetry (DSC). Moreover, solubility tests were conducted on the SMM in its deprotected state **(26)**.

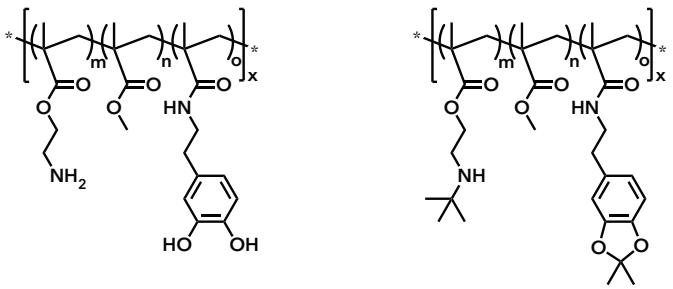

(25) **(26)**

Figure 2.7: Scheme of the mfp-5 mimetic SMM in its protected (p(AcDMA-bocAEMA-MMA)) **(25)** and deprotected state (p(DMA-AEMA-MMA)) **(26)**.

To implement the SMM **(25)** into an amphiphilic polymer containing PEG20MA, EHMA and the cohesive motif UPyHEMA, two different approaches were tested and compared. The SMM in its deprotected state was expected to augment the adhesive properties of both target polymers in comparison to the state-of-the-art-material p-(DMA-UPyHEMA-PEG20MA-EHMA).

For the first approach, the endgroup of the SMM was functionalized to yield a polymerizable methacrylate endgroup. The modified SMM was polymerized in a free radical polymerization into a random co-polymer to render p(p(DMA-AEMA-MMA)-UPyHEMA-PEG20-EHMA) **(27)** after a deprotection step. The second approach comprised a RAFT polymerization of the SMM to yield the block-co-polymer p(DMA-AEMA-MMA)-b-(UPyHEMA-PEG20-EHMA) **(28)** after deprotection. Intermediate stages and the polymerization processes itself were monitored by ^{1}H NMR measurements. Both polymers were processed into swellable films.

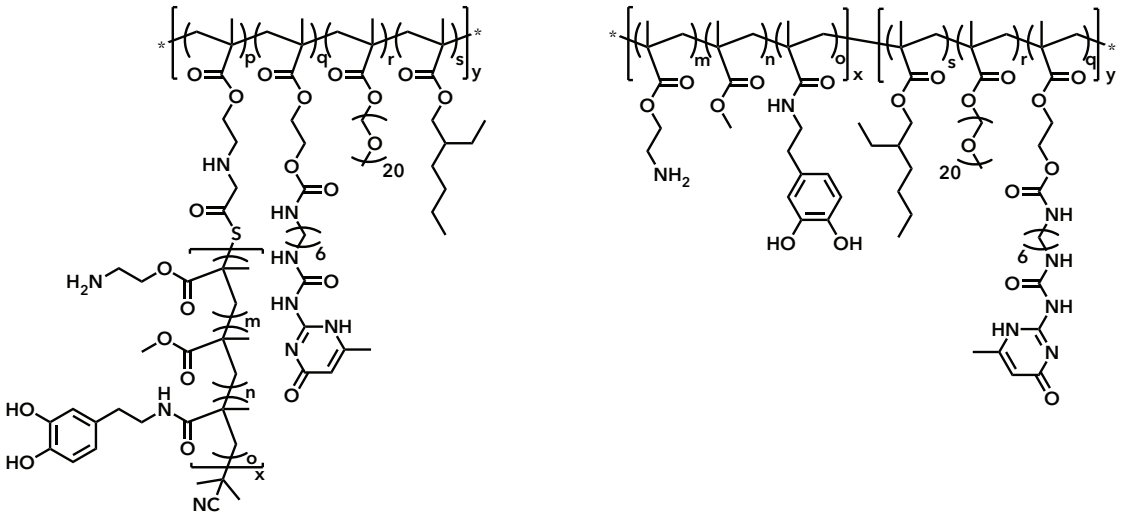

Figure 2.8: Scheme of the target polymers: p(p(DMA-AEMA-MMA)-UPyHEMA-PEG20-EHMA) **(27)** and p(DMA-AEMA-MMA)-b-(UPyHEMA-PEG20-EHMA) **(28)**.

To analyze the composition and film properties of the final polymers **27** and **28** (see figure 2.8), following techniques were applied: ^{1}H NMR, GPC and swelling experiments. Moreover, tensile testing on swollen samples as well as wet tissue shear adhesion were performed in order to gain understanding of the mechanical and adhesive properties. A cell viability study was conducted by courtesy of a Messersmith lab research fellow on the most promising polymer to provide first indications about biocompatibility.

By comparing the two approaches, it was thought possible to gain insights on the dopa and lysine synergy as well as the adhesion-cohesion interplay in methacrylic wet tissue adhesives. Furthermore, a comparison allowed for the identification of the polymeric material, which is better suited as a sealant for fetal surgery and therefore has the potential to drastically increase the survival rate of babies post-surgery.

Part IV

Results and Discussion

The ideal composition of a mussel mimetic wet tissue adhesive containing only dopa as an adhesive motif was studied in detail by Balkenende *et al.* and rendered the state-of-the-art-polymer (see figure 2.6 on page 16). Experiments had been carried out to determine the ideal components and molar composition of the amphiphilic monomer pair, and the combination of PEG20MA and EHMA was found to yield the best possible phase separation. Therefore, it provided the best matrix for individually tuning the cohesive and adhesive strength, as UPyHEMA would be located in the hydrophobic phase and dopa in the hydrophilic phase.[11]

This project deals with the synthesis and characterization of a refined polymeric adhesive based on the state-of-the-art-polymer developed by Balkenende and coworkers.[11] Initially, the synthesis of the bespoke monomers acetonide protected DMA (AcDMA) and tert-butyloxycarbonyl protected AEMA (bocAEMA) will be discussed, followed by a section about the polymerization and properties of the mfp-5 mimetic SMM containing the adhesive motifs. Ensuing, the implementation of the SMM into an amphiphilic matrix containing cohesive motifs *via* two different pathways will be covered. Both approaches are based on methacrylate chemistry. The implementation was achieved either by functionalizing the SMM's end group (see section 4.2) and using a free radical polymerization to obtain a random co-polymer (see chapter 5) or by using a second RAFT polymerization step to yield a block-co-polymer (see chapter 6). The compositional as well as mechanical analysis of both polymers will be looked at and compared. Especially the influence of the mfp-5 mimetic sequence on tissue adhesion properties and the failure mechanism will be elucidated.

3 Monomer Synthesis

The monomers AcDMA, bocAEMA and UPyHEMA were custom synthesized for their use in the polymerization of mussel-inspired adhesives. AcDMA and bocAEMA were prepared within the scope of this thesis, while UPyHEMA was provided by the courtesy of the research group.

3.1 Synthesis of AcDMA

As depicted in figure 3.1, the synthesis of AcDMA is a two step process that starts with the synthesis of DMA. In the first step, dopamine hydrochloride **(29)** engages in a condensation reaction with methacrylic anhydride **(30)** under basic conditions. This reaction yields the amide DMA **(18)**, which is easily extracted into an ethyl acetate (EA) phase after acidifying the reaction mixture to pH 2. From EA, DMA is precipitated into hexanes (Hex), filtered and vacuum dried. Literature suggests a precipitation duration of min. 12 h at 4 °C and recrystallization from tetrahydrofuran (THF) or Hex.[69,70] While the prolonged precipitation duration could increased the yield of product, it would render an additional recrystallization step necessary. In order to obtain a clean product, the duration of precipitation was kept at approx. 30 min. A light gray powder with a yield of 53 % and negligible EA residues (confirmed by ^{1}H NMR) was obtained.

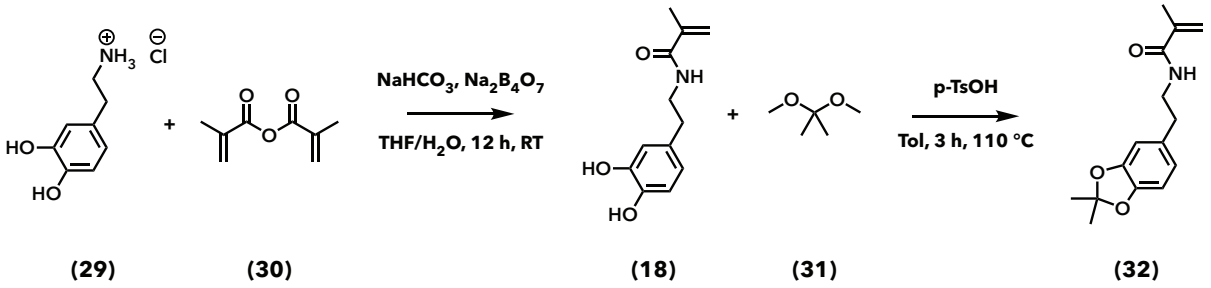

Figure 3.1: Preparation of Acetonide protected DMA: The first step shows the formation of DMA **(9)**, followed by a protection step toward acetonide-protected DMA (**(31)**.

As DMA is readily oxidized to dopamine quinone, the catechol is protected in a second reaction step.[71] The protecting group acetonide is introduced by refluxing the diol with 2,2-dimethoxypropane **(31)** in the presence of the catalyst p-toluensulfonic acid (p-TsOH) to give AcDMA **(32)**, a white powder. To remove volatile byproducts such as water and methanol (MeOH), 4 Å molecular sieves were employed. This enabled shifting the reaction equilibrium toward the product.[69,71]

3.2 Protection of AEMA

Protection of the amino group of 2-aminoethyl methacrylate was necessary, as RAFT technology is generally incompatible with unprotected primary or secondary amine functionalities.[61] The protecting group tert-butyloxycarbonyl (boc) was chosen to protect the amino group because it affords simultaneous cleavage of itself and the acetonide protecting group chosen for DMA. By employing one singular deprotection step with strong acid, both adhesive motifs can be deprotected.[72]

The synthetic procedure, derived from literature, comprised a reaction of 2-aminoethyl methacrylate hydrochloride (AEMA HCl) **(33)** with di-*tert*-butyl dicarbonate **(34)** in presence of the basic cat-

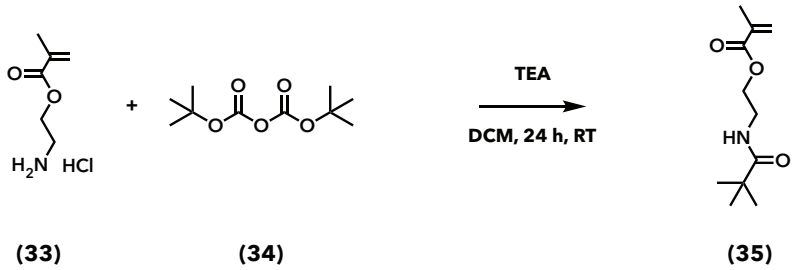

(33) **(34)** **(35)**

Figure 3.2: Protection of 2-aminoethyl methacrylate by introduction of a boc protecting group toward the boc-protected AEMA **(35)**.

alyst triethylamine (TEA).[73,74] After removing the solvent, the precipitate was cleaned of byproducts, unreacted educts and solvents by washing with water, freeze drying and recrystallization from Hex/dichlormethane (DCM). 2-(*tert*-butoxycarbonylamino)ethyl methacrylate (bocAEMA) **(35)** was obtained with a yield of 50 %.

4 Mfp-5 Mimetic Sequence Macromonomer

The adhesive motifs dopa and lysine were incorporated into a mfp-5 mimetic SMM in order to locate them in close proximity of each other, once the SMM was incorporated into the target polymers. This was hypothesized to replicate synergies between dopa and lysine and enhance the material's adhesion strength.

The SMM was designed to resemble the mfp-5 in its number of monomer units, its M_W and in its molar content of catechol and lysine moieties. Molecular weight control was established by RAFT polymerization, wherein the target M_W, comprising exactly 50 monomer units u, was calculated for a conversion of 80 % in order to prevent termination reactions toward the end of the polymerization to cause a sudden rise in M_W. The %mol of AcDMA and bocAEMA were chosen to resemble the molar content in mfp-5, 30 %mol of dopa and 20 %mol of lysine. A content of 25 %mol for each AcDMA and bocAEMA in the SMM was chosen, resulting in a theoretical amount of 12.5 monomer units u of each per SMM at 80 % conversion.

The theoretical molecular weight $M_{W,theor}$ at 80 % conversion was calculated using equation 4.1 (with $M_{W,CTA}$ being the M_W of the CTA and $M_{W,monomer}$ being the M_W of the respective monomers), while the amount of starting compounds was calculated according to a conversion rate of 100 % and a total of $u = 62.5$ monomer units.

$$M_{W,theor} = M_{W,CTA} + \sum u M_{W,monomer} \tag{4.1}$$

The resulting $M_{W,theor}$ of 8856,g/mol was found to be perfectly within range of the M_W reported

for mfp-5 (8.9 kDa).[75] Experimental measurements of the M_W were performed *via* ^{1}H NMR and GPC analysis of the polymerized SMM (see sections 4.3.1 and 4.3.3).

For the calculation of the amount of AcDMA, it was taken into account that literature reported dopa to cause retardation in (radical) polymerizations. This observation was attributed to the generation of a less reactive DMA-monomer-radical, respectively DMA-polymer-radical.[76–78] In order to ensure that this retarding effect would not decrease the target content of 25 %mol in the SMM, the amount of AcDMA used in the RAFT polymerization was increased. Prior experiments carried out by Balkenende *et al.* had shown that a factor of two, doubling the amount of AcDMA, was expedient. The resulting employed monomer mixture was constituted of 40 % MMA, 40 % AcDMA and 20 % bocAEMA.

4.1 Polymerization of p(AcDMA-bocAEMA-MMA)

The general synthetic pathway is depicted in figure 4.1 and comprises a RAFT polymerization of the three monomers AcDMA, bocAEMA and MMA using the RAFT chain transfer agent 2-cyano-2-propyl benzodithioate (CPBD). In reference to methacrylate polymerizations, the reaction was initiated by use of AIBN and carried out in dimethylformamide (DMF) at 70 °C under nitrogen atmosphere.[61]

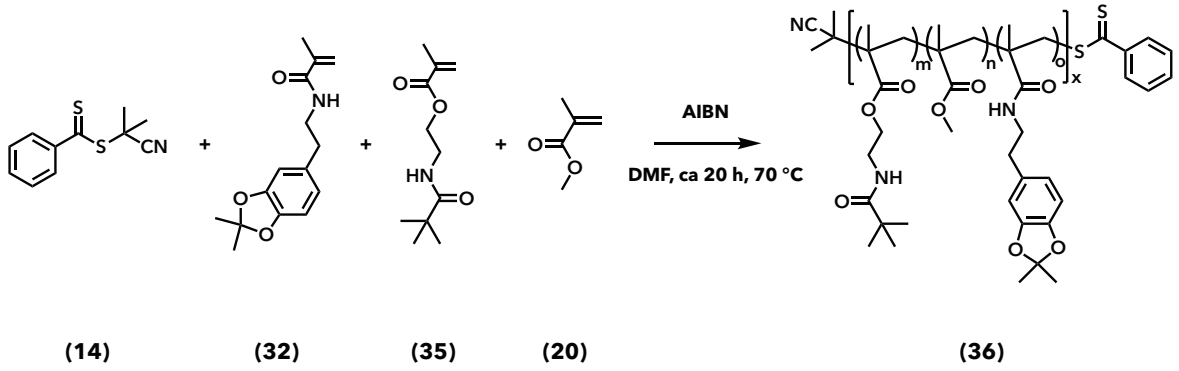

Figure 4.1: Preparation of the mfp-5 mimetic SMM p(AcDMA-bocAEMA-MMA) by RAFT polymerization.

Several samples were drawn over the course of the reaction and measured by ^{1}H NMR to determine the time point of 80 % conversion. The decrease of the effective methacrylate peaks (Int^t_{MA}) in respect to the aromatic dopamine peaks at 6.65 and 6.59 ppm ($Int_{Ar} = 3$) was used to determine the conversion. The six methacrylate peaks of AcDMA, bocAEMA and MMA were located between 6.1 - 5.3 ppm. As the secondary amine of AEMA caused a broad peak overlapping with the methacrylate peaks, its theoretical integral ($Int_{NH} = 1$) was removed from the sum of methacrylate integrals. Furthermore, the integral was reduced by the theoretical share of the excess AcDMA used (20 %mol) to give the integral attributed solely to the MA peaks of the reacting monomers. The conversion was calculated using equations 4.2 and 4.3.

$$Int^t_{MA} = ((\sum Int^t_{MAs}) - Int_{NH}) - 0.2((\sum Int^0_{MAs}) - Int_{NH}) \tag{4.2}$$

$$C_t = 1 - (\frac{Int^t_{MA}}{Int^0_{MA}}) \tag{4.3}$$

Int^t_{MA}...*Effective integral of the methacrylate peaks at time t*

Int^t_{MAs}...*Measured integral of all methacrylate and amine peaks between 6.1 - 5.3 ppm at time t*

Int_{NH}...*Theoretical integral of the secondary amine of AEMA (=1)*

C_t...*Conversion at time t*

A first reaction was carried out with a monomer concentration of 0.95 mol/L to determine the overall reaction kinetics and the reaction time for 80 % conversion.

Figure 4.2 depicts the reaction kinetics for the 0.95 molar reaction. By way of example, ^{1}H NMR spectra of the same reaction at t = 0 h (black) and t = 22 h (pink) are depicted in figure 4.3 to show the difference of the methacrylate integrals in the spectra. The ^{1}H NMR spectra corresponding to measurements at all time points are depicted in figure B.1 in the appendix B.1.

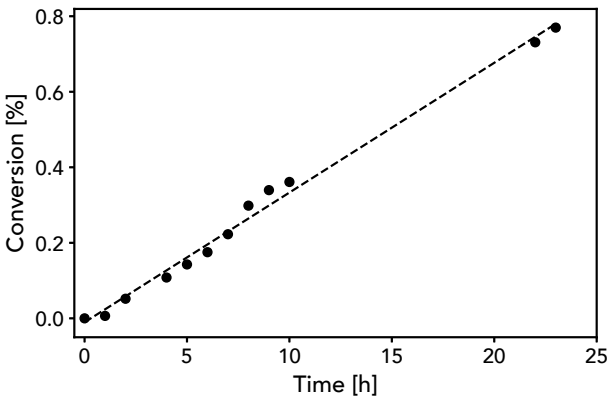

Figure 4.2: Monomer conversion plot of the polymerization of p(AcDMA-bocAEMA-MMA) at a molar concentration of 0.95 mol/L.

Due to the resulting reaction duration of 23 h, the monomer concentration for further SMM polymerizations was raised to 2.00 mol/L in order to reduce the required polymerization time.[79] As further SMM polymerizations were conducted overnight, this resulted in fewer samples being taken for the determination of the reaction's kinetics. Furthermore, increasing the molar concentration resulted in additional time savings due to a facilitated precipitation process.

Looking at the data points obtained from a set of three identical SMM polymerizations (identical reaction volume and molar monomer concentration of 2.00 mol/L) shown in figure 4.4, the reaction starts

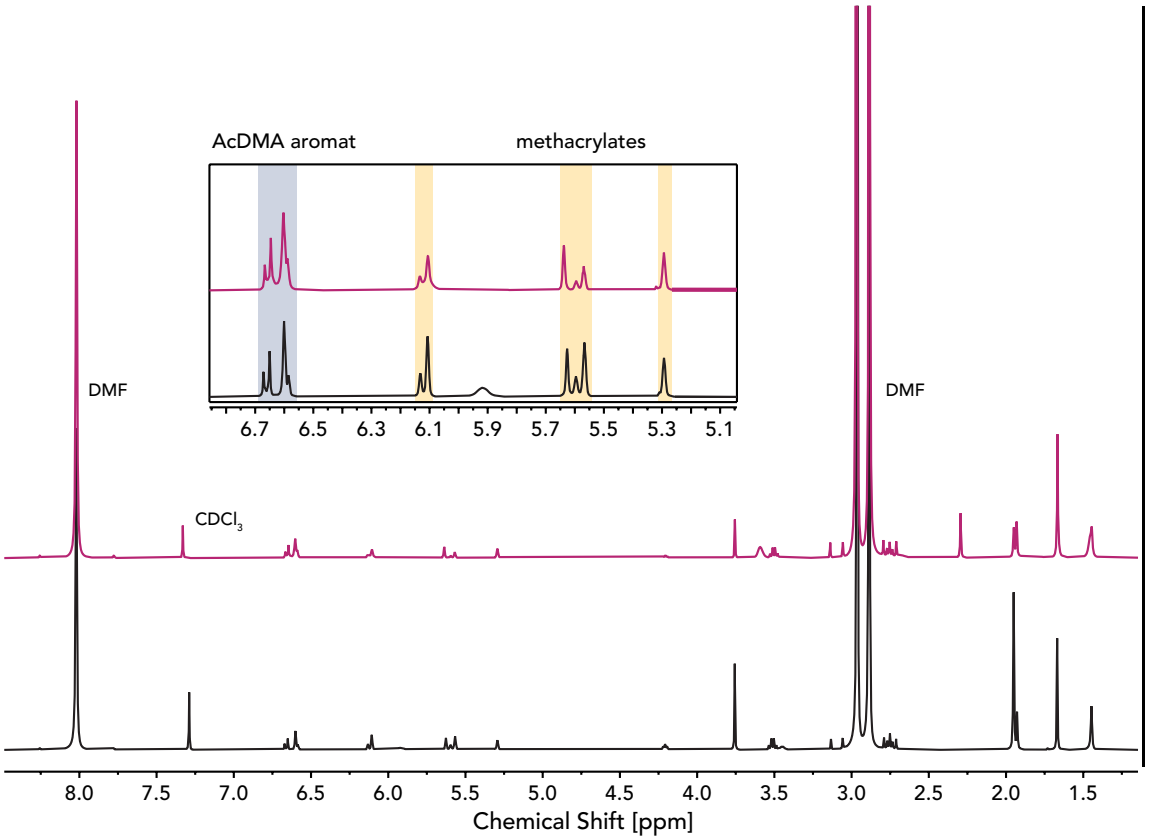

Figure 4.3: ^{1}H NMR spectra in $CDCl_3$ of the polymerization of p(AcDMA-bocAEMA-MMA) at t = 0 h (black) and t = 22 h (pink).

out with a virtually linear correlation between monomer conversion and time for each batch, before leveling off toward higher conversion. This suggests a termination of chain propagation, which imposes a limit on the monomer conversion. This could be explained by a decrease in monomer concentration and a raise in viscosity at higher conversions, both of which limit the chain mobility and render termination reactions, such as combination or disproportionation reactions, more likely.[80]

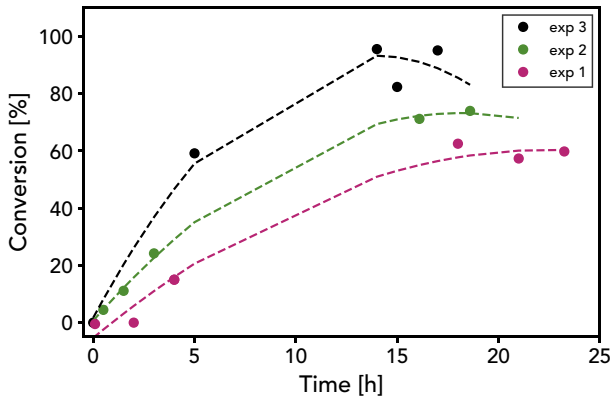

Figure 4.4: Monomer conversion plot of three identical polymerizations of p(AcDMA-bocAEMA-MMA) at a molar concentration of 2.00 mol/L.

Plotting $\ln(Int^{t}_{MA} / Int^{0}_{MA})$ versus time gives a linear correlation for monomer conversion below 60 %,

confirming the first-order kinetic behavior of a RAFT-polymerization.[81]

The duration of polymerization was not significantly shortened by the increase of monomer concentration, and varied strongly from batch to batch (17 - 23 h), as did the limiting maximum conversion. Therefore, ^{1}H NMR measurements of samples drawn at the beginning and toward the end of the reaction were performed for each batch to determine the limiting maximum conversion or the point of 80 % conversion respectively. As the ^{1}H NMR of the precipitated SMM showed similar monomer ratios for polymerizations at both molar concentrations (see section 33), all SMM polymerizations used for the incorporation into the supramolecular matrix polymer were conducted at 2.00 mol/L monomer concentration due to the facilitated workup.

After ^{1}H NMR evaluations indicated that the polymerization had reached the desired conversion, the reaction solution was quenched, one drop of solution was precipitated into ice/salt bath cooled diethylether (Et_2O), redissolved in DCM and precipitated two more times to yield a pink solid for characterization. The SMM in solution was used for further modifications and reactions without precipitation.

4.2 End Group Functionalization of the SMM p(AcDMA-bocAEMA-MMA)

In order to incorporate the SMM as a macromonomer unit into a random co-polymer, the benzodithioate end group imposed by the CTA was reacted to a carbamothioate methyl methacrylate (carbamothioate MMA) end group in a two step process. Model reactions with poly(methyl methacrylate) (p(MMA)) were conducted prior to functionalizing the SMM in order to determine ideal reaction conditions for the second reaction step. The following sections will evaluate two different sets of reaction conditions with the aid of the model system and discuss the application of the end group functionalization on the SMM.

4.2.1 Model Reactions

Using a p(MMA) system as a model system, a qualitative study of the end group functionalization from benzodithioate to carbamothioate MMA was conducted. The model compound p(MMA) was prepared by RAFT polymerization and the benzodithioate end group was cleaved by aminolysis to leave a thiol end group, as shown in figure 4.5. Subsequently a thiol-isocyanate click reaction with 2-isocyanatoethyl methylacrylate was conducted using two different sets of reaction conditions referred to in literature.[82,83] Figure 4.6 depicts the end group modification, with **A** and **B** each referring to one set of reaction conditions.

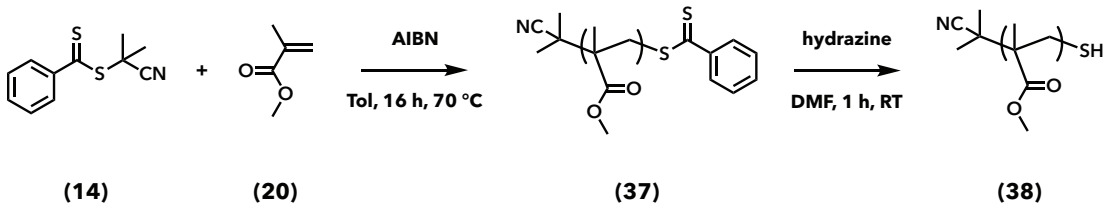

Figure 4.5: Preparation of p(MMA) by RAFT polymerization, followed by aminolysis to convert the benzodithioate end group to a thiol end group.

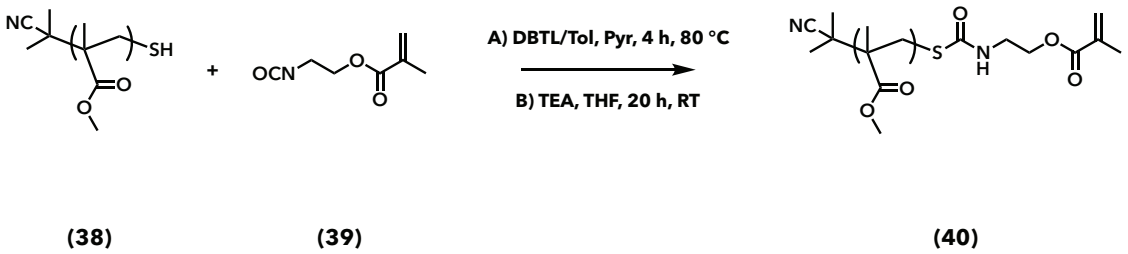

Figure 4.6: Click reaction of the thiol end group of p(MMA) toward a carbamothioate MMA group. **A** and **B** show the two different sets of reaction conditions tested.

Polymerization of p(MMA)

The RAFT polymerization of the model system p(MMA) was carried out under conditions similar to the SMM polymerization. CPBD was used as CTA, AIBN was used as initiator and the reaction was carried out in toluene (Tol) with a monomer concentration of 0.95 mol/L. The ratio of monomer to CTA and AIBN was initially chosen to correspond to the theoretical M_W of the SMM (8856 g/mol) at 80 % conversion. As this would equal an amount of 86 units per polymer chain, the reaction was quenched early after 16 h to obtain a p(MMA) similar to the SMM in unit size as well as in M_W. The reaction conversion was then determined to be 43 % by ^{1}H NMR measurement of the quenched reaction solution and weighting of the MMA integral at 3.75 ppm and the pMMA integral at 3.60 ppm.[84,85] The solution was reduced and precipitated into MeOH, before drying on high vacuum.

^{1}H NMR of the dried p(MMA) was used to determine the molecular weight by normalizing the spectrum to the aromatic benzodithioate peaks at 7.89 - 7.37 ppm. The integral of the -CH_3 peak of p(MMA) at 3.60 ppm was then used to determine the number of methyl methacrylates per CTA (approx. 63 units) and therefore the M_W of 6513 g/mol.

The conversion and molecular weight determined by ^{1}H NMR were found to be contradictory in regard to the amount of CTA and monomer used, as a conversion of 43 % would imply a M_W of 4849 g/mol and a chain length of 46 units. This might be caused by a flawed integration of the benzodithioate aromat peaks due to the weak signal in relation to the p(MMA) peak. However, with the weight as well as the unit number being in reasonable range of the SMM, the p(MMA) was considered to be an acceptable model polymer. Furthermore, the size of the polymer was expected to have a negligible impact on the end group modifications.

Synthesis of p(MMA)-thiol

In a second step, the benzodithioate end group was cleaved by aminolysis. Various methods using mainly primary amines have been reported to quantitatively convert the CTA end group to a thiol, though long reaction times, disulfide formation or complex reaction conditions were pointed out as a drawback to most procedures.[61] Referring to a method reported by Shen *et al.*, hydrazine was chosen as a nucleophile. It has been shown to accelerate aminolysis under simplified conditions, while suppressing the formation of disulfides.[86] The p(MMA) model polymer was dissolved in DMF to give a pink-colored solution, hydrazine was added and the solution was stirred for 1 h at RT. The resulting product was precipitated into MeOH and dried on high vacuum.

Conversion was determined by the distinct color change of the solution from pink to yellow within the first minute of the reaction, which was caused by the cleavage of the benzodithioate end group. Furthermore ^{1}H NMR measurements of p(MMA)-thiol showed no signs of the aromatic benzodithioate peaks at 7.89 - 7.37 ppm (see figure B.2 in appendix B.1), indicating full conversion to thiol end groups.

Synthesis of p(MMA)-carbamothioate MMA

For the synthesis of a carbamothioate MMA end group from a thiol end group, so called thiol-click-chemistry with the reactant 2-isocyanatoethyl methylacrylate was employed.[82,87] This reaction can either be catalyzed by a base such as TEA or a Lewis acid such as an organometallic tin compound. The nucleophilic base activates the thiol by formation of an anion that can then attack the isocyanate, while the electrophilic organometallic catalyst is proposed to coordinate to the isocyanate's oxygen or nitrogen atom, which can then be attacked by the thiol.[88,89]

The first method tested **(A)**, adapted from Lü and coworkers, employs the organometallic catalyst dibutyltin dilaurate (DBTL) in Tol in presence of 10 % pyridine (Py) under nitrogen atmosphere.[83] The reaction was conducted at 80 °C for 4 h. Due to the catalytic effect of the nucleophilic base Py, the reaction time was decreased in comparison to the literature procedure (9 h). The product was precipitated into Hex and the resulting white powder was dried on high vacuum.

In a second method **(B)**, the reaction was performed under mild reaction conditions (RT, 20 h) with TEA as a catalyst. Adapted from Li *et al.*, this reaction has been reported to proceed rapidly without any apparent side reactions or negative effects on the narrow M_W distribution.[82] The reaction was conducted under nitrogen atmosphere over night. Due to the long reaction duration and little amount of solvent deployed, most of the solvent THF had evaporated at the end of the reaction. Therefore, the solution was re-diluted before precipitating into Hex, in order to avoid complications due to high viscosity differences. The white powder obtained was dried on high vacuum.

For both methods, any 2-isocyanatoethyl methylacrylate residues were assumed to be removed dur-

ing the precipitation step due to the compound's solubility in Hex. The products of both method **(A)** and **(B)** were characterized *via* ^{1}H NMR in $CDCl_3$ by normalizing the integral of the methacrylate peak at 3.60 ppm to 188 H, according to the initial p(MMA). Both spectra are depicted in figure 4.7. The peaks corresponding to the targeted methacrylate end group are present in both spectra.

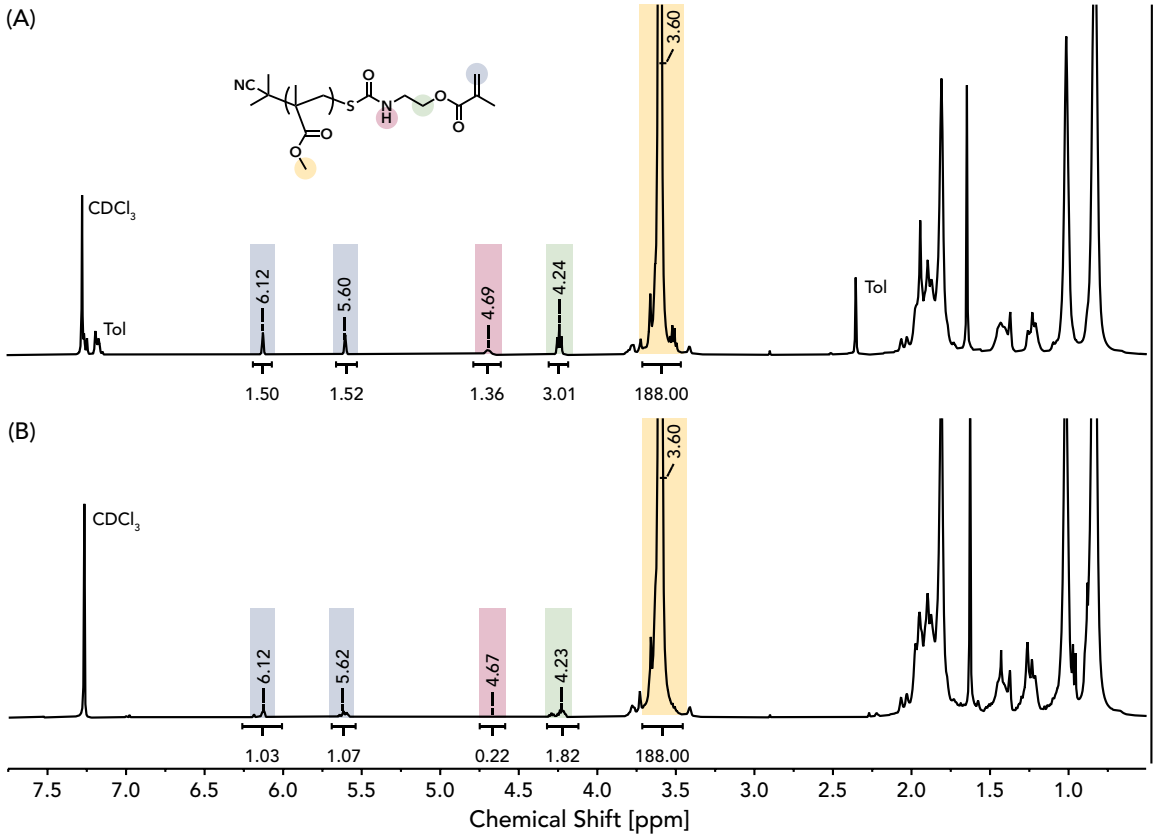

Figure 4.7: ^{1}H NMR of p(MMA)-carbamothioate MMA in $CDCl_3$. **A)** Product synthesized with DBTL as catalyst. **B)** Product synthesized with TEA as catalyst.

For method **(A)**, the singulets correlating to the $=CH_2$ protons of the end group are located at 6.12 and 5.60 ppm, and the triplets correlating to $-CH_2-CH_2-$ protons at 4.24 and 3.52 ppm. The second $-CH_2-$ peak at 3.52 ppm overlaps with the $-CH_3$ signal of p(MMA) at 3.60 ppm and could therefore not be integrated properly. The spectrum shows residues of the solvents Tol and Py, which could be easily removed by repeated precipitation and drying. The integrals of the methacrylate peaks ($-CH_2$: 1.50 and 1.52; $-CH_2-$: 3.01) and the -NH peak (1.36) show a theoretically correct ratio correlation. In regard to the p(MMA) $-CH_3$ integral of 188.00 however, the calculated ratio of 1.5 end groups per p(MMA) polymer chain suggests either shortening of the polymer chain by one third or a flawed integration of the aromatic peaks of the benzodithioate end group in section 4.2.1, which was conceived more likely. In order to counter check our assumption, the p(MMA) integral was calculated according to the conversion of the polymerization. This resulted in a reasonable ratio of end groups to polymer chains of 1.11:1.00. This calculation furthermore supported the presumption that the integration of the aromatic peaks of

the benzodithioate end group is to be considered imprecise due to high differences in concentration and therefore signal intensities.

For method **(B)**, peaks correlating to the methacrylate end group are found at 6.12, 5.62, 4.23 and 3.51 ppm, however they appear quite broad and of incorrect multiplicity. As observed in spectrum **(A)**, the second -CH_2- peak in spectrum **(B)** at 5.51 ppm overlaps with the -CH_3 signal of the p(MMA) at 3.60 ppm and proper integration was therefore not possible. As THF as well as TEA peaks would overlap with the polymer's signals, it was not possible to conclude the polymer's purity. The integral of the =CH_2 protons (1.03 and 1.07) and the integral of the -CH_2-CH_2- protons (1.82) show the expected ratio of 100 % conversion to carbamothioate MMA end groups. However, this conversion is based on the M_W calculations of the p(MMA) according to the benzodithioate end group, which is presumably faulty. This fact, as well as the odd shape of the peaks, the non-traceable contamination by solvents and existence of other impurities and the inconclusive integral of the -NH peak (0.22) are an indication for the appearance of byproducts or incomplete conversion of the end group.

Overall, method **(A)** proved to be a faster and easier controllable method and was therefore chosen to be employed for the end group functionalization of the SMM.

4.2.2 End Group Functionalization of the SMM

The end group functionalization of the SMM was conducted in a two-step process adapted from literature and tested on p(MMA). Figure 4.8 depicts the aminolysis to a thiol end group followed by a so called click-reaction to a carbamothioate methyl methacrylate.[82]

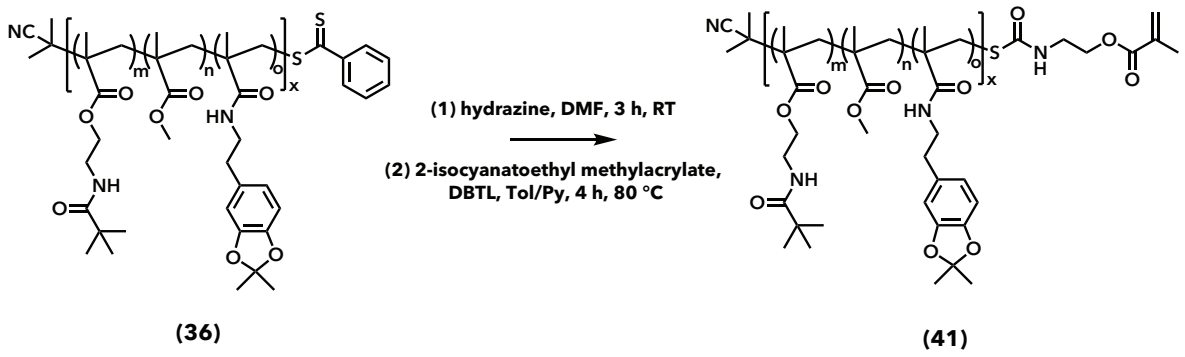

Figure 4.8: Synthetic pathway toward the carbamothioate methyl methacrylate end group functionalized SMM.

For the aminolysis, the solution of polymer in DMF obtained from the p(AcDMA-bocAEMA-MMA) synthesis (see section 4.1) was reacted with hydrazine. No precipitation steps were performed prior to the aminolysis in order to maximize yields. As shown in section 4.3.1, ^{1}H NMR measurements of a droplet of precipitated p(AcDMA-bocAEMA-MMA) were used to determine the molecular weight of the polymer (8471 g/mol). These initial calculations were used to calculate the amount of a 5 mol eq. of

hydrazine for the aminolysis. As will be detailed in section 4.3.1, the interpretation of the spectrum, particularly of the indicatory aromatic benzodithioate peaks, was afflicted with severe difficulties. Therefore, the initially calculated and employed mol eq. of 5 was found to rather equal a value of 8.3 mol eq. according to the re-evaluation of the spectrum, which rendered a M_W of 14341 g/mol for the SMM. As the disappearance of the aromatic benzodithioate peaks at 7.84 - 7.36 ppm in the ^{1}H NMR spectrum of the polymer carrying the thiol end group was deemed unreliable, full conversion of the benzodithioate group to the thiol was confirmed by a distinct change in color (see figure 4.9). The SMM-thiol was precipitated into Et_2O and the resulting white powder was dried on high vacuum.

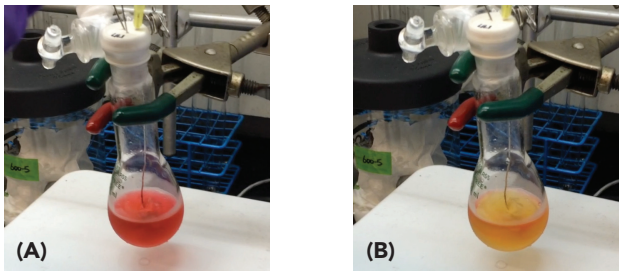

Figure 4.9: Color change during the aminolysis of p(AcDMA-bocAEMA-MMA)-benzodithioate. **(A)** Pink color caused by the benzodithioate end group before addition of hydrazine. **(B)** Light yellow color of p(AcDMA-bocAEMA-MMA)-thiol after reacting with hydrazine for 2 min.

As the reactions conducted with the model system p(MMA)-thiol had shown the method adapted from Lü *et al.* to be successfully working and easily applicable, this method was employed for the end group functionalization of the SMM-thiol as well.[83] Again, the initial M_W inferred from the ^{1}H NMR spectrum of the particular SMM p(AcDMA-bocAEMA -MMA)-benzodithioate batch was used to calculate the entry amount of 2-isocyanatoethyl methylacrylate (1.2 mol eq) and the solvent amount (0.015 M). After careful re-evaluation of the ^{1}H NMR spectrum, the employed amounts were shown to correspond to 2.3 mol eq. of 2-isocyanatoethyl methylacrylate and a concentration of 0.007 mol/L (see detailed NMR evaluation in section 4.3.1 and GPC measurements in section 4.3.3). The procedure comprised redissolving the SMM-thiol in Tol/Py and reacting it with 2-isocyanatoethyl methylacrylate in the presence of the catalyst DBTL for 4 h at 80 °C. The resulting white powder was obtained after repeated precipitation in Et_2O, dried on high vacuum and characterized *via* ^{1}H NMR.

The superimposed spectra of SMM-thiol and SMM-carbamothioate MMA are depicted in figure 4.10. The spectrum of the resulting p(AcDMA-bocAEMA-MMA)-carbamothioate MMA in DMSO-d6 shows distinct methacrylate peaks at 6.05 and 5.67 ppm, which indicate the successful end group functionalization of the SMM. However, the integrals of the methacrylate peaks show values twice as big as expected. As the ratio of the SMM peaks is reproduced accurately in the ^{1}H NMR spectra of all end group modifications, two explanations for the high methacrylate integrals are deemed possible. On one hand, it could be caused by an inaccurate determination of the M_W, which has already been shown to pose a difficulty by the synthesis of the sample compound p(MMA). On the other hand, the acciden-

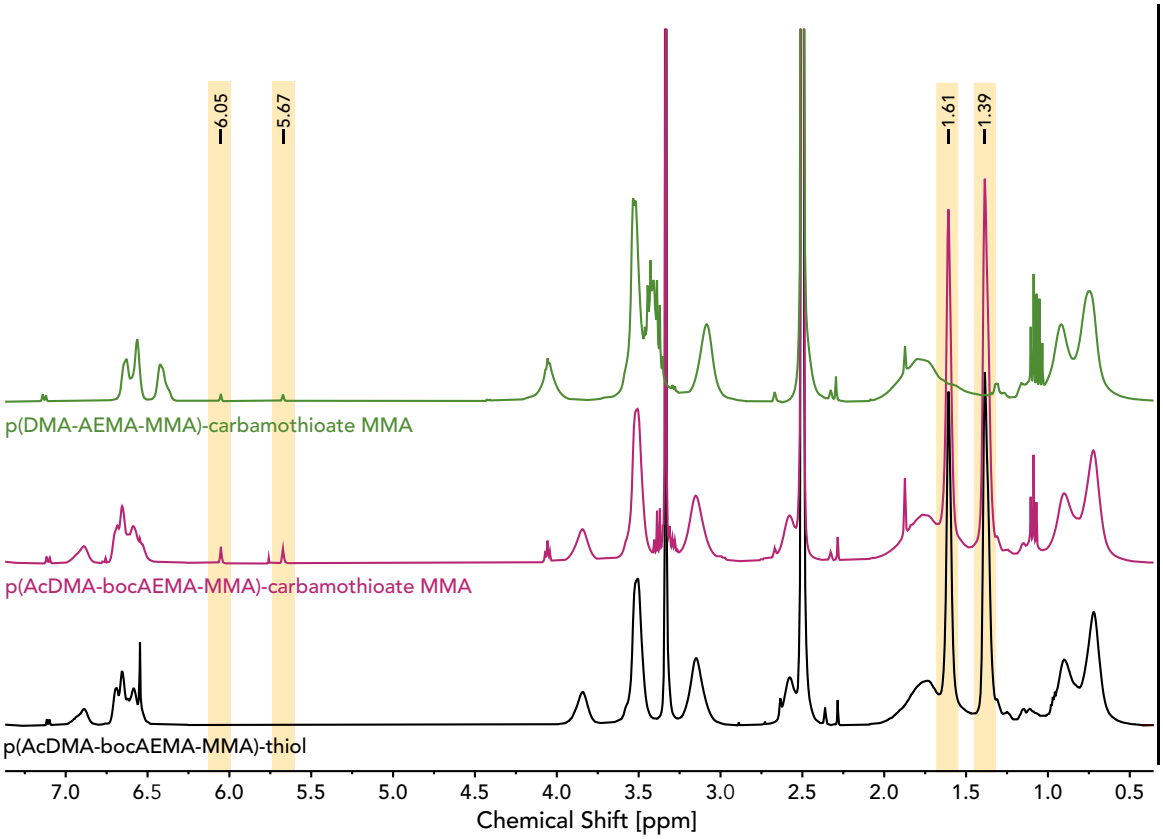

Figure 4.10: ^{1}H NMR spectra in DMSO-d6 of the SMM in different stages of the end group modification: p(AcDMA-bocAEMA-MMA)-thiol in black, p(AcDMA-bocAEMA-MMA)-carbamothioate MMA in pink and p(DMA-AEMA-MMA)-carbamothioate MMA in green. Control peaks for a successful reaction are highlighted in yellow.

tally employed excess amount of 2-isocyanatoethyl methylacrylate (2.3 mol eq.) could have not been removed properly and thus cause a superposition of the relevant peaks in the ^{1}H NMR spectrum. As GPC data (see section 4.3.3) confirmed the calculated M_W and the ^{1}H NMR spectrum of the SMM in its deprotected state rendered matching integral values for the methacrylate peaks of 0.88 (6.05 ppm) and 1.01 (5.68 ppm), it is considered most likely that the excess of 2-isocyanatoethyl methylacrylate was not removed entirely from the SMM-carbamothioate MMA.

Reproducibility of End Group Functionalization

The end group functionalization of the SMM was repeated with two more batches of p(AcDMA-bocAEMA-MMA) with molecular weights of 11956 and 14333 g/mol (determined by ^{1}H NMR) to test its reproducibility. In both cases, the removal of the benzodithioate end group after aminolysis was clearly shown by ^{1}H NMR measurements (see appendix B.1 figure B.3, pink line). The click reaction to carbamothioate MMA, however, was not reproduced successfully, as both ^{1}H NMR spectra were void of methacrylate peaks from 6.05-5.67 ppm (see appendix B.1 figure B.3, green line).

Initially this was assumed to be caused by misinterpretation of the ^{1}H NMR spectra, leading to mis-

taken M_W calculations and an insufficient amount of 2-isocyanatoethyl methylacrylate used. However, the employed amount of 2-isocyanatoethyl MA corresponded to an excess molar equivalent of 1.2 and 2.5 resp., therefore confounding this hypothesis, as the SMM should have been at least partially end group functionalized.

Fourier-transform infrared spectroscopy (FTIR) spectra were recorded at the beginning (t = 0 h) and during the reaction (t = 2 h) for one batch in order to monitor the isocyanate band caused by 2-isocyanatoethyl MA at 2260 cm^{-1}. The spectrum of the reaction at t = 0 h, which was expected to show a significant isocyanate band, did not show any signals caused by asymmetrical N=C=O stretching (see appendix B.1, figure B.4). Whether this was caused by background effects, a low concentration or a reaction of the thiol end groups with the 2-isocyanatoethyl MA in the sample container was not investigated.

For reasons of practicability, experiments concerning the end group functionalization were stopped at this point as they were deemed non-reproducible, complicated to synthesize and did not result in the random co-polymer material being of superior performance compared to the block-co-polymer, as shown in chapter 7.

4.3 Characterization of the SMM p(AcDMA-bocAEMA-MMA)

4.3.1 ^{1}H NMR Measurements of the SMM

^{1}H NMR spectra of the SMM with benzodithioate end group were measured in $CDCl_3$. Measurements were used to confirm the presence and molar content ratios of AcDMA, bocAEMA and MMA and to determine the molecular weight of the polymer. As depicted in the exemplary spectrum in figure 4.11, peaks were assigned to each polymer component, demonstrating that all motifs were successfully incorporated. Most signals showed a slightly different chemical shift than the corresponding monomer signal, caused by the polymerization and associated coupling and chemical environment effects. The spectrum does not show any significant impurities besides solvent residues of $CHCl_3$, DMF, Et_2O and H_2O. Additional peaks caused by impurities might be superimposed by the polymer's broad aliphatic peaks in the lower field region.

The spectrum was normalized to the integral of the benzodithioate signal at 7.84 ppm (aromatic, 2H) and following peaks were used to determine the ratio of monomers: 6.64 - 6.58 ppm for AcDMA (aromatic, 3H), 4.03 ppm for bocAEMA (-O-CH_2-C, 2H) and 3.59 ppm (-O-CH_3, 3H) for MMA. The M_W was calculated according to the monomer units per CTA. In table 4.1, the M_W as well as the resulting monomer ratios and the percental difference to the ideal ratios (50 % MMA, 25 % AcDMA and 25 % bocAEMA) are shown for relevant batches of SMM. Calculations for all batches of p(AcDMA-bocAEMA-

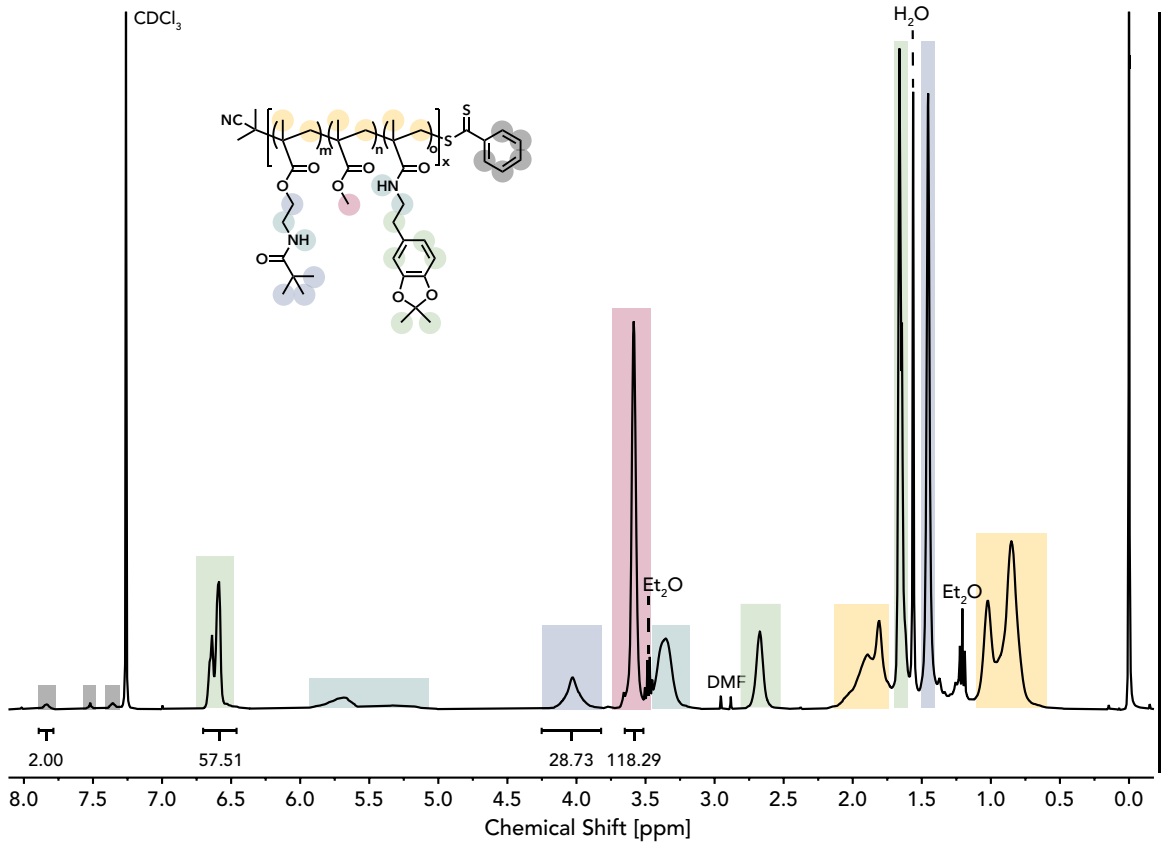

Figure 4.11: ^{1}H NMR spectrum of p(AcDMA-bocAEMA-MMA)benzodithioate in $CDCl_3$. Solvent signal at 7.26 ppm. Et_2O peaks at 3.49 and 1.21 ppm, DMF peaks at 2.95 and 2.88 ppm, H_2O peak at 1.56 ppm. Gray labels: benzodithioate end group, blue labels: bocAEMA motif, pink label: MMA motif, green labels: AcDMA motif, turquoise labels: bocAEMA and AcDMA -NH and N-CH_2-C protons, yellow labels: polymer backbone.

MMA) are shown in the appendix B.1 in table B.1.

Table 4.1: Molecular weight M_W and monomer ratio derived from ^{1}H NMR measurements.

SMM batch	Mw [g/mol]	monomer ratio [%mol]			difference to calculated ratio [%]		
		MMA	AcDMA	bocAEMA	MMA	AcDMA	bocAEMA
3	14341	51.3	27.2	21.6	2.6	8.8	-13.6
4	21680	55.2	24.2	20.7	10.4	-3.2	-17.2
6	(38256)*	57.2	24.7	18.1	14.4	-1.2	-27.6

* A peak in the benzodithioate region was only visible upon changing exponential apodiziation along t1 to 5 Hz and no proper calculation of the M_W was possible.

It should be noted that the M_W values obtained from ^{1}H NMR calculations are substantially higher than theoretically anticipated even for 100 % conversion, suggesting longer polymer chains. Thus, the M_W indicates that not the every unit of CTA employed led to the formation of one polymer chain respectively, possibly due to the low ratio of radical starter used.

As expected, employing twice the amount of AcDMA desired resulted in the targeted molar content of approx. 25 %mol. With individual exceptions (e.g. the low bocAEMA content of SMM batch 6), the molar contents are within reasonable range of the initially calculated ratios and of sufficient resemblance to the mfp-5.[32] No significant correlation was found between the amount of monomer entry, molar

concentration, conversion and monomer ratios.

4.3.2 Solubility Testing of the SMM

Dopa and lysine, the adhesive motifs incorporated into the SMM, need to be facing the wet tissue surface in order to form strong covalent interactions in physiological conditions. As the matrix for the SMM is designed to phase separate upon contact with water, the SMM needs to be located in the hydrophilic phase to be turned outwards toward the tissue. To derive in which phase of the amphiphilic matrix the sequence macromonomer was likely to be located, its solubility in water was tested.

In order for the protective groups not to interfere with the solubility tests, the SMM was deprotected according to literature.[72] A small amount of p(AcDMA-bocAEMA-MMA)-carbamothioate MMA (M_W 14341 g/mol) was dissolved in $CHCl_3$ and TFA and reacted in presence of a catalytic amount of H_2O for 4 h. After precipitation into Et_2O, the cleavage of the protective groups acetonide and tert-butyloxycarbonyl was confirmed *via* ^{1}H NMR by the absence of the acetonide aliphatic peak at 1.66 ppm and the boc aliphatic peak at 1.45 ppm.

The solubility of the deprotected SMM in H_2O was evaluated qualitatively by immersing a small amount of SMM in a scintillation vial filled with water. Upon gentle shaking, the sample dissolved without any solid residues.

As presumed, the solubility of the SMM in water confirmed its polar character and hydrophilicity. Therefore, its hypothesized location in the hydrophilic phase of the polymer matrix (see chapters 5 and 6 for incorporation of the SMM into the matrix) was confirmed.

4.3.3 GPC Measurements of the SMM

In order to verify the SMM's molecular weight calculated from the ^{1}H NMR spectrum (14341 g/mol), gel permeation chromatography was conducted in THF on one batch of the SMM. Signals were recorded with a UV detector at 282 nm, as absorption experiments had shown this to be the absorbance maximum of AcDMA. The chromatogram, depicted in figure 4.12 **(A)**, shows a sharp signal at 24.2 min, confirming the narrow M_W distribution expected for a polymer synthesized by RAFT polymerization. According to the PMMA calibration data, the SMM's molecular weight is 14582 g/mol. This value is in accordance with the M_W calculated from the ^{1}H NMR spectrum and therefore confirms the weight of the SMM.

A chromatogram of the end group functionalized SMM (p(AcDMA-bocAEMA-MMA)carbamothioate MMA) was recorded in order to evaluate the effect of the functionalization procedure on the M_W. The chromatogram is shown in figure 4.12 **(B)** and shows a narrow signal at 24.3 min, correlating to a M_W of 16624 g/mol.

This increase in M_W of 14 % was assumed to be caused by the end group modification, the sample

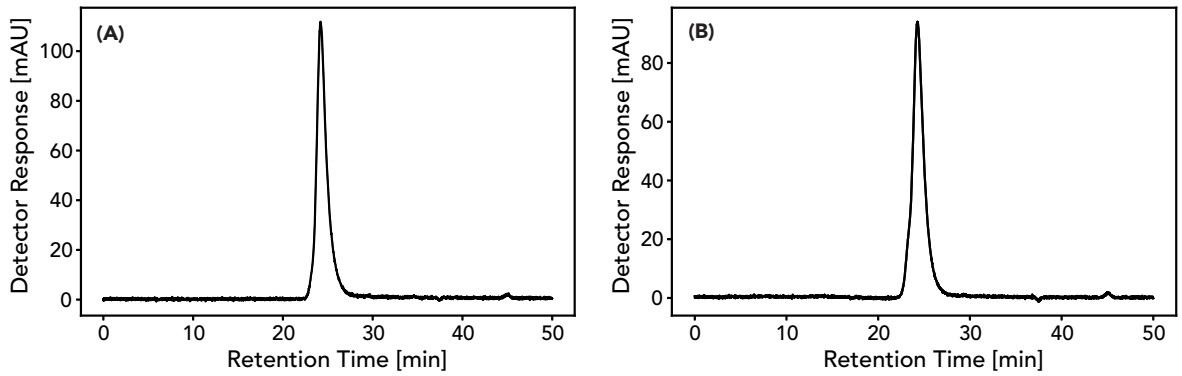

Figure 4.12: Chromatogram of the SMM in THF. **(A)** Unmodified SMM with benzodithioate end group, GPC signal at 24.2 min correlating to a M_W of 14582 g/mol. **(B)** SMM with end group modification to carbamothioate MMA, GPC signal at 24.3 min correlating to a M_W of 16624 g/mol.

preparation and measurement deviations. The M_W increase was considered too small to cause a significant change in the properties of the SMM once embedded into the supramolecular matrix and therefore the deviation was not investigated any further. No repetition of the GPC measurements was performed.

4.3.4 DSC Measurements of the SMM

Differential scanning calorimetry measurements were performed on the modified SMM p(AcDMA-bocAEMA-MMA)-carbamothioate MMA in order to assess the potential of the SMM to be used as an adhesive on its own behalf and to establish whether the SMM was a one-phase system.

The modified SMM p(AcDMA-bocAEMA-MMA)-carbamothioate MMA with a M_W of 14341 g/mol calculated from the ^{1}H NMR spectrum was analyzed. The SMM underwent three cycles from -100 to +200 °C (for the heating profile, see figure B.5 in the appendix B.1), the second cycle of which is depicted in figure 4.13.

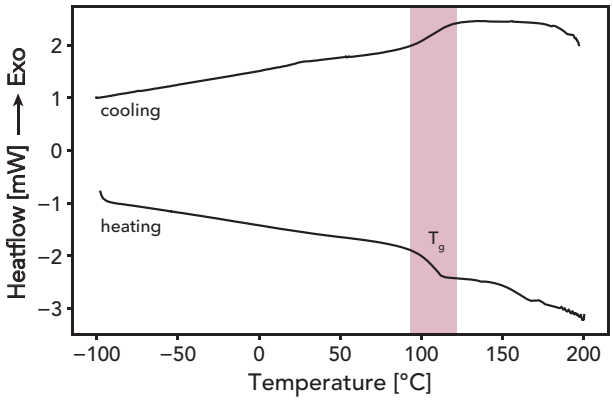

Figure 4.13: DSC heating and cooling curve from -100 to 200 °C at a heating rate of 10 °C/min for p(AcDMA-bocAEMA-MMA)carbamothioate MMA. The endothermic glass transition temperature T_g is highlighted by a pink box.

Prior to the glass transition with an onset of 102.27±0.78 °C and a midpoint of 108.74±1.96 °C, the

SMM does not show any thermal events. This indicates a single phased material, as anticipated. The high glass transition temperature (T_g) renders the SMM a quite brittle polymer, not suited on its own to comprise a tissue adhesive.

4.4 Discussion of the SMM

So as to enhance its adhesive behavior, the sequence macromonomer was designed and synthesized to resemble the mfp-5 in respect to its M_W and its molar content of dopa and lysine. ^{1}H NMR measurements confirmed molar ratios of the adhesive motifs within reasonable range of the 25 %mol target, with 27.2 %mol of AcDMA and 21.6 %mol of bocAEMA. The molecular weight of 14341 g/mol determined by ^{1}H NMR was confirmed by GPC analysis (14582 g/mol) and was twice as high as anticipated. This might indicate that not every CTA unit led to the formation of a polymer chain. As the monomer ratios were appropriate regardless of the high M_W, the SMM was deployed in further polymerizations and functionalizations toward the wet tissue adhesive.

The end group functionalization of p(AcDMA-bocAEMA-MMA)-benzodithioate toward p(AcDMA-bocAEMA-MMA)-carbamothioate MMA was successfully conducted on one batch of the SMM. However, the procedure was deemed unreproducible after attempts on two more batches failed.

Solubility testing on the deprotected p(DMA-AEMA-MMA)-carbamothiate MMA confirmed its polar character and indicated that it would be located within the hydrophilic phase of the amphiphilic, supramolecular matrix. DSC measurements showed, that the SMM was a one-phased system with a T_g of 108.74 ± 1.96 °C. As a quite brittle polymer, the SMM therefore was not suitable to be processed into a tissue adhesive on its own behalf.

5 Random Co-polymer

In order to provide the mfp-5 mimetic SMM with cohesive properties and render it processable into a tissue adhesive, it was embedded into an amphiphilic, supramolecular matrix *via* one of two synthesis routes.

In this chapter, the implementation of the end group functionalized SMM p(AcDMA-bocAEMA-MMA)-carbamothioate MMA (see section 4.2.2) into the supramolecular cohesive matrix by free radical polymerization, its deprotection and characterization will be discussed.

The random co-polymer was designed to contain about 10 %mol of DMA, corresponding to 1.2 %mol of SMM. As those values were calculated according to the M_W obtained from a first ^{1}H NMR interpretation (7318 g/mol), the employed amount of SMM according to corrected calculations (M_W = 14310 g/mol)

corresponded to 0.6 %mol of SMM.

In regard to the SMM, molar percentages were designed to resemble the ideal molar ratios determined by Balkenende and coworkers (10 %mol UPyHEMA, 60 %mol EHMA and 20 %mol PEG20MA) and resulted in ratios of 11 %mol of UPyHEMA, 65.8 %mol of EHMA and 22 %mol of PEG20MA.[11] In regard to all motifs, this resulted in a constitution of 9.3 %mol AcDMA, 7.3 %mol bocAEMA, 17.5 %mol MMA, 7.3 %mol UPyHEMA, 14.7 %mol PEG20MA and 43.9 %mol EHMA.

The theoretical M_W of the random co-polymer, resulting from the molar ratios and the assumption that each AIBN molecule would start two polymer chains, was 23588 g/mol.

5.1 Polymerization of p(p(DMA-AEMA-MMA)-UPyHEMA-EHMA-PEG20MA)

Figure 5.1 depicts the general synthetic pathway toward the random co-polymer.

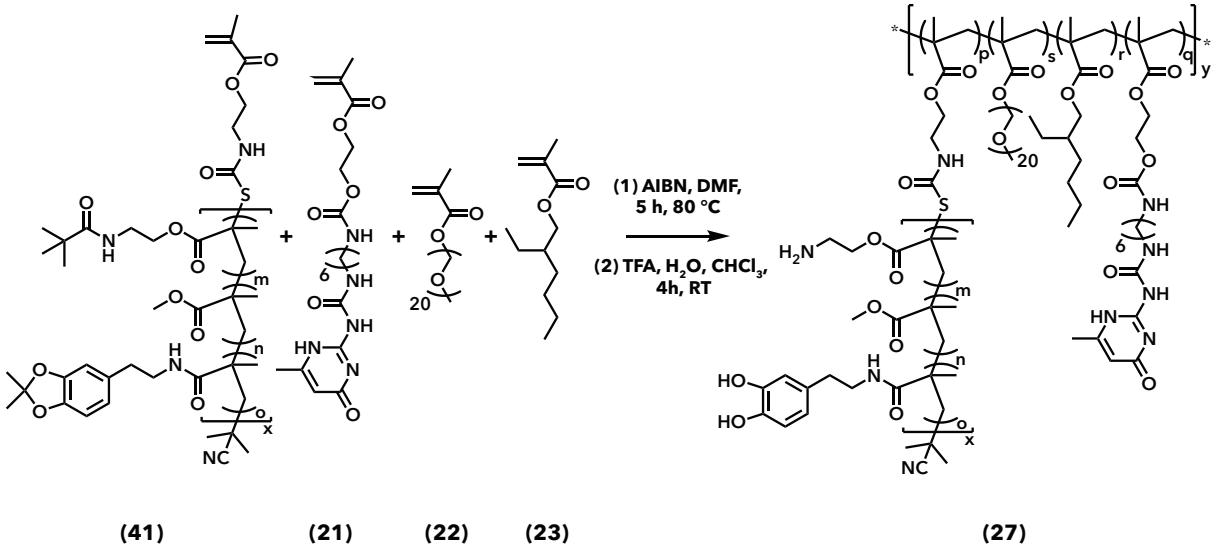

Figure 5.1

The end group functionalized SMM-carbamothioate MMA was polymerized with UPyHEMA, EHMA and PEG20MA in a free radical polymerization in DMF under nitrogen atmosphere with AIBN as radical starter. The obtained random co-polymer p(p(AcDMA-bocAEMA-MMA)-UPyHEMA-EHMA-PEG20MA) was precipitated and dried on high vacuum.

The adhesive motifs dopa and lysine had to be deprotected for the block-co-polymer to exhibit adhesive interaction with tissue proteins. To that end, TFA in $CHCl_3$ with a catalytic amount of H_2O was employed in a deprotection step. The acetonide and boc groups were cleaved off and rendered the DMA and AEMA motifs unprotected.[72] After precipitation and drying on high vacuum, an opaque off-white polymer was obtained.

Cleavage of the protective groups was confirmed by the absence of the respective peaks at 1.61 ppm and 1.39 ppm in the ^{1}H NMR spectrum of the polymer, as can be observed in figure 5.2.

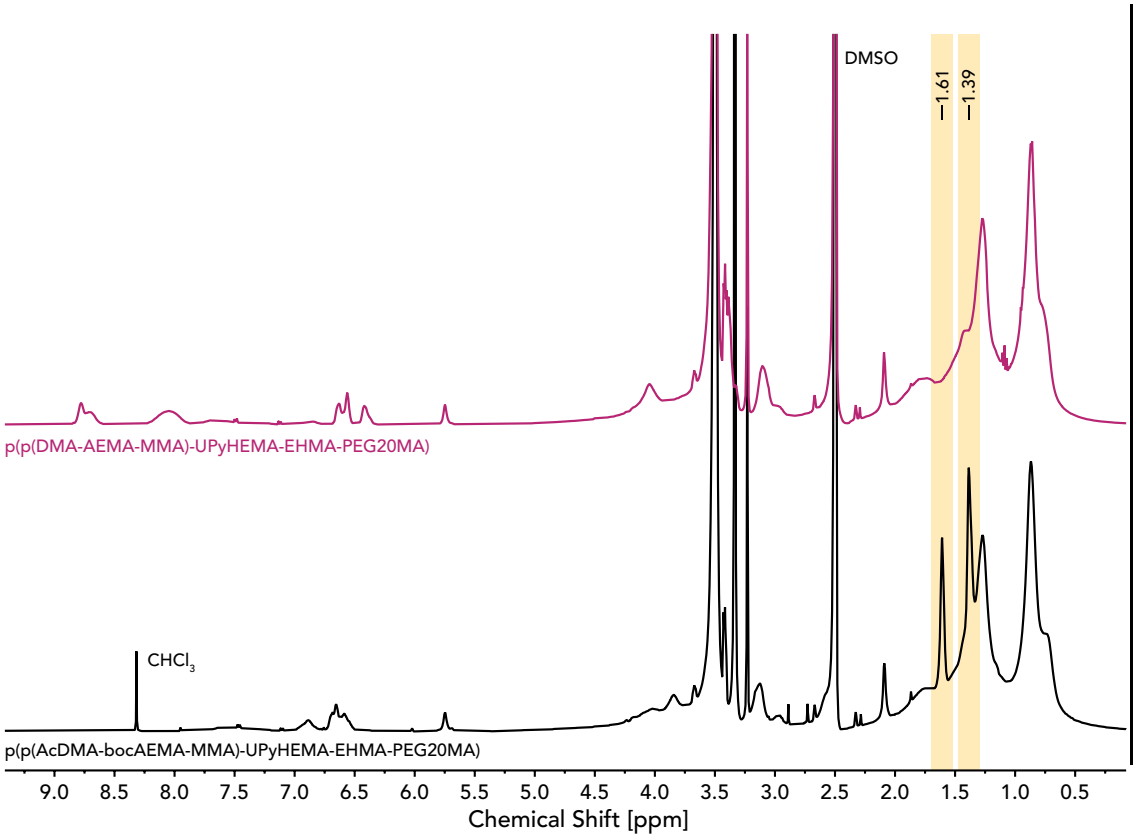

Figure 5.2: ^{1}H NMR spectra of the random co-polymer in DMSO-d6 before (black line: p(p(AcDMA-bocAEMA-MMA)-UPyHEMA-EHMA-PEG20MA)) and after deprotection (pink line: p(p(DMA-AEMA-MMA)-UPyHEMA-EHMA-PEG20MA)). The disappearance of the signals corresponding to the protective groups boc (1.39 ppm) and acetonide (1.61 ppm) is highlighted in yellow.

5.1.1 Preparation of Compression Molded Polymer Patches

Polymer patches were produced by compression molding in order to measure swelling behavior, tensile properties and tissue adhesion strength. A typical procedure included transferring the polymer between two Teflon films and employing a Teflon spacer of 0.127 mm thickness to ensure even thickness distribution over the entire area of the polymer film. The polymer was then pressed at 207 bar and 65 °C for 30 seconds. This process was repeated several times to ensure a homogeneous film without enclosed air bubbles. The obtained polymer film was stored overnight prior to testing.

5.2 Characterization of p(p(DMA-AEMA-MMA)-UPyHEMA-EHMA-PEG20MA)

5.2.1 ^{1}H NMR Measurements of the Random Co-Polymer

The ^{1}H NMR spectrum of the deprotected random co-polymer in DMSO-d6 was used to confirm the presence of the SMM and the matrix motifs employed.

Figure 5.3 shows the assignment of peaks to the respective motifs used. Due to the change in solvent, the SMM peaks were located slightly shifted in comparison to the SMM spectrum in $CDCl_3$. The signals used to determine the molar composition of the polymer were 6.63 - 6.42 ppm for DMA (aromatic, 3H), 4.05 ppm for EHMA and AEMA (-O-CH_2-C-, 2H), 3.23 ppm for PEG20MA (-O-CH_3, 3H) and 2.09 ppm for UPyHEMA (heterocyclic -CH_3, 3H).

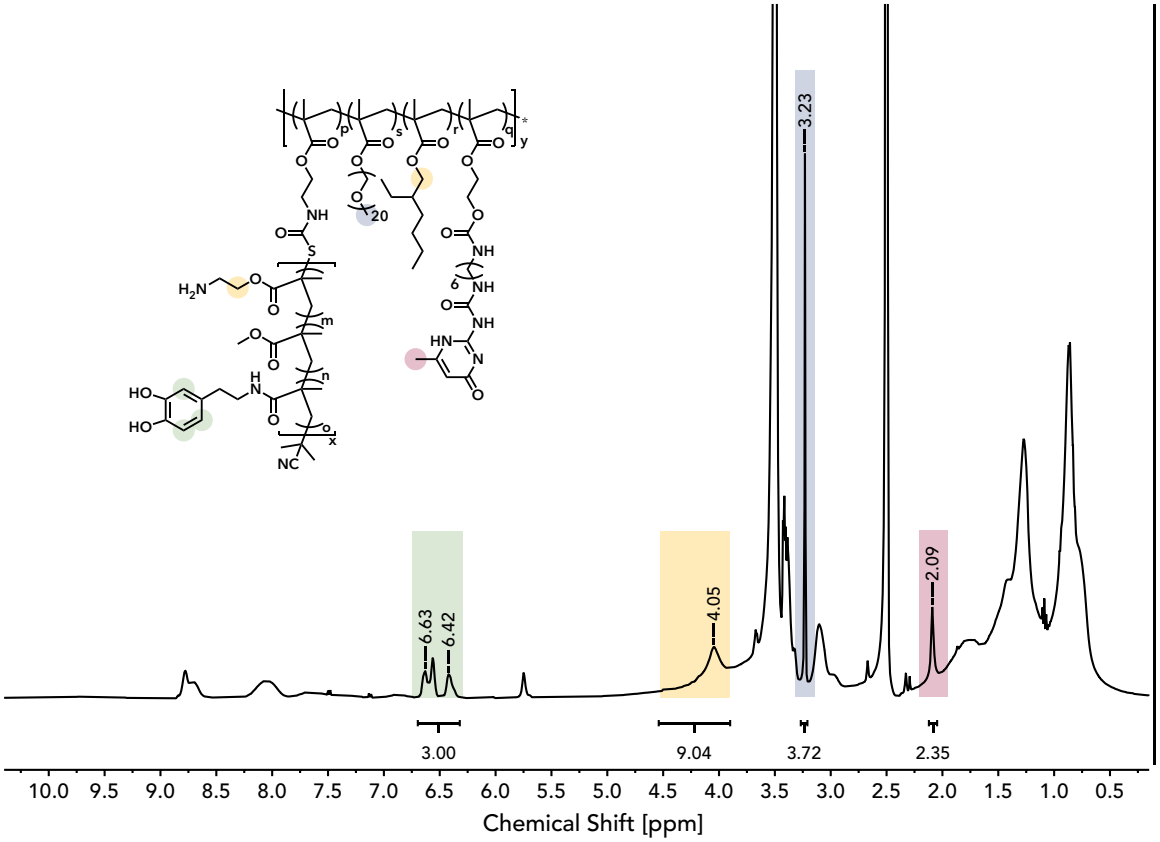

Figure 5.3: ^{1}H NMR of the random co-polymer p(p(DMA-AEMA-MMA)-UPyHEMA-EHMA-PEG20MA) in DMSO-d6. Solvent signal at 2.50 ppm. Green label: DMA motif, yellow label: AEMA and EHMA motifs, blue label: PEG20MA motif, pink label: UPyHEMA motif.

The implemented SMM had already been characterized thoroughly, therefore the monomer ratios of AEMA and MMA determined from the ^{1}H NMR spectrum of the SMM were transferred to the spectrum of the random co-polymer according to the integral of the DMA signal at 6.63 - 6.42 ppm. This afforded the deduction of the AEMA integral from the overlapping signal for EHMA and AEMA at 4.05 ppm.

Results of the ^{1}H NMR evaluation are summarized in table 5.1 for two batches of random co-polymer using the same batch of SMM. Table 5.2 shows the ratios calculated from the spectra of the protected random co-polymers.

Table 5.1: Monomer ratios of two batches of random co-polymer using the same SMM, derived from ^{1}H NMR measurements. Δ indicates the percentual deviation from the theoretically calculated ratios.

deprotected	theoretical	batch 1		batch 2	
	ratio [%mol]	monomer ratio [%mol]	Δ [%]	monomer ratio [%mol]	Δ [%]
DMA	9.27	10.70	15.4	13.07	41.0
AEMA	7.32	8.54	16.7	10.43	42.6
MMA	17.54	20.19	15.1	24.67	40.6
UPyHEMA	7.33	7.50	2.2	6.93	-5.6
EHMA	43.87	39.81	-9.3	33.67	-23.3
PEG20MA	14.67	13.27	-9.6	11.24	-23.4

Table 5.2: Monomer ratios of two batches of random co-polymer in the protected state using the same SMM derived from ^{1}H NMR measurements. Δ indicates the percentual deviation from the theoretically calculated ratios.

protected	theoretical	batch 1		batch 2	
	ratio [%mol]	monomer ratio [%mol]	Δ [%]	monomer ratio [%mol]	Δ [%]
AcDMA	9.27	9.57	3.3	9.49	2.4
bocAEMA	7.32	7.61	4.0	7.57	3.5
MMA	17.54	18.07	3.0	17.90	2.1
UPyHEMA	7.33	7.08	-3.5	7.02	-4.3
EHMA	43.87	44.33	1.1	44.93	2.4
PEG20MA	14.67	13.33	-9.1	13.09	-10.8

For both batches of the protected random co-polymer, the monomer ratios determined from the ^{1}H NMR differed little from the theoretical ratios, with PEG20MA exhibiting the largest deviation of -10.8 %. Generally, an increase of the SMM's motifs is observed at the expense of the matrix motifs PEG20MA and UPyHEMA. After the deprotection step, however, the ratios exhibited larger deviations from the theoretical molar percentages. A large increase in SMM content connected to a relative increase of the integral of DMA is shown, particularly distinctive for the second batch. This change in monomer ratios before and after the deprotection step can be explained by unsuccessful incorporation of the end group functionalized SMM into the random co-polymer (compare section 5.2.2). Due to the missing covalent linkage, the precipitation steps after the deprotection step led to different loss of material in the matrix-co-polymer and the SMM respectively.

As no specific detectable end group was attached to the polymer, the length of a polymer chain and thus the M_W could not be determined *via* ^{1}H NMR measurements.

Although the incorporation of the SMM into the random co-polymer was not successful for either batch, it was possible to reproduce the experiment successfully. The same batch of SMM was used for both batches of random co-polymer and similar molar ratios were achieved, as confirmed by ^{1}H NMR

measurements.

5.2.2 GPC Measurements of the Random Co-Polymer

To verify the assumption that the SMM was not covalently linked to the matrix polymer, GPC measurements were performed. The random co-polymer in its protected state was used, as not to damage the column. DMF with 0.02 M LiBr (100 %) was employed as eluent. Signals were recorded with a UV detector at 282 nm, as absorption experiments had shown this wavelength to offer optimal detection of the AcDMA motif as well as the UpyHEMA motif. The resulting chromatogram is depicted in figure 5.4 **(A)**.

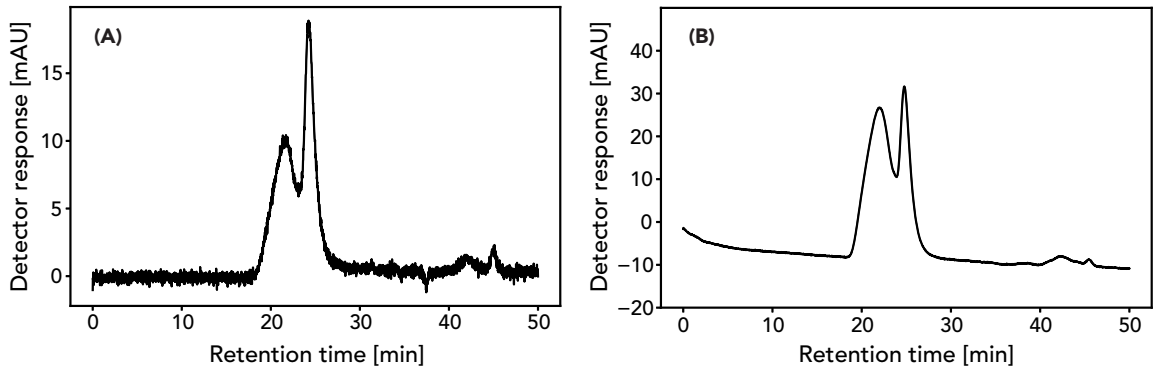

Figure 5.4: GPC chromatogram of **(A)** the protected random co-polymer p(p(AcDMA-bocAEMA-MMA)-UPyHEMA-EHMA-PEG20MA), **(B)** a mixture of the SMM and the matrix polymer.

The random co-polymer shows a bimodal distribution in the chromatogram, providing evidence that the SMM is not covalently bonded to the supramolecular matrix. The M_W determined according to a PMMA calibration is 172792 g/mol for the signal at 21.7 min and 15538 g/mol for the signal at 24.2 min. The second signal corresponds well with the GPC measurements of the SMM (see section 4.3.3). These findings were confirmed by the GPC measurements of the second batch of random co-polymer in its protected state (see figure B.6 in appendix B.2).

Furthermore, GPC measurements were carried out with a sample containing both the SMM and a matrix polymer in solution. The supramolecular matrix polymer was synthesized from molar equivalents of UPyHEMA, EHMA and PEG20MA, in a procedure identical to the random co-polymer's polymerization. The chromatogram of the mixture is shown in figure 5.4 **(B)** and exhibits a similar bimodal distribution with two signals at 22.0 and 24.7 min, corresponding to the matrix polymer and the SMM respectively. The difference in signal intensities between measurement **(A)** and **(B)** is ascribed to the sample being a qualitative experiment, for which the amounts of SMM and matrix polymer used have only been approximated.

5.2.3 Swelling Studies of the Random Co-Polymer

Swelling studies were carried out to assess the co-polymer's behavior upon contact with bodily fluids. They were performed on the processed polymer films in phosphate buffered saline (PBS), a saline solution reconstructing physiological conditions. Figure 5.5 depicts the average results with standard deviation for both batches of random co-polymer (values are listed in table B.2 in appendix B.2).

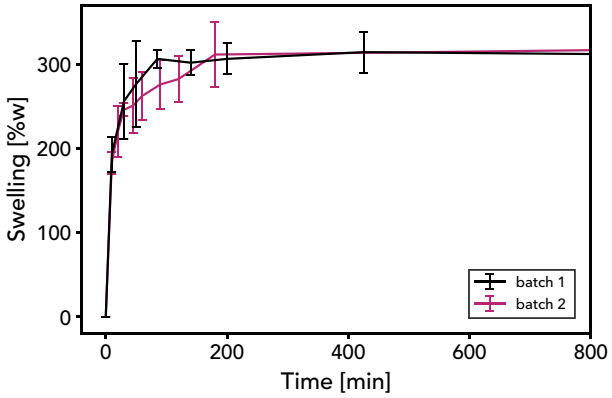

Figure 5.5: Average weight gain over time for two batches of random co-polymer in PBS. Vertical lines show the standard deviation for a sample size of n = 3 (black) and n = 4 (pink).

Initially, the polymer takes up approximately half of its total intake of PBS within the first 10 min, followed by rapidly reaching an equilibrium after about 2 h.

The equilibrium PBS content of 312.5±30.7 %w is quite large and is of concern, as it could potentially have a negative impact on the tissue adhesion properties over time. Excessive swelling might induce mechanical strain, leading to strained covalent links, which would eventually break.

5.2.4 DSC Measurements of the Random Co-Polymer

DSC measurements were performed on the processed polymer patch in its dry and swollen state in order to assess phase separation behavior upon swelling, and to determine the T_g of the material. For the dry sample, three heating and cooling cycles from -100 to +200 °C were performed (see figure B.5 in appendix B.1), of which the second cycle is depicted in figure 5.6 **(A)**. The swollen samples were stored in PBS over night to ensure equilibrium swelling, and then underwent one cycle of heating from +5 to +80 °C and cooling to +25 °C, as shown in figure 5.6 **(B)**.

For the dry random co-polymer sample, a broad T_g with an onset of -66.0±1.4 °C and a midpoint of -58.2±2.4 °C was determined. Additionally, an endothermic event was recorded at 18.4±0.4 °C. This is hypothesized to be caused by the reorganization of the hydrogen bonds of UPyHEMA upon heating above the glass transition and once sufficient mobility is available.[90] No further thermal events were recorded, suggesting that the random co-polymer in its dry state is a single phased system.

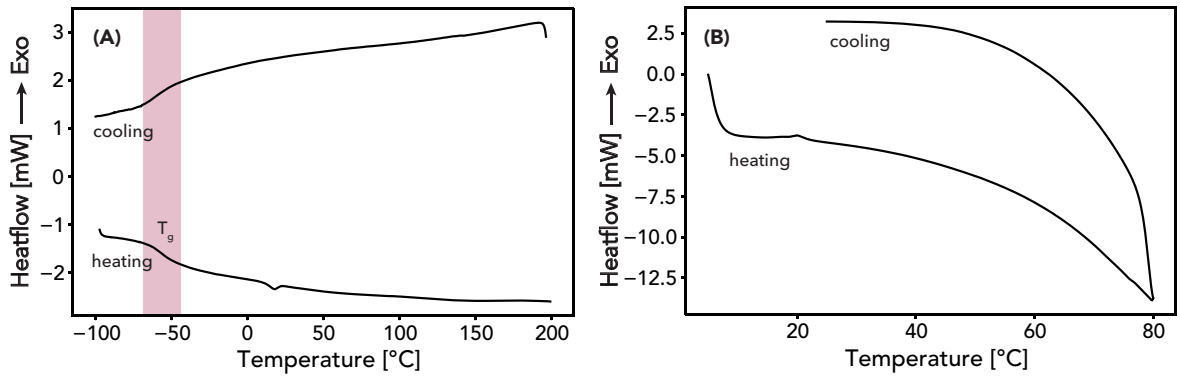

Figure 5.6: DSC heating and cooling curves of the processed random co-polymer in its **(A)** dry state and **(B)** swollen state at a rate of 10 °C/min.

For the swollen random co-polymer patch, the appearance of a T_g at 20.9±1.5 °C was recorded in the DSC trace. This thermal event, which was not recorded in the dry polymer patch's DSC trace, is indicative of a phase separated morphology upon swelling.[11]

5.2.5 Tensile Tests of the Random Co-Polymer

The random co-polymer's tensile properties in its swollen state were assessed by tensile tests. Dogbone shaped samples were prepared and swollen in PBS for 2 h to reach equilibrium swelling. They were tested with a strain rate of 25 %/min.

A considerably low elastic modulus of 0.17±0.02 MPa, a strength of 0.04±0.03 MPa and a strain at break of 46±5 % were recorded. The small stress at break implies relatively low UPy-UPy interaction strength or insufficient crosslink density. The excessive equilibrium swelling of 312.5±30.7 %w is considered to be a possible cause for the random co-polymer's weak mechanical properties. This most likely results from the hydrophilic SMM not being covalently bonded to the amphiphilic matrix.

5.2.6 Tissue Adhesion Tests of Random Co-Polymer

Tissue adhesion tests were performed to study the adhesive and cohesive strength of the polymer, especially in respect to the newly implemented mfp-5 mimetic motif.

Testing Procedure

Tests were performed according to the standard ASTM-2255-05. The procedure is depicted in figure 5.7 and explained in detail below.

The processed polymer patch was cut into pieces of 1 cm^2 and attached to strips of polycarbonate (PC) with cyanoacrylate glue. Bovine pericardium tissue was used as a surrogate collagenous tissue to resemble actual surgical conditions. It was prepared freshly by thawing the frozen tissue in PBS and

attaching it onto PC substrate strips. The tissue area on the strips was adjusted to a width of 1 cm. Typical appearance of the prepared samples is shown in figure 5.7 **(1)**, with the polymer placed on the left side and the tissue sample on the right side. The tissue and polymer surfaces were then overlapped and gently pressed together to form adhesive joints **(2)** before immersing the samples in PBS in a petri dish. A weight of 200 g was placed on the overlapping area to exert a force of 2 N **(3)**. The samples were incubated at 37 °C for 15 - 150 min.

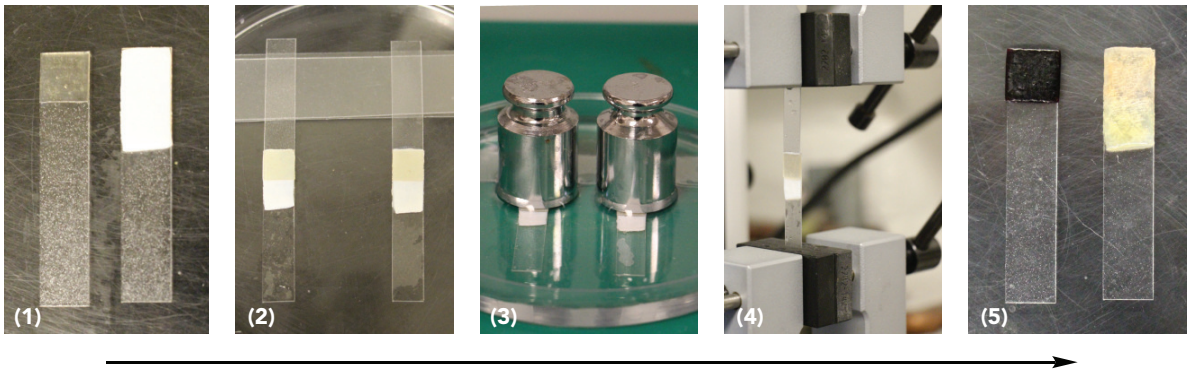

Figure 5.7: Procedure for shear adhesion testing. **(1)**: Polymer and tissue sample before incubation. **(2)**: Overlapping samples with tissue-polymer interface. **(3)**: Incubation at 37 °C in PBS with a force of 2 N applied to the interface. **(4)**: Shear adhesion test. **(5)**: Samples after testing and staining with Arnow stain.

Following incubation, the samples were tested in a shear adhesion setup on a universal testing machine **(4)**. After the lap shear tests, the separated polymer and tissue surfaces were stained to obtain information about the mode of failure **(5)**.

For the determination of the failure mechanism, Arnow stain was used.[91] This stain is based on the nitration of aromatic diols and triols by subsequent acidification with HCl, nitration with a $NaNO_2/Na_2MoO_4$ solution and alkalinization with NaOH. The selective reaction with DMA causes a clearly visible, reddish discoloration. Dependent on whether this discoloration occurs solely on the

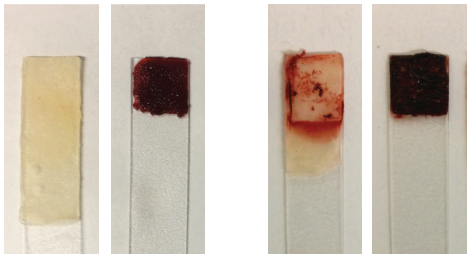

Figure 5.8: Exemplary depiction of the failure mode determined by Arnow stain.

polymer surface or as well on the tissue surface, the failure mode can be assessed. Red discolorations on both surfaces imply DMA residues, representing polymer residues, on the tissue surface. This is indicative for cohesive failure. Contrarily, if the polymer surface alone shows red discolorations, adhesive failure is concluded. Exemplary, figure 5.8 depicts samples discolored with Arnow stain for adhesive

failure (left) and cohesive failure (right).

Evaluation

Average results of the random co-polymer's tissue shear adhesion strength with standard deviation and statistical significance are depicted in figure 5.9 for batch 1 **(A)** and batch 2 **(B)**. Values are listed in the appendix B.2 in table B.3.

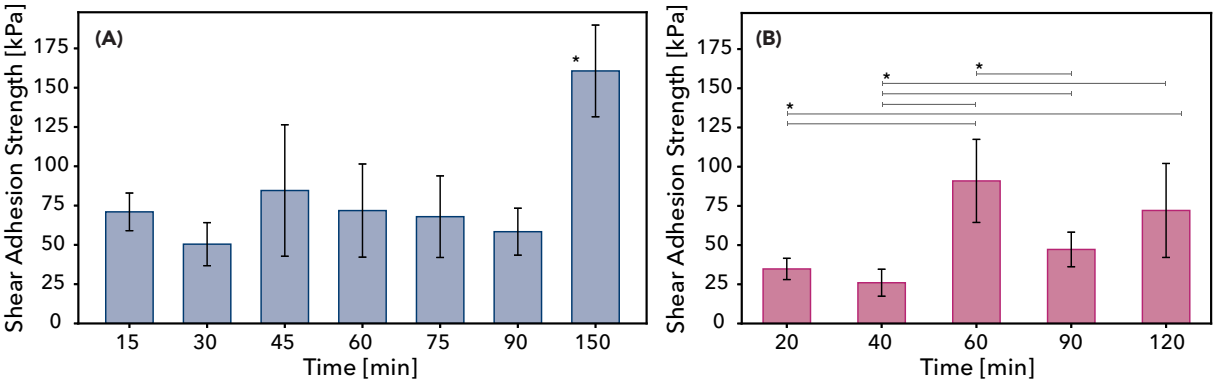

Figure 5.9: Tissue shear adhesion strength of the random co-polymer batch 1 **(A)** and batch 2 **(B)**. Average values for n = 4 samples (for batch 1 at 60 min, n = 10) are shown with standard deviation. Statistical significance ($p > 0.05$) is indicated with a star * and lines.

The highest adhesion strength was recorded for an incubation time of 150 min with 160.7±29.2 kPa.

Large standard deviations are owed to the restricted amount of material available for testing at each incubation time (n = 4) as well as biological variations between harvested tissues.[11] Statistically significant differences between batch 1 and batch 2 are limited to experiments at 15 resp. 20 min and 150 resp. 120 min incubation time. Overall, no trend of tissue adhesion strength with time could be allocated. This is an indication that, unlike the state-of-the-art material, adhesive strength does not deteriorate over time.[11]

Figure 5.10 shows the tissue adhesion specimens of batch 1 after staining them with Arnow stain (specimens of batch 2 are depicted in figure B.8 in appendix B.2).

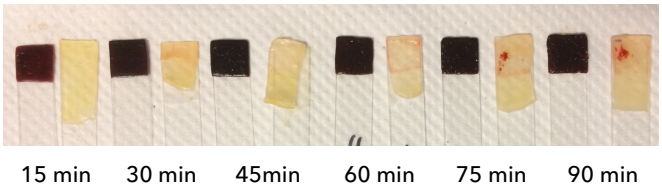

Figure 5.10: Random co-polymer batch 1 tissue adhesion samples of different incubation times after shear adhesion testing. Samples were discolored with Arnow stain to determine the failure mode.

At short incubation times (<60 min), samples showed adhesive failure, whereas at prolonged incubation times (≥60 min) cohesive failure was observed. This observation indicates that prolonged incubation and contact with tissue supported by a force of 2 N enables DMA to form stronger interfacial bonds.

However, as extensive swelling of the random co-polymer at the beginning of incubation induces strain on those bonds, no significant change in adhesion strength is observed when the failure mode switches from adhesive to cohesive failure.

Additional tests were performed to assess whether pre-swelling had the potential to minimize the strain induced by swelling during incubation. To that end, prepared PC strips with polymer patch attached (batch 1) to them were stored in PBS for 1 h to reach a nearly equilibrated state. The adhesion strength to bovine pericardium was then tested according to the previously employed procedure with a sample size of n = 6. A very low tissue adhesion strength of 8.3±2.1 kPa compared to 71.8±29.6 kPa for identical incubation time with the dry polymer patch was determined. Apparently, reducing the strain caused by swelling during incubation stands in no relation to the interfacial coverage that can be realized with dry polymer patches.

5.3 Discussion of the Random Co-polymer

With adhesion strengths greater than 55 kPa at 60 min incubation time, the random co-polymer shows good adhesive properties toward the bovine pericardium tissue. Up to the tested maximum duration of incubation (150 min), no declining trend of adhesion strength with time was recorded. This is unexpected, as swelling experiments in PBS showed excessive swelling of more than 300 %w within the first 2 h, which could potentially strain the cohesive network and covalent adhesive bonds.

Failure mechanism tests revealed that at short incubation times, the polymer showed adhesive failure, whereas at longer incubation times (≥60 min), cohesive failure was observed. This change in failure mechanism could be decisive for the polymer's constant adhesion strength over time, as the strain on the covalent network induced by swelling is hypothesized to compromise the increase in adhesive bonds over time. An approach to avoid the negative influence of excessive swelling failed, as pre-swelling of the polymer patches prior to tissue adhesion tests resulted in very poor adhesion.

Concerning the materials constitution, ^{1}H NMR measurements showed the expected monomer ratios in the protected state for both batches. Once deprotected, however, the ratios changed toward higher contents of SMM motifs and lower contents of matrix motifs. This difference in loss of material after precipitations indicated, that the SMM was not covalently bonded to the matrix polymer. GPC analysis confirmed this hypothesis by displaying a bimodal distribution in the chromatogram.

The chromatogram was further used to determine the M_W of the matrix polymer (172792 g/mol), which exceeded the theoretically calculated M_W of the random co-polymer (23588 g/mol) by a factor of seven. This deviation can be ascribed to the negligence of chain transfer reactions and AIBN recombination reactions in the theoretical calculations.

DSC measurements of the random co-polymer indicated excellent processability in its dry state due

to its low T_g of -58.2±2.4 °C. This had already been observed as an advantage during processing and sample preparation. Upon swelling in PBS, the amphiphilic matrix phase separated, as shown by the DSC trace of the swollen polymer. The phase separation and the excessive swelling are thought responsible for the poor performance of the swollen random co-polymer in tensile tests.

Overall, in terms of tissue adhesion strength and processability, the random co-polymer poses a promising surgical tissue adhesive. However, as the crucial end group functionalization of the SMM could not be reproduced, this approach of implementing the SMM into a supramolecular matrix does not have any prospects.

6 Block-co-polymer

In order to facilitate the implementation of the adhesive SMM into a supramolecular, cohesive matrix, a synthetic route that avoided the SMM's end group functionalization altogether, was designed.

Said easier, simpler route comprises the implementation of the SMM into a supramolecular block-co-polymer by reactivation of the CTA end group of the SMM and subsequent RAFT polymerization. This step is followed by the cleavage of the end group and a deprotection step, all of which will be elucidated within this chapter. Subsequently, the characterization of the polymer in terms of composition and tissue adhesion properties will be discussed.

The target M_W for the block-co-polymer was defined according to 80 % conversion, similar to the SMM, and an overall content of 1.0 %mol of SMM correlating to 10 %mol of DMA within the block-co-polymer.

For the calculations, the monomer amounts employed in the SMM and in the block-co-polymer were summarized, as no precipitation step was performed between the RAFT polymerization of the SMM and the RAFT polymerization of the block-co-polymer, and therefore unreacted monomer units from the SMM polymerization were still present in the reaction mixture. The precipitation step was omitted as to minimize the loss in material related to multiple precipitations. Furthermore, the influence of the remaining SMM monomer units, were they to be incorporated in the amphiphilic supramolecular block of the polymer, was considered negligible in regard to the amount of new monomer introduced.

The ideal molar ratio of motifs determined by Balkenende and coworkers was modified to accommodate the additional monomer units of bocAEMA and MMA.[11] Consequentially, the targeted molar contents were 10.7 %mol AcDMA, 10.7 %mol bocAEMA, 6.3 %mol UPyHEMA, 37.9 %mol EHMA, 12.7 %mol PEG20MA and 21.6 %mol MMA. The molar equivalents used in the polymerization were identical with those used for the synthesis of the random co-polymer, resulting in a better comparability in respect to the molar composition.

The theoretical M_W was calculated according to equation 4.1 to equal 37860 g/mol. Considering the complications in the determination of the M_W of the SMM and the significant probability of a lesser amount of polymer chains present after the RAFT polymerization of the SMM, the real M_W will likely differ substantially from the theoretical M_W.

6.1 Polymerization of p(DMA-AEMA-MMA)-(UPyHEMA-EHMA-PEG20MA)

Figure 6.1 depicts the general synthetic pathway toward the block-co-polymer.

The pink reaction mixture obtained after quenching the RAFT polymerization of the SMM (see section 4.1) was further co-polymerized with UPyHEMA, EHMA and PEG20MA by restarting the RAFT polymerization with anew addition of AIBN and re-dilution in DMF under nitrogen atmosphere.

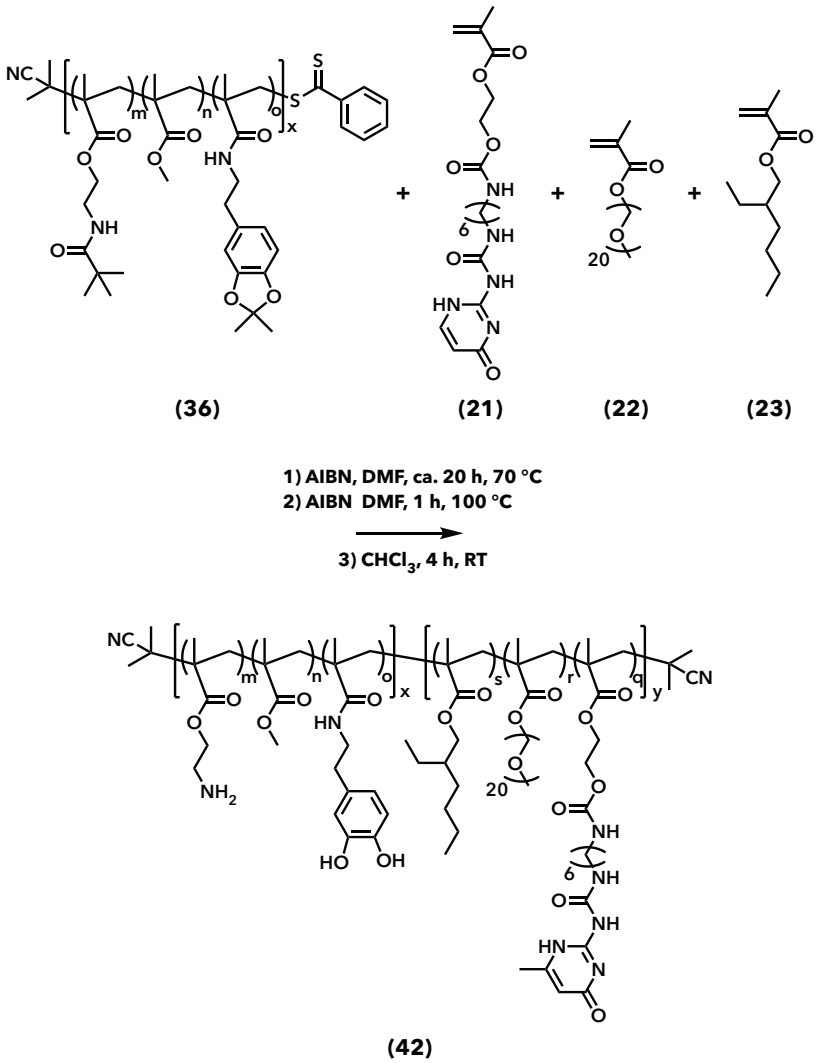

Figure 6.1: Scheme of the RAFT polymerization of p(AcDMA-bocAEMA-MMA)-b-(PEG20MA-EHMA-UPyHEMA) **(1)** with subsequent cleavage of end groups **(2)** and a deprotection step **(3)**.

To determine the duration of reaction to 80 % conversion, ^{1}H NMR samples were taken and measured at the beginning and toward the end of the reaction. The decrease of the methacrylate peaks at 6.13-6.10 ppm, 5.62-5.56 ppm and 5.31-5.29 ppm in respect to the aromatic dopa peaks at 6.65-6.60 ppm was used to determine the conversion based on equation 4.3. The sum of the methacrylate peaks was reduced by the theoretical share of excess AcDMA (9.7 % in the block-co-polymer).

Figure 6.2 shows the progress of the reaction with time. After 19 h at a conversion of 84 %, the reaction was quenched and one drop of the solution was precipitated into ice/salt bath cooled Et_2O with 10 % Hex for ^{1}H NMR analysis.

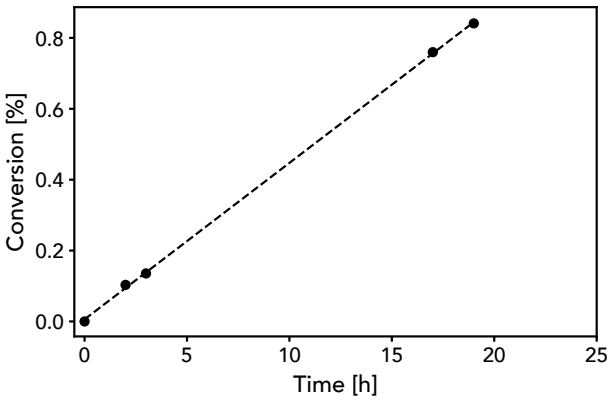

Figure 6.2: Conversion of the RAFT polymerization of the block-co-polymer with time. The dashed line indicates the linear trend line.

In order to remove the CTA's benzodithioate end group, an excess of AIBN was employed for an addition-fragmentation coupling reaction toward a cyanoisopropyl end group.[61] The reaction conversion was assessed by means of the reaction solution's change in color from pink to yellow, and confirmed in the ^{1}H NMR spectrum of the block-co-polymer (see figure 6.3). The block-co-polymer was precipitated in Et_2O and Hex and the resulting transparent off-white polymer was dried on high vacuum.

For the deprotection step, TFA in $CHCl_3$ with a catalytic amount of H_2O was employed to remove the protective groups acetonide and boc from the DMA and AEMA motifs. After precipitation and drying on high vacuum, a transparent polymer with a yellow hue was obtained. Cleavage of the protective groups was confirmed by the absence of the respective peaks at 1.66 ppm and 1.45 ppm in the ^{1}H NMR spectrum of the polymer (see figure 6.3).

Polymeric patches were compression molded according to the steps described in section 5.1.1.

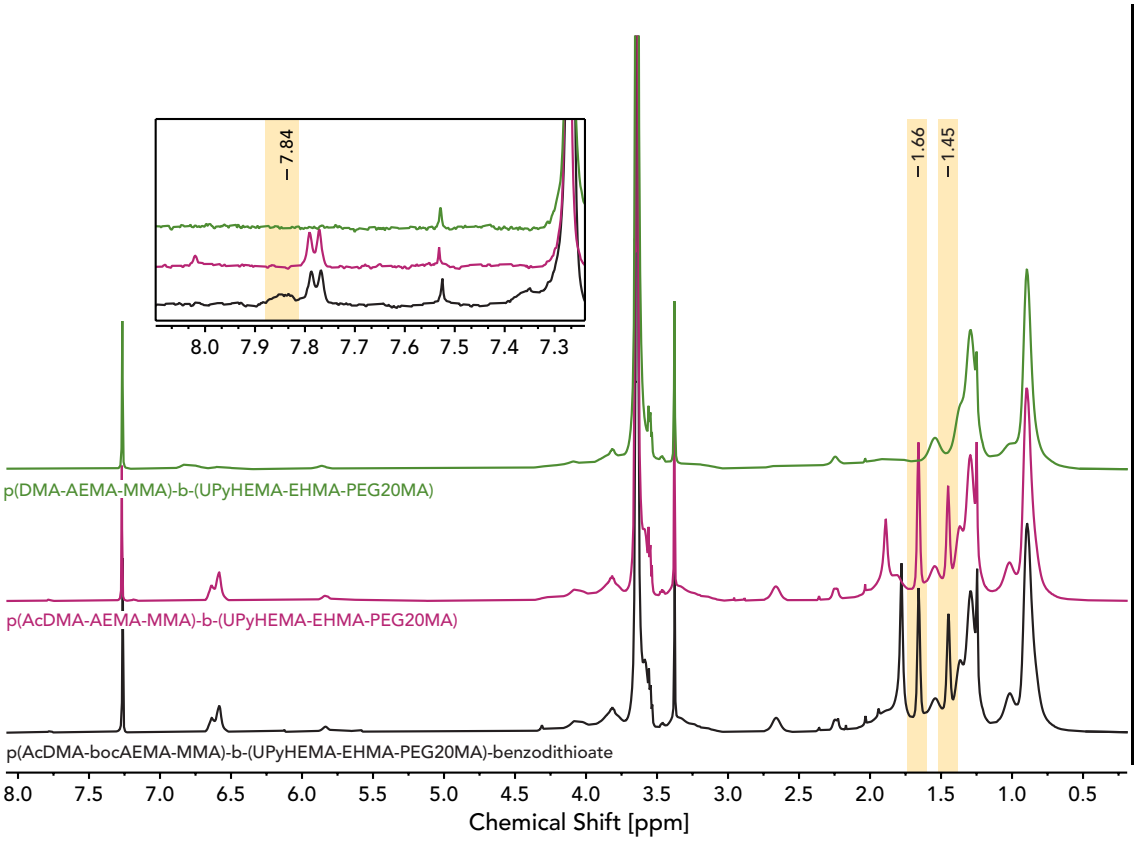

Figure 6.3: ^{1}H NMR in CDCl^{3} of the block-co-polymer at different reaction stages: The black graph depicts p(AcDMA-bocAEMA-MMA)-b-(UPyHEMA-EHMA-PEG20MA)-benzodithioate, the pink line depicts p(AcDMA-bocAEMA-MMA)-b-(UpyHEMA-EHMA-PEG20MA) after the end group cleavage and the green line depicts p(DMA-AEMA-MMA)b-(UPyHEMA-EHMA-PEG20MA) after deprotection. Control signals for successful reactions are highlighted in yellow.

6.2 Characterization of p(DMA-AEMA-MMA)-(UPyHEMA-EHMA-PEG20MA)

6.2.1 ^{1}H NMR Measurements of the Block-co-polymer

In order to confirm the success of the polymerization and determine the molar composition of the block-co-polymer, a ^{1}H NMR spectrum of the unprocessed polymer with the benzodithioate end group in $CDCl_3$ was recorded.

Peaks were assigned to each polymer component, as depicted using the example of batch 1 in figure 6.4. They showed a slight shift compared to the monomer spectra due to coupling and chemical environment effects. However, characteristic peaks were assigned to each motif, thus confirming that all monomers were successfully incorporated into the block-co-polymer.

The spectrum was normalized to the benzodithioate signal at 7.84 ppm (aromatic, 2H) and following peaks were used to determine the ratio of monomers: 11.88 ppm for UPyHEMA (heterocyclic -NH-, 1H), 6.64 - 6.59 ppm for AcDMA (aromatic, 3H), 4.08 ppm for EHMA (-O-CH_2-C-, 2H), 3.59 ppm for MMA

(-O-CH_3, 3H), 3.38 ppm for PEG20MA (-O-CH_3, 3H) and 1.45 ppm for bocAEMA (boc group -CH_3, 9H).

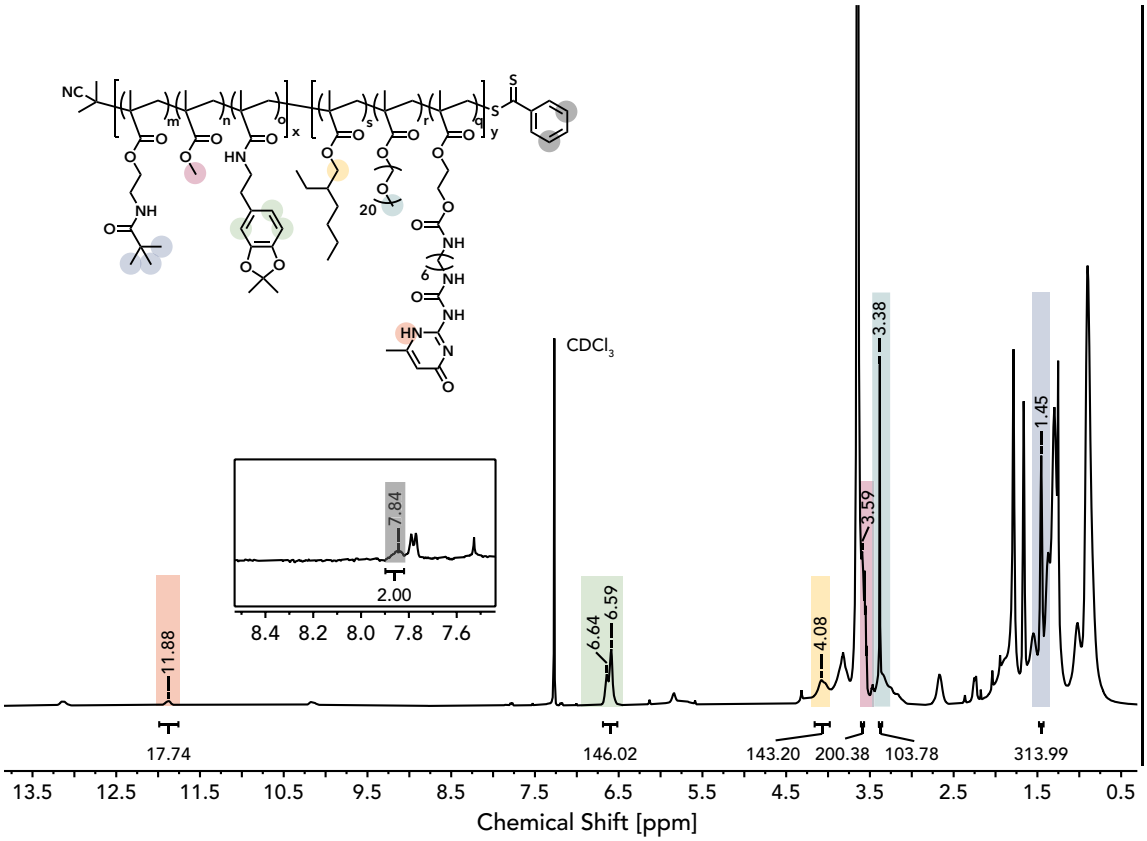

Figure 6.4: ^{1}H NMR spectrum of the block-co-polymer p(DMA-AEMA-MMA)-b-(PEG20MA-HEMA-UPyHEMA) in $CDCl_3$. Solvent signal at 7.26 ppm. Gray labels: benzodithioate end group, blue labels: bocAEMA motif, pink label: MMA motif, green labels: AcDMA motif, yellow label: EHMA motif, turquoise label: PEG20MA motif, orange label: UPyHEMA motif.

The molar percentages calculated for both batches of block-co-polymer are listed in table 6.1 with their deviations from the ideal values.

Table 6.1: Monomer ratios of two batches of block-co-polymer derived from ^{1}H NMR measurements, listed with deviation from theoretically calculated ratio Δ.

	batch 1		batch 2	
	monomer ratio [%mol]	Δ [%]	monomer ratio [%mol]	Δ [%]
AcDMA	17.75	64.5	17.56	62.8
bocAEMA	12.72	17.9	12.22	13.2
MMA	24.35	12.9	26.79	24.1
UPyHEMA	6.47	2.2	5.18	-18.2
EHMA	26.1	-31.1	24.41	-35.5
PEG20MA	12.6	-0.4	13.84	9.4

The determined ratios were confirmed by the spectra of the block-co-polymer without the benzodithioate end group, by normalizing the spectra to the AcDMA signal at 6.64-6.59 ppm. Furthermore, it was possible to achieve similar molar ratios in both polymerizations (batch 1 and batch 2), thus rendering the polymerization reproducible.

As shown in table 6.1, the molar percentages of motifs derived from ^{1}H NMR show large deviations

from the theoretically calculated ratios. This is especially true for EHMA and AcDMA with deviations of up to 64.5 % for the latter. This rise in molar content of AcDMA can be attributed to the excess amount employed in the SMM polymerization, as this was not removed by an intermediate precipitation and therefore was able to react again in the ensuing block-co-polymer polymerization. This hypothesis also offers an explanation for the elevated MMA and bocAEMA contents, as the 20 %mol of MMA and bocAEMA remaining after the SMM polymerization were theoretically still present in the reaction mixture and available to react in the co-polymerization. This furthermore adds up to the recorded deficits of the matrix motifs UPyHEMA, EHMA and PEG20MA within the block-co-polymer.

The determination of the molar ratios from the spectrum of the unprotected block-co-polymer was attempted. However, due to immense difficulties caused by overlapping peaks, broadened and shifted signals, multiple ambiguous peak areas could not be integrated reasonably. Notably, the MMA -O-CH_3 peak had shifted to overlap with the PEG20MA -O-CH_2-O- signal in its entirety and the EHMA -O-CH_2-C- protons and the AEMA -O-CH_2- protons rendered one indistinguishable broad peak. Further tests were made under the assumption that all motifs remained incorporated in the material after the deprotection procedure. This was confirmed in part by the results of the tissue adhesion measurements (see section 6.2.6).

The molecular weight calculated from the ^{1}H NMR spectrum, with a value of 82201 g/mol, deviated substantially from the theoretical M_W of 37860 g/mol. Due to the size of the polymer, excessive differences in signal intensities between the decisive benzodithioate end group peaks and the motif signals exist, rendering the M_W's calculation from the ^{1}H NMR spectrum inefficient and prone to errors. GPC measurements were regarded as a better suitable alternative for the determination of the M_W.

6.2.2 GPC Measurements of the Block-co-polymer

GPC measurements were conducted on the block-co-polymer in its protected state. They were used to investigate the M_W distribution of the block-co-polymer and to determine its M_W. The distribution provides information about the connectivity between the p(AcDMA-bocAEMA-MMA)-block and the p(UpyHEMA-EHMA-PEG20MA)-block.

Figure 6.5 depicts the chromatograms of both batches of block-co-polymer.

As derived from the PMMA calibration, the M_W of batch 1 **(A)** and batch 2 **(2)** was calculated to be 64085 g/mol and 66876 g/mol respectively. These values roughly confirm the M_W derived from ^{1}H NMR measurements.

Both chromatograms show one large narrow peak with a smaller narrow shoulder at longer retention times. Overall, the narrow size distribution as well as the high ratio of peak to shoulder suggest a reasonable ratio of implementation of the SMM into the block-co-polymer. Additionally, the chro-

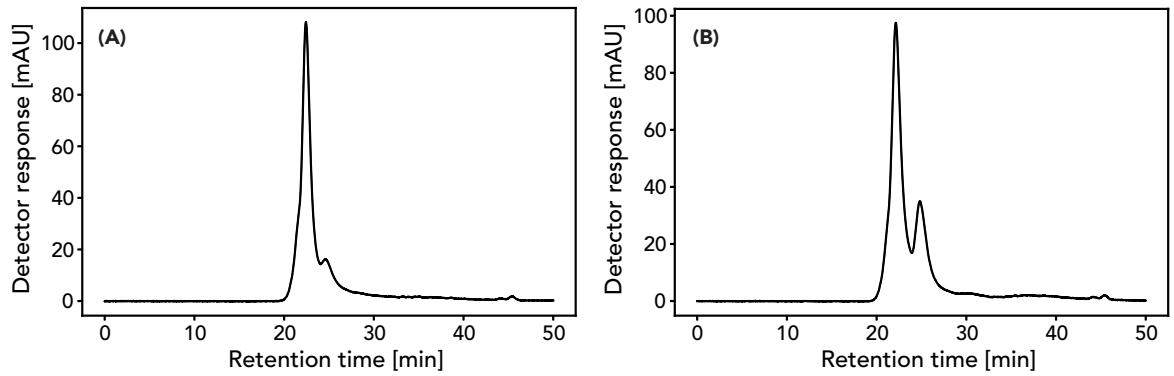

Figure 6.5: GPC chromatograms of the block-co-polymer p(AcDMA-bocAEMA-MMA)-b-(PEG20MA-HEMA-UPyHEMA). **(A)**: batch 1, **(B)**: batch 2.

matograms confirm a covalent bonding between the SMM and the supramolecular matrix, resulting in the block-co-polymer with a controlled M_W.

The shoulders at 24.6 min **(A)** and 24.8 min **(B)** correspond to a portion of the SMM that did not engage in further co-polymerization and remained mechanically trapped in the material upon precipitation. A possible explanation for this occurrence is offered by the reaction mechanism of the block-co-polymerization, which relies on restarting the reaction with anew addition of AIBN. A locally high concentration of AIBN at an early stage in the reaction could lead to cleavage of the RAFT end group from the SMM and therefore remove a portion of the SMM from the pool of polymers to be added onto. The shoulder is more distinct in the second batch of block-co-polymer, suggesting slight differences in polymerization and precipitation procedures between the two batches.

6.2.3 Swelling Studies of the Block-co-polymer

In order to assess the extent of swelling of the block-co-polymer in physiological environments, swelling experiments were carried out in PBS. Figure 6.6 depicts the resulting weight gain of the block-co-polymer over time (values are listed in table B.2 in appendix B.2).

About two thirds of the block-co-polymer's total PBS intake happen during the first 10 min. A swelling equilibrium of 146.3±6.6 %w is then reached after approx. 3 h.

Both batches show small standard deviations and generally correspond well with each other, confirming that the batches are very similar to each other in their molar content of the matrix motifs.

During the process of swelling, the polymeric network expands and the motifs EHMA and PEG20MA cause a phase separated morphology, as confirmed by DSC measurements (see section 6.2.4).[11] The hydrophobic EHMA phase of the polymer is expected to embed the UPyHEMA motif, therefore shielding the -NH groups from hydration and enabling strong cohesive strengths. The hydrophilic PEG20MA phase is expected to embed the SMM, containing the adhesive motifs. This phase faces outwards to-

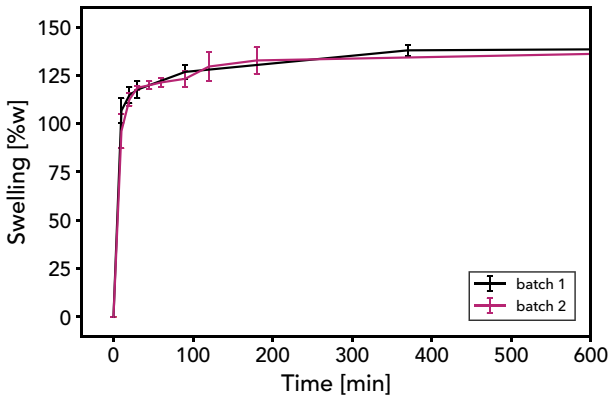

Figure 6.6: Average weight gain with time for two batches of block-co-polymer in PBS. Vertical lines show standard deviation for a sample size of n = 6 (black) and n = 4 (pink).

ward physiological liquids and the tissue surface, providing an interface for the adhesive motifs within the SMM.

This hypothesis of phase separation and good UPy interactions within the hydrophobic phase is further backed by the observation that after several days, even though the polymer had reached equilibrium swelling, the block-co-polymer did not start to disintegrate and was still tangible without inducing breakage.

After the samples were stored in PBS for several days, the PBS was tested for DMA residues. This test was used to determine whether non-covalently linked, DMA containing polymer chains (*e.g.* mechanically trapped SMM, which was shown by GPC to be present in the block-co-polymer) had leeched out of the polymer film. By adding sodium nitrite ($NaNO_2$) to the liquid, residual catechol groups would be oxidized to dopa-quinone, resulting in a red-brown discoloration. As no such discoloration was observed in the PBS, it was considered highly unlikely that polymer chains within the material had leeched into the liquid.

6.2.4 DSC Measurements of the Block-Co-Polymer

As to confirm the block-co-polymer's phase separation upon swelling, DSC measurements of the processed polymer film were performed in its dry state and after equilibrium swelling. For the dry sample, three heating and cooling cycles from -100 to +200 °C were performed (see figure B.5 in appendix B.1). The second cycle is depicted in figure 6.7 **(A)**. For the swollen samples, one cycle of heating from +5 to +80 °C with subsequent cooling to +25 °C was recorded (see figure 5.6 **(B)**).

For the dry block-co-polymer patch, a very broad glass transition was recorded in the DSC curve with an onset of -49.5±4.2 °C and a midpoint of -29.0±7.7 °C. As no further thermal events were detected, the polymer in its dry state was confirmed to be a single phased system.

The trace of the swollen polymer patch showed the presence of a T_g at 20.2±0.6 °C, which was not

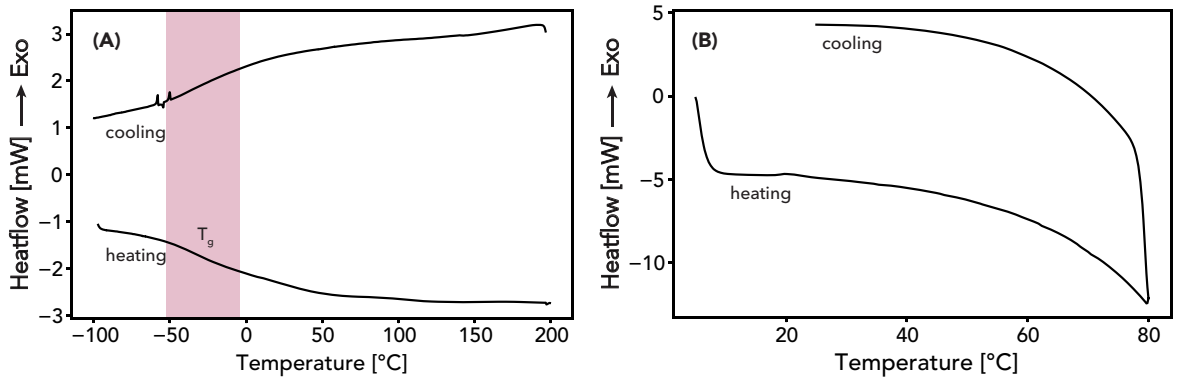

Figure 6.7: DSC heating and cooling curves of the processed block-co-polymer in its **(A)** dry state and **(B)** swollen state at a rate of 10 °C/min.

recorded in the dry sample's trace. This confirmed, that upon swelling the supramolecular polymer takes on a phase separated morphology.

6.2.5 Tensile Tests of Block-Co-Polymer

The mechanical properties of the block-co-polymer were assessed by tensile tests in the dry and swollen state. For swollen specimens, dogbone shaped samples were immersed in PBS for 2 h to reach a nearly equilibrated state prior to measurements. Specimens were tested with a strain rate of 25 %/min. Characteristic stress-strain curves of both dry and swollen patches are depicted in figure B.7 in the appendix B.2.

Tests of dry samples were aborted early, as tensile strain values easily exceeded 100 %. This characteristic confirms the dynamic character of the UPy crosslinks, bestowing the dry block-co-polymer patches with enormous elasticity.

For the swollen polymer patches, an elastic modulus of 6.12±0.27 MPa, a strength of 0.40±0.03 MPa and a strain at break of 12.2±6.2 % were determined. Those values are well in range of the mechanical properties of the fetal membrane. Calvin *et al.* for example reported a strength of 1.0 MPa and an elastic modulus of 5 MPa for chorioamnion samples of 250 μm thickness.[92] Matching the mechanical behavior of the amniotic tissue is highly desirable in order to avoid stress concentration at the interface between the polymeric patch and the fetal membrane. Thus, delamination of the patch due to premature failure could be prevented.[93]

6.2.6 Tissue Adhesion Tests of the Block-co-polymer

Tissue shear adhesion tests were performed as to determine the adhesion strength of the block-co-polymer toward bovine pericardium tissue, a fetal membrane surrogate, and to analyze the adhesive behavior over time.

As previously described in section 5.2.6, the testing procedure was conducted according to the standard ASTM-2255-05.

Average values and standard deviations of tissue shear adhesion were calculated for both batches of block-co-polymer with n = 4 samples for each incubation duration (for batch 1 at 45 min, n = 7). The results are depicted in figure 6.8 **(A)** for batch 1 and **(B)** for batch 2. Corresponding values are listed in table B.3 in the appendix B.2.

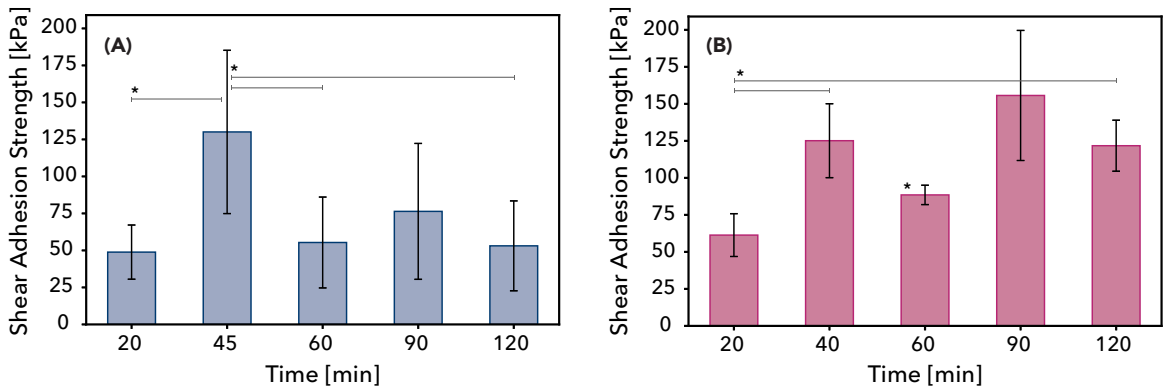

Figure 6.8: Tissue shear adhesion strength of the block-co-polymer batch 1 **(A)** and batch 2 **(B)**. Average values for n = 4 (for batch 1 at 45 min, n = 7) samples are shown with standard deviation. Statistical significance ($p > 0.05$) is indicated with a star * and lines.

Figure 6.9 depicts the assessment of the failure mode *via* Arnow stain for batch 1 (batch 2 is depicted in figure B.9 in the appendix B.2).

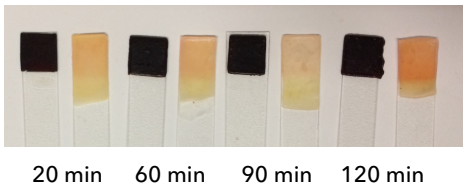

Figure 6.9: Block-co-polymer batch 1 tissue adhesion samples of different incubation times after shear adhesion testing. Arnow stain was employed to determine the failure mode.

The considerable high standard deviations, found especially in batch 1, were attributed on one hand to biological variations between the bovine pericardium tissues used, and on the other hand to the limited number of specimens measured. Overall, consistently high adhesion strengths above 48.9 kPa were achieved, with higher average strengths recorded for batch 2. The highest value of 155.7±43.9 kPa was measured for batch 2 at 90 min incubation time.

Statistical analysis showed no significant deviation between the two batches for incubation times ≤90 min. This is consistent with the molar monomer ratios determined by ^{1}H NMR (see table 6.1), which are almost identical for both batches. Measurements at 120 min, however, showed a significant variation between a shear adhesion strength of 121.7±17.2 kPa for batch 2 and 53.1±30.4 kPa for batch 1. This increase could be attributed to the marginally higher hydrophilic monomer ratios. Higher concen-

trations of PEG20MA might positively affect the amount of interface coverage upon phase separation and thus increase the quantity of DMA and AEMA available at the interface for covalent bonding.

However, assessment of the failure mode did not confirm this hypothesis, as batch 1 did not appear more prone to adhesive failure than batch 2. Throughout, the failure mode shifted from adhesive failure at short incubation times ($\leq$40 min) to cohesive failure at longer incubation times ($\geq$60 min). This change in failure mode implies, that the cohesive strength of the polymer initially exceeds the adhesive strength and at longer incubation times then is superseded by the adhesive strength. Nonetheless, said change in failure mechanism does not seem to influence tissue adhesion strengths, as no significant trend of adhesion strength with time was found.

Considering both the failure mode and the adhesion strength, the following mechanism was suggested: Upon incubation, a state close to equilibrium swellling is reached before adhesive covalent bonds are formed or even begin to form. This is consistent with adhesive failure observed at short incubation times. Adhesive bonds can then form without being strained by further swelling and the formation of new bonds can compensate for any strained bonds. Concurrently, the cohesive network and UPy-UPy interactions are slightly weakened over time by further hydration.

Similar observations of time-independent adhesion strength have been made for the random co-polymer, in contrast to findings about the time-dependent adhesion behavior of the state-of-the-art polymer.[11]

6.2.7 Cytocompatibility Study of the Block-Co-Polymer

As a promising candidate for a fetal membrane adhesive, the block-co-polymer's cytocompatibility was assessed in a first cell viability study. Tests were performed on in vitro cell culture models, according to the standard ISO 10993-5.[94] NIH 3T3 (mouse fibroblast) and CCD-32sk (human fibroblast) cells were employed and treated with media conditioned with block-co-polymer (batch 2) films.

Cytocompatibility was assessed by absorption measurements at 540 nm and subsequent transformation into percentage points of cell viability. Results for the tested concentrations of 5, 10 and 20 mg/mL as well as positive and negative control groups are depicted in figure 6.10. While positive control groups were treated with unmodified media, cells in negative control groups were intentionally killed by addition of 0.2 mg/mL sodium lauryl sulfate.

Per standard, a survival rate of more than 70 % of the treated cells relative to the positive control group is defined as cytocompatible.

As can be seen in figure 6.10 (corresponding values are listed in table B.4 in the appendix B.2), the block-co-polymer was found to be cytocompatible even at high concentrations. This observation is well in accordance with literature reporting little inflammatory or other negative cell response for catechol-

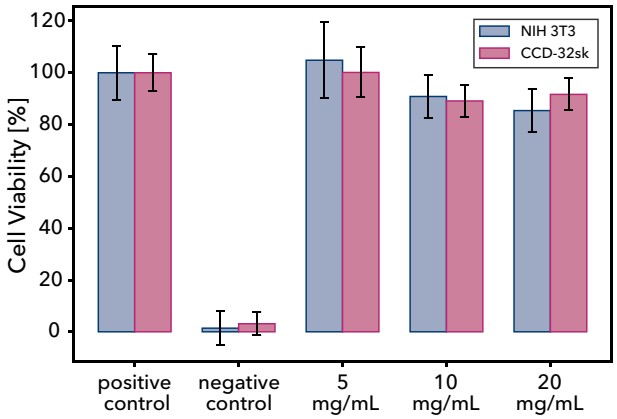

Figure 6.10: Cell viability of NIH 3T3 cells (blue) and CCD-32sk cells (pink) at different concentrations of block-co-polymer.

containing materials.[95] However, for 20 mg/mL a dose-dependent viability response was expected, similar to what had been reported by Balkenende *et al.* for the state-of-the-art polymer. This dose-dependency is hypothesized to be caused by the increase in DMA and its potential to generate H_2O_2 upon (auto)oxidation.[11]

The considerably improved biocompatibilty was attributed to the implementation of the catechol-containing motif DMA into the SMM.

6.3 Discussion of the Block-co-polymer

With average adhesive strengths above 48.9 kPa for incubation times of up to 120 min, the block-co-polymer poses a promising material for surgical adhesives.

The implementation of the adhesive SMM into the supramolecular matrix was shown to have worked successfully by means of ^{1}H NMR measurements and GPC analysis. It was further established, that the adhesive and the cohesive block are covalently linked to each other, as the GPC chromatogram showed one narrow peak with a small shoulder at higher retention times. The narrow shoulder corresponds to SMM residues, which were mechanically trapped within the polymer upon precipitation. The share of SMM, that could not be reactivated for the RAFT polymerization of the block-co-polymer, is thought to be responsible for the substantial difference of the M_W determined by GPC (64085 g/mol) and the theoretically calculated M_W (37860 g/mol). As not all SMM chains were available for the addition of matrix monomers, the resulting block-co-polymer chains grew longer than anticipated.

Notwithstanding the deviations in M_W and related changes in monomer ratios, the ^{1}H NMR spectrum and GPC data revealed that all motifs were present and covalently linked. The effect of covalent bonds within the material could also be observed in the swelling behavior of the block-co-polymer, which showed an equilibrium swelling of only 146.3±6.6. %w. DSC data of the swollen block-co-

polymer furthermore provided proof for the predicted phase separation, as a glass transition, that had not been observed in the DSC trace of the dry polymer, was recorded at 20.2±0.6 °C.

Tissue adhesion experiments showed overall high adhesion strengths, with the highest value of 155.67±43.93 kPa being recorded for batch 2 at an incubation time of 90 min. Even though single data points showed significantly higher values than others (*e.g.* batch 1 at 45 min), no correlation could be found between the shear adhesion strength and time. What did change however, was the failure mode. For incubation times ≥60 min, a transition from adhesive to cohesive failure was observed, which was hypothesized to be caused by following mechanism: Excessive swelling takes place within the first 10 min, during which only a small amount of cohesive bonds between dopa and the tissue surface is formed. Initially, adhesive failure is observed. Over time, more covalent bonds form and the adhesive strength exceeds the cohesive network strength, which is further weakened by swelling to the equilibrium state. Therefore, cohesive failure is observed.

The swollen block-co-polymer patches showed mechanical properties similar to the target tissue, as well as cytocompatibility up to concentrations of 20 mg/mL. These highly desirable properties, combined with the polymer's high adhesive strength, make the block-co-polymer a promising candidate for fetal surgery.

7 Comparison of Tissue Adhesion Properties

This chapter will cover the tissue adhesive properties' comparison of the two approaches covered in previous chapters with the state-of-the-art polymer, as well as with commercially available surgical glues.

As the random co-polymer and the block-co-polymer were designed to show similar molar constitution, they can be compared independent of molar ratios. This affords a conclusion about the effect of the redistribution of monomers on the tissue adhesion properties.

In terms of swelling, an enormous improvement of PBS intake was observed from the random co-polymer to the block-co-polymer. Although the block-co-polymer still exhibits a high swelling equilibrium of 146.3±6.6 %w, the covalent links between the SMM and the matrix presumably reduced the equilibrium substantially. In comparison, the random co-polymer, which barely contains any covalent links between the hydrophilic SMM and the amphiphilic matrix, has a swelling equilibrium of 312.5±30.7 %w.

Nonetheless, the swelling behavior is not reflected in the shear adhesion strength, as no significant difference between the measurements of both batches of random co-polymer and block-co-polymer was detected for incubation times ≤60 min (see figure B.10 in appendix B.2). As the majority of swelling

takes places within the first 20 min, effects of the excessive swelling on the adhesive interface would have been expected to appear within the same time frame. Overall, the redistribution of monomers from random co-polymer (with the SMM not incorporated properly) to block-co-polymer did neither significantly influence the adhesive strength, nor the failure mode.

The block-co-polymer, however, was easier to synthesize, reproducible and proved superior in regard to M_W control and swelling properties.

For ensuing comparisons, only data of batch 1 of the random co-polymer and batch 2 of the block-co-polymer was used, as those batches exhibited superior adhesive properties.

Figure 7.1 depicts the shear adhesion strength as a function of time for both polymers as well as for the state-of-the-art polymer p(DMA-UPyHEMA-EHMA-PEG20MA). Data for the state-of-the-art polymer was provided by Dr. Balkenende.

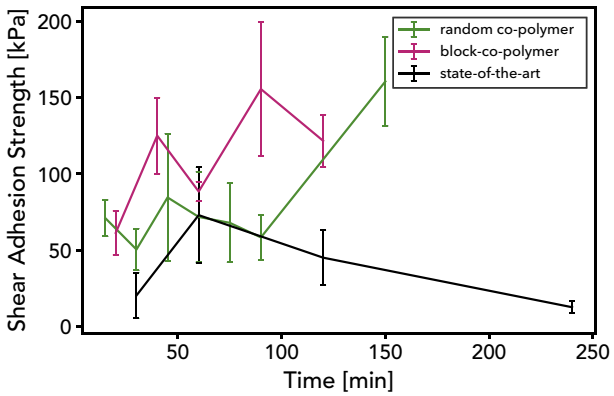

Figure 7.1: Tissue adhesion strength as a function of time for the random co-polymer, the block-co-polymer and the state-of-the-art-polymer. Vertical lines represent standard deviations.

As discussed in sections 5.2.6 and 6.2.6, no significant trend of tissue adhesion with time was recorded. In contrast, the state-of-the-art polymer was reported to show declining tissue adhesive strength with increasing duration of incubation.[11] As anticipated, the incorporation of lysine in form of a mfp-5 mimetic SMM had a distinctly positive effect on the tissue adhesion strength. This can be observed especially at short incubation times ($\leq$40 min) and extended incubation times ($\geq$100 min), for which the SMM containing polymers show significantly higher adhesion values than the state-of-the-art polymer. However, studies including adhesion data at extended incubation times (>150 min) are necessary to confirm the trend observed within the scope of this thesis.

Commercially available tissue sealants such as cyanoacrylate adhesives and fibrin glues were easily outperformed by both the random co-polymer and the block-co-polymer, as depicted in figure 7.2. Literature values were used for the comparison, if they employed the same testing procedure based on the standard ASTM F2255-05 at an incubation time of 1 h.[96–98]

Statistical significance levels were determined by comparison of means with the software MedCalc.[99]

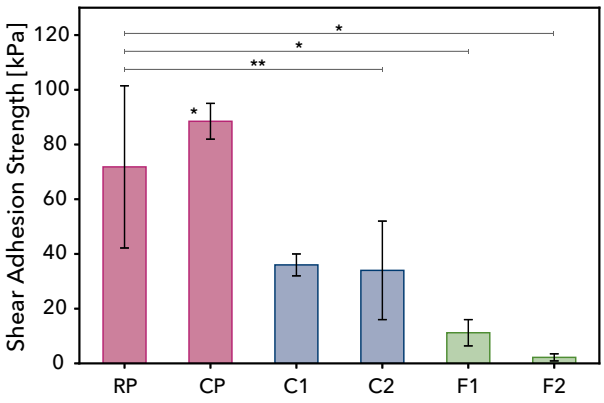

Figure 7.2: Comparison of tissue adhesion strengths tested with lap shear experiments after 1 h of incubation. Random co-polymer (RP, pink) and block-co-polymer (CP, pink) were compared to following commercially available tissue adhesives: Cyanoacrylate-based adhesives Beriplast HS (Behringwerke AG)[98] (C1, blue) and Dermabond™(Ethicon)[97] (C2, blue). Fibrin glues Tisseel™(Baxter Healthcare)[97] (F1, green) and Tissucol™(Baxter Healthcare)[96] (F2, green). * $p \leq 0.0001$, ** $p<0.01$.

With a shear adhesion strength of 88.5±6.5 kPa, the block-co-polymer proved significantly stronger than even the cyanoacrylate glue Beriplast HS (36±4 kPa). The random co-polymer showed significantly higher tissue adhesion strength than the surgical adhesives Dermabond™, Tisseel™and Tissucol™.[96,97] Due to the small sample size of n = 3 reported for Beriplast HS, the comparison of means for the determination of the statistical significance level rendered a p-value of 0.0676, marginally above the limit for significance of $p = 0.05$.

Overall, comparisons to the state-of-the-art polymer and commercially available tissue adhesives confirmed the efficacy of the mfp-5 mimetic SMM in increasing the adhesion strength. Both approaches of incorporating the SMM into a supramolecular matrix rendered polymers capable of outperforming commercially available fibrin and even cyanoacrylate adhesives. Additionally, both the random co-polymer as well as the block-co-polymer were able to retain their adhesive strength after equilibrium swelling was reached.

Part V

Conclusion and Outlook

In summary, this thesis aimed at and achieved the synthesis of a wet tissue sealant with enhanced adhesive properties.

Initially, a **mfp-5 mimetic sequence macromonomer**, that resembled the model system in molecular weight and monomer ratios, was **successfully synthesized** by RAFT polymerization. It contained both the motifs **dopa** (in the form of DMA), which is widely used as an **adhesive motif**, and **lysine** (in the form of AEMA), which is often found adjacent to dopa in mfps. It was hypothesized that the synergy of these biomimetic motifs (DMA and AEMA) would improve the adhesion strength of wet tissue adhesives. The SMM was characterized thoroughly in order to test its potential to be used as an adhesive independently. DSC measurements revealed a high glass transition temperature of more than 102 °C, showing that the SMM is quite brittle at RT and unsuited to be used as a tissue adhesives on its own behalf. Furthermore, the SMM's solubility in water was demonstrated by qualitative solubility tests, adding to its ineptness to be employed under physiological conditions without a matrix.

In an ensuing step, **the SMM was successfully incorporated into a supramolecular matrix**, employing an orthogonal chemistry approach to combine dopa's adhesive properties with the cohesive strength of **UPy-dimers' hydrogen bonding**. Two synthetic pathways, resulting in different distributions of similar molar monomer ratios, were employed. The first approach included an end group functionalization of the SMM toward SMM-carbamothioate MMA and a subsequent free radical polymerization into a random co-polymer. The second approach was based on re-activating the CTA endgroup of the SMM in a second RAFT polymerization with the matrix monomers to render a block-co-polymer.

Both approaches produced polymeric materials with a T_g below -29 °C and **excellent tissue adhesive properties** of up to 160.7±29.2 kPa, easily outperforming commercially available surgical glues. This suggests that the synergy between AEMA and DMA, which allows for the cationic amino group to displace hydrated salt ions and provide DMA with a nearly dry surface to adhere to, greatly impacts the strength of the adhesive interface.

Concerning the random co-polymer, two major difficulties were observed: In the first place, the end group functionalization of the SMM could not be reproduced after an initial success in synthesizing SMM-carbothioate MMA (determined by ^{1}H NMR and FT-IR). Secondly, the GPC chromatograms of

the random co-polymer showed a bimodal distribution, indicating that the SMM was not covalently bonded to the matrix. This assumption was further confirmed by measurements of a reference sample containing both the matrix polymer and the SMM separately. The block-co-polymer, on the other hand, was synthesized as planned and results were reproduced successfully.

Regarding the properties of both polymers, the monomer's redistribution evidently affected the swelling behavior. The swelling equilibrium of the random co-polymer with 312.3±30.7 %w was more than twice as high as the block-co-polymer's with 146.3±6.6 %w. The extreme swelling of the random co-polymer was attributed to the lack of covalent bonds between the SMM and the matrix, and was expected to affect the tissue adhesive properties as well. However, no significant differences between the tissue adhesion strengths of both polymers (apart from batch-to-batch variations) were detected. Both polymers showed adhesive failure at incubation times below 60 min and cohesive failure at longer incubation durations. This change in the failure mechanism is thought to result from strong initial swelling of the polymer ($\leq$60 min), which interferes with the adhesive bond formation. Once nearly equilibrated ($\geq$60 min), covalent bonds between dopa and the tissue's amino acid residues are formed. Adhesion strengths were not influenced by the shift in failure mode, and measurements did not reveal any significant trend between adhesive strength and incubation time. This is ascribed to the synergy between lysine and dopa, once more **confirming the efficacy of the SMM as adhesive motif**.

Altogether the block-co-polymer was deemed better suitable as a tissue adhesive due to its more facile and reproducible synthesis, its better controllable M_W and molar ratios, and its limited equilibrium swelling. Initial cell viability studies were conducted on the block-co-polymer *in vitro* to test its potential to operate in a biological system. Gratifyingly, the material was shown to be **cytocompatible** even at concentrations of 20 mg/mL.

Notwithstanding its exceptional adhesive properties, additional adhesion strength measurements are needed to confirm the longevity of the adhesive bonds at extended incubation times ($\geq$150 min). Furthermore, block-co-polymers with fine tuned ratios of DMA, AEMA and UPyHEMA should be polymerized and tested, so as to optimize the interplay of adhesive and cohesive strength. Besides, further experiments are necessary in order to gain a better understanding of the block co-polymer's polymerization kinetics in both RAFT polymerization steps. This would allow for the reproducible synthesis of a polymer with a clearly defined M_W and exact molar ratios. In a last step, the applicability of the final polymer patch in the environment of a real fetoscopic surgery, its removal and the design of a medical trial, would need to be given thought.

Overall, within the scope of this thesis, a wet tissue adhesive of remarkably high adhesion strength was designed and synthesized. Apart from its application in fetal surgery, the polymer has potential to be used as a general surgical adhesive.

Part VI

Experimental Part

8 Synthesis and Preparation

8.1 Chemicals

Methacrylate anhydride (94 %), sodium hydroxide (97 %), sodium borate (anhydrous, 99 %), magnesium sulfate (≥97 %), dimethoxy propane (≥97 %), p-toluenesulfonic acid (≥98.5 %), 2-aminoethyl methacrylate hydrochloride (90 %), bis(*tert*-butyl)dicarbonate (≥98 %), triethyl amine (≥99 %), hydrazine (64 %), 2-isocyanatoethyl methylacrylate (98 %), dibutyltin dilaurate (95 %) and sodium nitrite (≥97 %) were purchased from Sigma-Aldrich and used as received.

Sodium bicarbonate (>99.7 %, Fisher Scientific), trifluoroacetic acid (99 %, Fisher Scientific), sodium molybdate (≥99 %, Fisher Scientific), hydrochloric acid (37 %, J.T. Baker), 2-cyano-2-propyl benzodithioate (≥97 %, Strem Chemicals), dopamine hydrochloride (99 %, Alfa Aesar) and Al_2O_3 (activated, basic, Brockmangrade 1, Alfa Aesar) were used as received.

Ureido-4-pyrimidinone hydroxyethyl methacrylate was provided by courtesy of the research group and used as received.

Azobis(isobutyronitril) (98 %, Sigma-Aldrich) was recrystallized from MeOH and dried on high vacuum prior to use.

Methyl methacrylate (≥99.8 %, TCI) and 2-ethyl-hexyl methacrylate (98 %, Alfa Aesar) were filtered over basic Al_2O_3 prior to use. Poly(ethylene glycol) methyl ether methacrylate (average M_n 950, Sigma-Aldrich) was dissolved in DCM, filtered over basic Al_2O_3, reduced by rotary evaporation and dried on high vacuum prior to use.

The solvents ethyl acetate (≥95 %), hexanes (≥98.5 %), dichloromethane (≥99.5 %), methanol (≥99.8 %), dimethylformamide (≥99.8 %), toluol (≥98 %) and chloroform (≥99.8 %) were purchased from VWR and used as received. Tetrahydrofuran (99.9 %) was purchased from Fisher Scientific and used as received.

Anhydrous pyridine (99 %, Fisher Scientific), diethylether (99 %, Fisher Scientific) and anhydrous toluol (99.8 %, Sigma-Aldrich) were purchased and used without further purification.

$CDCl_3$ (99.8 % D, 0.03 % TMS, Sigma-Aldrich) and DMSO-d6 (99.9 % D, Sigma-Aldrich) were used for ^1H NMR measurements as purchased.

Water was purified on a Millipore Synergy-R apparatus.

8.2 Synthesis of monomers

Synthesis of 3,4-dihydroxyphenylalanine methacrylate (DMA)

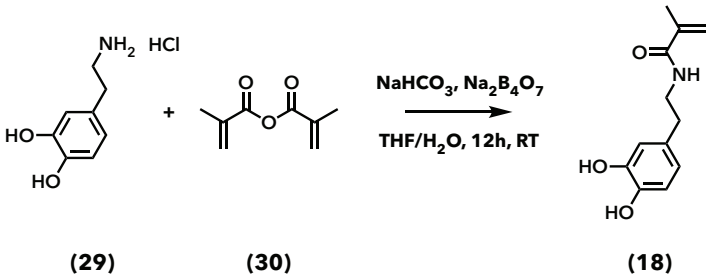

Figure 8.1

compound	eq.	n [mmol]	m [g]	V [mL]
dopa hydrochloride	1.0	79.10	15.0	
methacrylate anhydride	1.2	94.92		14.1
THF				60.0
H_2O				300.0
$NaHCO_3$			12.0	
$Na_2B_4O_7$			30.0	

$NaHCO_3$ and $Na_2B_4O_7$ were dissolved in H_2O in a three-neck flask equipped with a magnetic stir bar, two septa and a dropping funnel. A nitrogen inlet and outlet were installed in the septa and the solution was degassed with nitrogen for 20 min. The nitrogen flow was kept at a medium flow rate for the subsequent reaction. Methacrylate anhydride and THF were mixed in an Erlenmeyer flask, degassed with nitrogen for 10 min and transferred to the dropping funnel. Dopa hydrochloride was added into the three-neck flask. The mixture of methacrylate anhydride in THF was gradually added to the reaction solution over the course of 20 min. The dropping funnel was removed and replaced with a septum. The solution was stirred overnight at room temperature. The solution was washed with 150 mL EA twice and acidified with 3 N HCl to pH 2. The product was extracted into 150 mL EA three times. The three EA fractions were combined and dried with $MgSO_4$. The solution was filtered and evaporated under reduced pressure at room temperature until first precipitates had formed. The solution was precipitated into 600 mL hexanes cooled by an ice/salt bath, filtered and dried on high vacuum.

yield: 9.34 g (53.4 % of theory), light gray powder.

^{1}H NMR (400 MHz, DMSO-d6): δ [ppm] 8.76 (s, 1H), 8.64 (s, 1H), 7.94 (t, 1H), 6.63 - 6.61 (d, 1H), 6.56 (s, 1H), 6.43 - 6.41 (d, 1H), 5.61 (s, 1H), 5.30 (s, 1H), 3.22 - 3.19 (q, 2H), 2.56 - 2.51 (t, 2H), 1.83 (s, 3H)

Synthesis of Acetonide protected Dopamine Methacrylate (AcDMA)

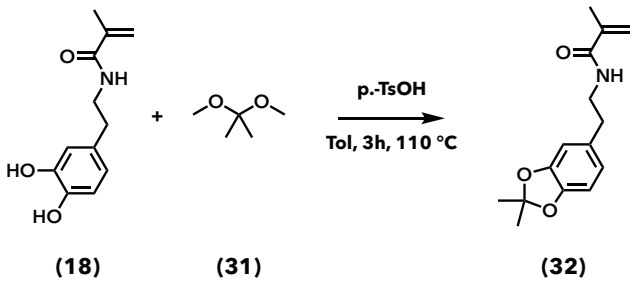

Figure 8.2

compound	eq.	n [mmol]	m [g]	V [mL]
DMA	1.000	18.1	4.0	
dimethoxy propane	8.000	144.6		17.7
p-TsOH	0.045	0.8	0.155	
anhydrous toluol				127.0

A single neck flask equipped with a magnetic stir bar was charged with DMA, dimethoxy propane and 117 mL of anhydrous toluol and degassed with nitrogen for 1 h. The remaining 10 mL of toluol were transferred to an Erlenmeyer flask and degassed with nitrogen simultaneously. p-TsOH was added to the single neck flask and degassed for further 5 min. A dean stark setup with a reflux cooler and a drying tube was attached to the flask. The dean stark was charged with 4 Å molecular sieves and 10 mL of degassed toluol. The solution was gradually heated to 111 °C and refluxed for 3 h. The solution was cooled in an ice/salt bath and reduced to 50 mL by rotary evaporation at 40 °C and reduced pressure. The resulting solution was precipitated into 200 mL of ice/salt bath cooled hexanes to yield a white precipitate. The precipitate was filtered and washed with cold hexanes three times. The white powder was dried on high vacuum.

yield: 2.5 g (52.9 % of theory), white powder.

^{1}H NMR (400 MHz, DMSO-d6): δ [ppm] 7.97 (t, 1H), 6.71 - 6.70 (d, 1H), 6.67 (s, 1H), 6.59 - 6.57 (d, 1H), 5.60 (s, 1H), 5.30 (s, 1H), 3.27 - 3.25 (q, 2H), 3.26 - 3.62 (t, 2H), 1.83 (s, 3H), 1.61 (s, 6H)

Synthesis of Boc-Aminoethyl Methacrylate

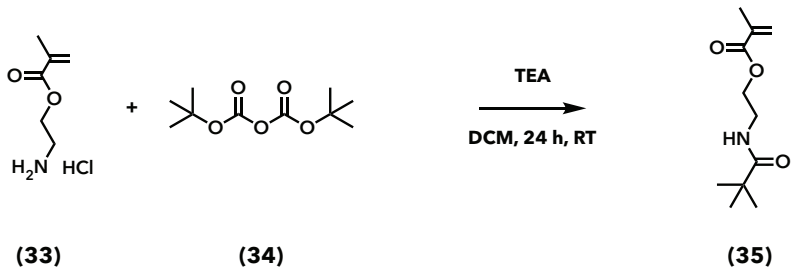

Figure 8.3

compound	eq.	n [mmol]	m [g]	V [mL]
AEMA HCl	1.0	21.8	3.6	
bis(*tert*-butyl)dicarbonate	1.2	26.2		6.0
TEA	2.0	43.6		6.1
DCM				72.6

A single neck flask equipped with a magnetic stir bar was charged with AEMA HCl and 62.6 mL DCM. The solution was cooled to 0 °C with an ice/salt bath and TEA was added dropwise. The flask was equipped with a septum and an argon in- and outlet and the solution was degassed with argon for 20 min. Bis(*tert*-butyl)dicarbonate was dissolved in 10 mL DCM and slowly added to the single neck flask. The solution was warmed to room temperature and stirred for 24 h under argon atmosphere. The resulting solution was mixed with 150 mL EA, filtered and reduced to a solid by rotary evaporation at reduced pressure. The precipitate was washed with H_2O thrice and freeze dried. The resulting product was recrystallized from a mixture of hexanes and DCM. The obtained white crystalline product was dried on high vacuum.

yield: 2.5 g (50.0 % of theory), white crystals.

^{1}H NMR (400MHz, DMSO-d6): δ [ppm] 7.00 - 6.97 (t, 1H), 6.06 (s, 1H), 5.67 (s, 1H), 4.06 - 4.03 (t, 2H), 3.22 - 3.18 (q, 2H), 1.87 (s, 3H), 1.37 (s, 9H)

8.3 Polymerization of Polymers

8.3.1 Model polymer p(MMA)

Polymerization of p(MMA)

(14) **(20)** **(37)**

Figure 8.4

compound	eq.	n [mmol]	m [g]	V [mL]
MMA	107.5	36.518		3.9
CPBD	1.00	0.340	0.075	
AIBN	0.20	0.068	0.011	
Tol				38.3

A Schlenk flask equipped with a magnetic stir bar was charged with MMA, CPBD, AIBN and Tol and sealed with a septum. The stopcock valve was closed and the solution was frozen in a bath of liquid nitrogen. The valve was then opened to vacuum and the flask was evacuated for 2 min. After closing the valve, the solution was thawed completely and the freeze-pump-thaw cycle was repeated twice. The flask was charged with nitrogen atmosphere and put in a 70 °C oil bath. The polymerization's conversion was monitored by drawing samples over the course of the reaction. Samples were analyzed by ^{1}H NMR to determine conversion. The polymerization was quenched after 16 h with liquid nitrogen and air. The solution was reduced to 10 mL by rotary evaporation and precipitated into a 10-fold amount of ice/salt bath cooled MeOH. After redissolving in Tol, two more precipitation steps were performed. The obtained pink powder was dried on high vacuum.

^{1}H NMR (400 MHz, $CDCl_3$): δ [ppm] 7.89 - 7.37 (m, 5 H), 3.60 (s, 188H), 2.36 - 1.24 (br, 188 H), 1.02 - 0.83 (s, 188H)

Synthesis of p(MMA)-thiol

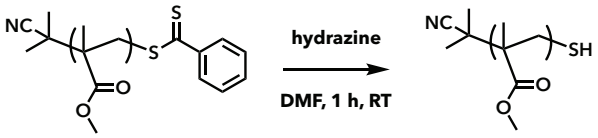

(37) **(38)**

Figure 8.5

compound	eq.	n [mmol]	m [g]	V [mL]
p(MMA)	1.0	0.15	0.8	
hydrazine 64 %	6.2	0.75		0.0375
DMF				5.0

A scintillation vial was charged with p(MMA) and DMF and vortexed until the polymer was dissolved completely. The vial was equipped with a stir bar, a septum and two needles for degassing the solution with nitrogen for 1 h. Hydrazine was added with a μL-syringe and the solution was stirred in nitrogen atmosphere for 1 h. The solution was precipitated into a 10-fold amount of ice/salt bath cooled MeOH and dried on high vacuum.

yield: 0.35 g (44.6 % of theory), white powder.

^{1}H NMR (400 MHz, $CDCl_3$): δ [ppm] 3.60 (s, 188H), 2.36 - 1.24 (br, 188 H), 1.02 - 0.81 (s, 188H)

Synthesis of p(MMA)-carbamothioate methyl methacrylate - I

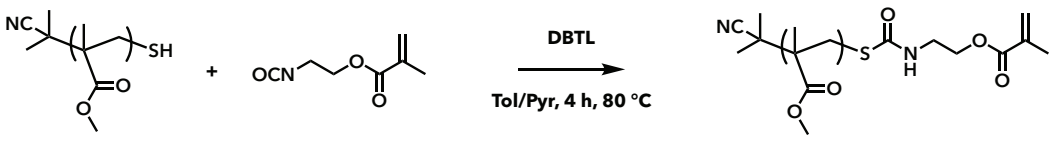

(38) **(39)** **(40)**

Figure 8.6

compound	eq.	n [mmol]	m [g]	V [mL]
p(MMA)-thiol	1.0	0.016	0.1	
2-isocyanatoethyl methylacrylate	1.3	0.020		0.0029
DBTL				1 drop
anhydrous Tol				1.8
anhydrous Py				0.2

A scintillation vial equipped with a stir bar was charged with p(MMA)-thiol, the anhydrous solvents Tol and Py and sealed with a septum. Two needles served as in- and outlet to flush the vial with nitrogen for 20 min. The outlet needle was removed and under nitrogen atmosphere, DBTL and 2-isocyanatoethyl methylacrylate were added to the solution. The solution was then heated to 80 °C in an oil bath and stirred for 4 h. The solution was removed from the oil bath and allowed to cool to RT before precipitating it into a 10-fold amount of ice/salt bath cooled Hex. The obtained white powder was dried on high vacuum.

^{1}H NMR (400 MHz, $CDCl_3$): δ [ppm] 6.12 (s, 1H), 5.60 (s, 1H), 4.69 (br, 1H), 4.24 (t, 2H), 3.60 (s, 188H), 3.51 (t, 2), 2.36 - 1.24 (br, 188 H), 1.02 - 0.83 (s, 188H)

Synthesis of p(MMA)-carbamothioate methyl methacrylate - II

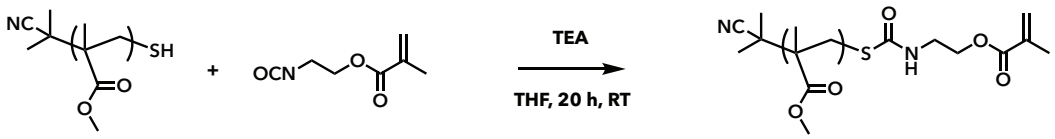

(38) **(39)** **(40)**

Figure 8.7

compound	eq.	n [mmol]	m [g]	V [mL]
p(MMA)-thiol	1.0	0.016	0.1	
2-isocyanatoethyl methylacrylate	1.9	0.030		0.0042
TEA				0.0137
THF				2.5

A scintillation vial was filled with THF and degassed with nitrogen for 20 min. A second scintillation vial was equipped with a stir bar, charged with p(MMA)-thiol and 2-isocyanatoethyl methylacrylate and sealed with a septum. Two needles were added for purging the vial with nitrogen for 5 min. 1 mL of degassed THF was added and the vial was purged with nitrogen for another 2 h. TEA in 1 mL of degassed THF was added to the solution the reaction was stirred at RT under nitrogen atmosphere for 20 h. 0.5 mL of THF were added to the solution for proper redissolving before precipitating it into a 10-fold amount of ice/salt bath cooled Hex. The obtained white powder was dried on high vacuum.

^{1}H NMR (400 MHz, $CDCl_3$): δ [ppm] 6.13 (s, 1H), 5.62 (s, 1H), 4.67 (br, 1H), 4.24 (t, 2H), 3.60 (s, 188H), 3.52 (t, 2), 2.31 - 1.21 (br, 188 H) 1.02 - 0.84 (s, 188H)

8.3.2 Sequence Macromonomer

Polymerization of p(AcDMA-bocAEMA-MMA)

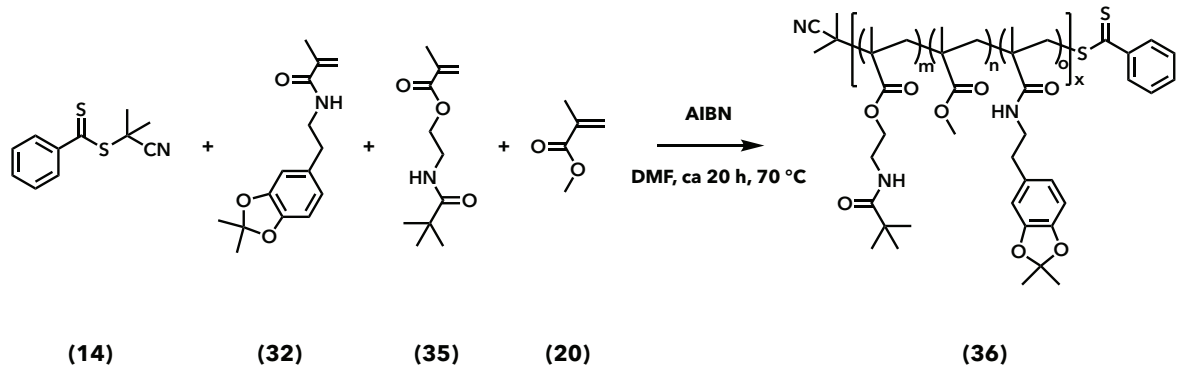

Figure 8.8

Entry	
MMA	31.25 eq.
AcDMA	31.25 eq.
bocAEMA	15.63 eq.
CPBD	1.00 eq.
AIBN	0.20 eq.
DMF	2 M

A Schlenk flask equipped with a magnetic stir bar was charged with MMA, AcDMA, bocAEMA, CPBD, AIBN and DMF and sealed with a septum. The stopcock valve was closed and the solution was frozen in a bath of liquid nitrogen. The valve was then opened to vacuum and three freeze-pump-thaw cycles were performed. The flask was charged with nitrogen atmosphere and put in a 70 °C oil bath. The polymerization kinetics and conversion were monitored by drawing samples over the course of the reaction. Samples were analyzed by ^{1}H NMR to determine 80 % conversion. After complete polymerization (17-23 h) the reaction was quenched with liquid nitrogen and air. At least one drop of solution was precipitated into a 10-fold amount of ice/salt bath cooled Et_2O. After redissolving in DCM, two more precipitation steps were performed. The product was dried on high vacuum. For endgroup-modifications and additional RAFT-polymerization steps, the solution was used without any precipitation.

yield: 67.0 % of theory at 80 % conversion, pink powder.

^{1}H NMR (400 MHz, $CDCl_3$): δ [ppm] 7.84 (t, 2H), 7.52 (t, 1H), 7.36 (d, 2 H), 6.64 - 6.60 (m, 67H), 4.03 (br, 36H), 3.59 (s, 126H), 3.36 (br), 2.64 - 1.81 (br), 1.66 (s, 134H), 1.45 (s, 162H), 1.02 - 0.85 (br)

Synthesis of p(AcDMA-bocAEMA-MMA)-thiol

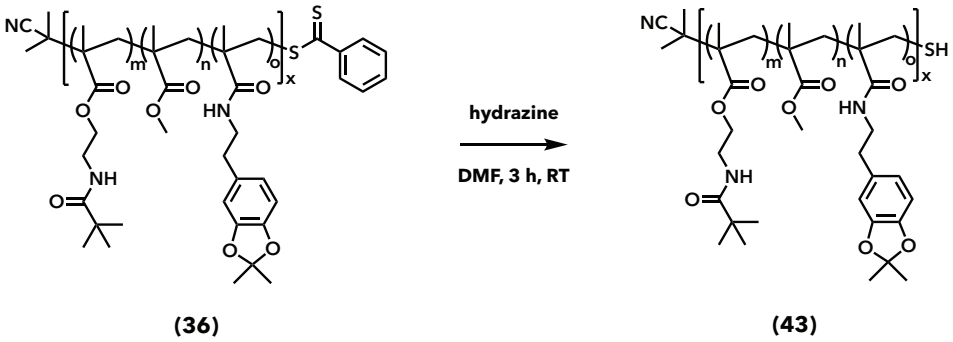

Figure 8.9

Entry	
p(AcDMA-bocAEMA-MMA)-benzodithioate	1 eq.
hydrazine 64 %	5 eq.
DMF	2 M

The polymer solution in the Schlenck flask obtained from the RAFT polymerization of p(AcDMA-bocAEMA-MMA)-benzodithioate in DMF (2 M) was used as received. Under nitrogen flow, the flask was charged with hydrazine. The flask was closed and the reaction was stirred for 3 h at RT under nitrogen. The solution was diluted with Tol and the DMF/Tol solvent mixture was reduced by rotary evaporation. The solution was precipitated into a 10-fold excess of ice/salt bath cooled Et_2O, redissolved in DCM and reprecipitated twice.

yield: 73.9 % of theory, white powder.

^{1}H NMR (400 MHz, $CDCl_3$): δ [ppm] 6.64 - 6.59 (m, 67H), 4.03 (br, 36H), 3.59 (s, 126H), 3.36 (br), 2.67 - 1.81 (br), 1.66 (s, 134H), 1.45 (s, 162H), 1.02 - 0.85 (br)

Synthesis of p(AcDMA-bocAEMA-MMA)-carbamothioate methyl methacrylate

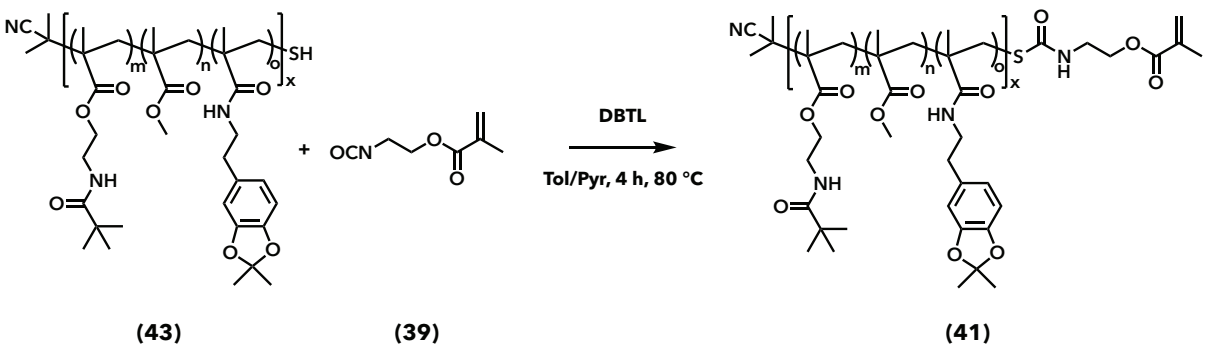

Figure 8.10

Entry	
p(AcDMA-bocAEMA-MMA)-thiol	1.0 eq.
2-isocyanatoethyl methylacrylate	1.2 eq.
DBTL	1 drop
Tol	0.015 M
Py	0.015 M

A one necked flask equipped with a magnetic stir bar was charged with the polymer p(AcDMA-bocAEMA-MMA)-thiol, Tol and Py to give a 0.015 M solution. The flask was sealed with a septum and equipped with two needles as a nitrogen in- and outlet. The solution was degassed with nitrogen for 20 min. DBTL and 2-isocyanatoethyl methylacrylate were added with a μL-syringe and the flask was heated to 80 °C in an oil bath. The reaction was conducted under nitrogen for 4 h. The solution was precipitated into a 10-fold amount of ice/salt bath cooled Et_2O, redissolved in DCM and reprecipitated twice. The obtained product was dried on high vacuum.

yield: 0.80 % of theory, white powder.

^{1}H NMR (400 MHz, DMSO-d6): δ [ppm] 6.66 - 6.59 (m, 67H), 6.05 (s, 1H), 5.67 (s, 1H), 3.84 (br, 36H), 3.52 (s, 126H), 3.15 (br), 2.58 - 1.76 (br), 1.87 (s, 6H), 1.61 (s, 134H), 1.39 (s, 162H), 0.90 - 0.72 (br)

Deprotection of p(AcDMA-bocAEMA-MMA)-carbamothioate methyl methacrylate

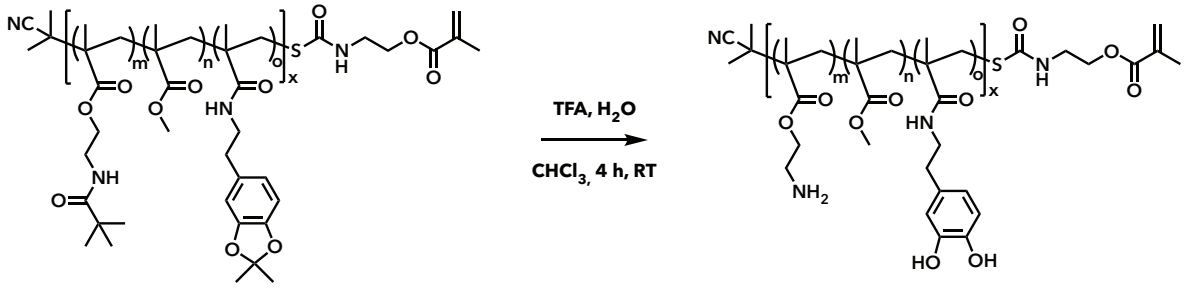

(41) **(44)**

Figure 8.11

Compound	m [g]	V [mL]
p(AcDMA-bocAEMA-MMA)-carbamothioate MMA	0.1	
TFA		0.25
H_2O		0.05
$CHCl_3$		0.75

A scintillation vial equipped with a magnetic stir bar was charged with the polymer p(AcDMA-bocAEMA-MMA)-carbamothioate MMA, TFA and $CHCl_3$. The vial was sealed with a septum and equipped with two needles as a nitrogen in- and outlet. The solution was degassed with nitrogen for 5

min. H_2O was added to the solution and the mixture was reacted for 4 h at RT under nitrogen atmosphere. The solution was precipitated into a 10-fold amount of ice/salt bath cooled Et_2O, redissolved in DCM and reprecipitated twice. The obtained white powdered product was dried on high vacuum.

^{1}H NMR (400 MHz, DMSO-d6): δ [ppm] 6.66 - 6.42 (m, 67H), 6.05 (s, 1H), 5.68 (s, 1H), 4.05 (br, 36H), 3.54 (s, 126H), 3.08 (br), 2.29 - 1.76 (br), 1.87 (s, 6H), 0.91 - 0.75 (br)

8.3.3 Random Co-Polymer

Polymerization of p(p(AcDMA-bocAEMA-MMA)-UPyHEMA-EHMA-PEG20MA)

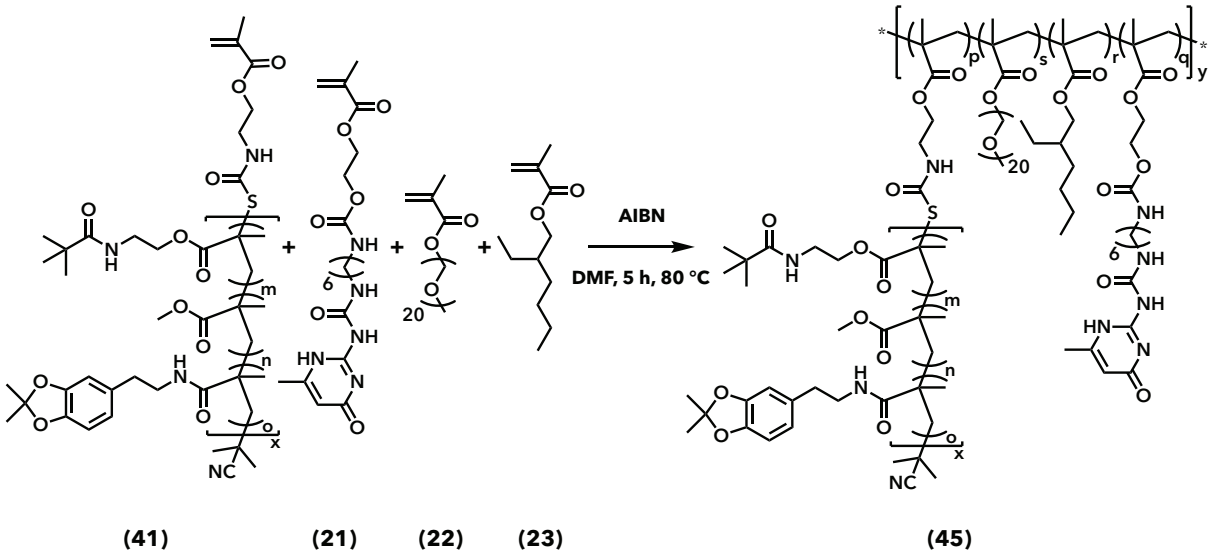

Figure 8.12

Entry	
SMM-carbamothioate MMA	0.6 eq.
UPyHEMA	11.0 eq.
EHMA	65.8 eq.
PEG20MA	22 eq.
AIBN	1 eq.
DMF	0.95 M

PEG20MA was weighed into a scintillation vial and dissolved in one fifth of the DMF by vortexing. A Schlenk flask equipped with a magnetic stir bar was charged with the dissolved PEG20MA, SMM-carbamothioate MMA, UPyHEMA, EHMA, AIBN and the remainder of DMF. The flask was sealed with a septum and three freeze-pump-thaw cycles were performed. The flask was charged with nitrogen atmosphere and put in a 80 °C oil bath for 5 h. The reaction was removed from the oil bath to let it cool down and the solution was precipitated into a 10-fold amount of ice/salt bath cooled Et_2O with 10 %

Hex. After redissolving in $CHCl_3$ with 10 % of MeOH, two more precipitation steps were performed. The product was dried on high vacuum.

yield: 75.9 % of theory, translucent off-white polymer.

Deprotection of p(p(AcDMA-bocAEMA-MMA)-UPyHEMA-EHMA-PEG20MA)

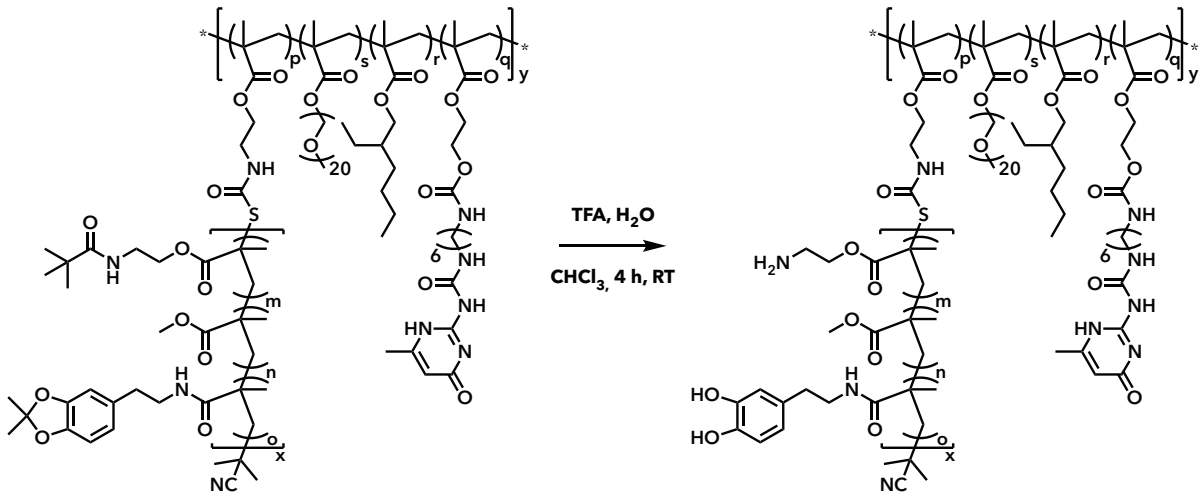

Figure 8.13

Entry	
p(p(AcDMA-bocAEMA-MMA)-UPyHEMA-EHMA-PEG20MA)	1.0 eq.
TFA	0.018 M
H_2O	5 drops
$CHCl_3$	0.006 M

A single neck flask equipped with a stir bar was charged with the polymer p(p(AcDMA-bocAEMA-MMA)-UPyHEMA-EHMA-PEG20MA), $CHCl_3$ and TFA. The flask was closed with a septum and the mixture was stirred until completely dissolved. Two needles were inserted through the septum and a constant stream of nitrogen through the solution was induced. Five drops of H_2O were added with a syringe and the solution was stirred at RT for 4 h. The solution was then precipitated into a 10-fold amount of ice/salt bath cooled Et_2O with 10 % Hex. After redissolving in $CHCl_3$ with 10 % of MeOH, two more precipitation steps were performed. The product was dried on high vacuum.

yield: 74.6 % of theory, opaque off-white polymer.

8.3.4 Matrix Polymer

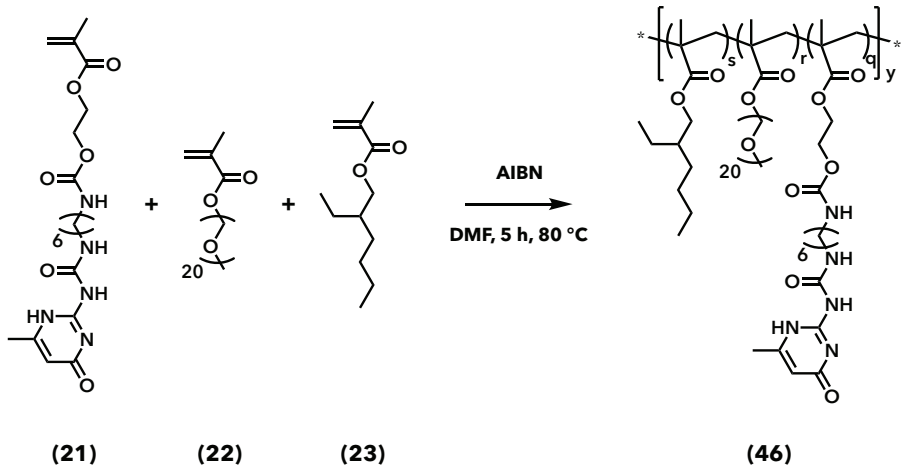

Figure 8.14

Entry	
UPyHEMA	11.0 eq.
EHMA	65.8 eq.
PEG20MA	22 eq.
AIBN	1 eq.
DMF	0.95 M

PEG20MA was weighed into a scintillation vial and dissolved in one fifth of the DMF by vortexing. A Schlenk flask equipped with a magnetic stir bar was charged with the dissolved PEG20MA, UPyHEMA, EHMA, AIBN and the remainder of DMF. The flask was sealed with a septum and three freeze-pump-thaw cycles were performed. The flask was charged with nitrogen atmosphere and put in a 80 °C oil bath for 5 h. The reaction was removed from the oil bath to let it cool down and the solution was precipitated into a 10-fold amount of ice/salt bath cooled Et_2O with 10 % Hex. After redissolving in a 3:1 mixture of DCM:MeOH, two more precipitation steps were performed. The resulting translucent polymer was dried on high vacuum.

8.3.5 Block-Co-Polymer

Polymerization of p(AcDMA-bocAEMA-MMA)-b-(UPyHEMA-EHMA-PEG20MA)-benzodithioate

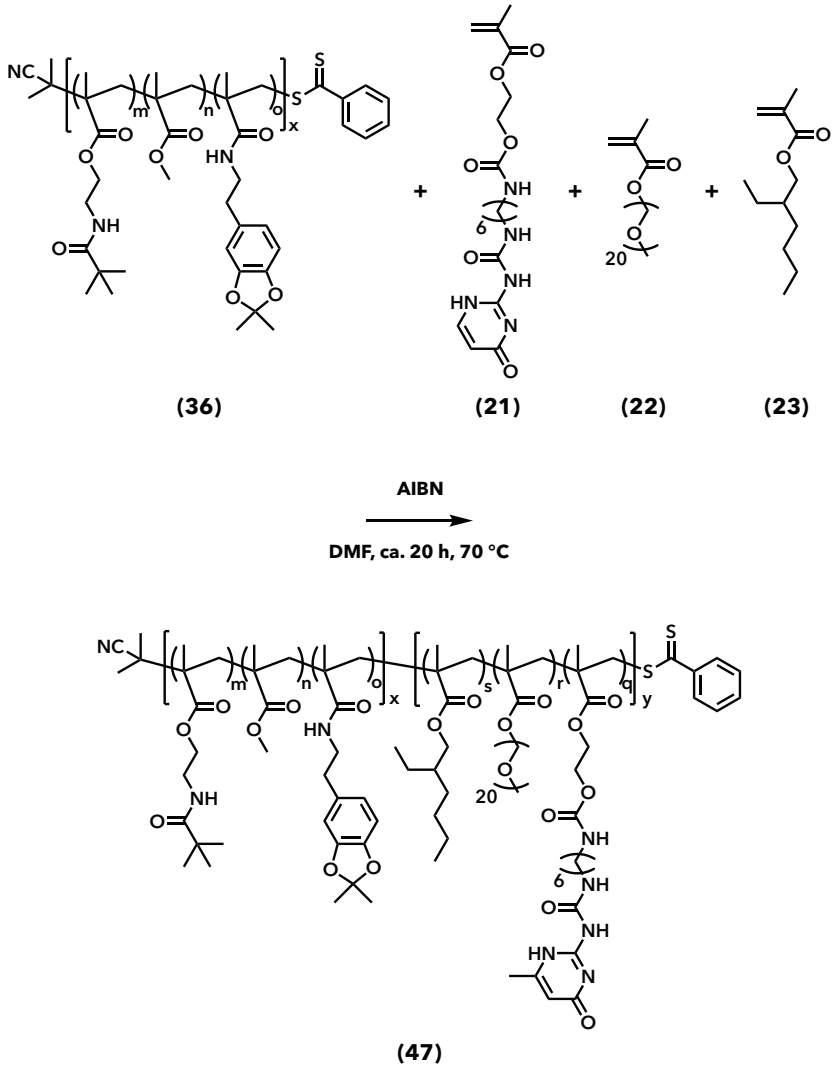

Figure 8.15

Entry	
SMM	1 eq.
UPyHEMA	9.16 eq.
EHMA	54.83 eq.
PEG20MA	18.33 eq.
AIBN	0.20 eq.
DMF	2 M

PEG20MA was weighed into a scintillation vial and dissolved in 2 mL of the DMF by vortexing. The reaction solution from the synthesis of p(AcDMA-bocAEMA-MMA) was used without any further precipitation steps. The Schlenk flask equipped with a magnetic stir bar containing the SMM in DMF

was charged with UpyHEMA, EHMA, PEG20MA in DMF and AIBN. It was sealed with a septum and three freeze-pump-thaw cycles were performed. The flask was charged with nitrogen atmosphere and put in a 70 °C oil bath. Samples were drawn and analyzed by ^{1}H NMR at the beginning and toward the end of the reaction to determine 80 % conversion. After complete polymerization (about 20 h) the reaction was quenched with liquid nitrogen and air. One drop of solution was precipitated into a 10-fold amount of ice/salt bath cooled Et_2O with 10 % Hex. After redissolving in $CHCl_3$ with 10 % MeOH, two more precipitation steps were performed. The product was dried on high vacuum. The bulk of the reaction solution was used without any precipitation for the end group cleavage.

Synthesis of p(AcDMA-bocAEMA-MMA)-b-(UPyHEMA-EHMA-PEG20MA)

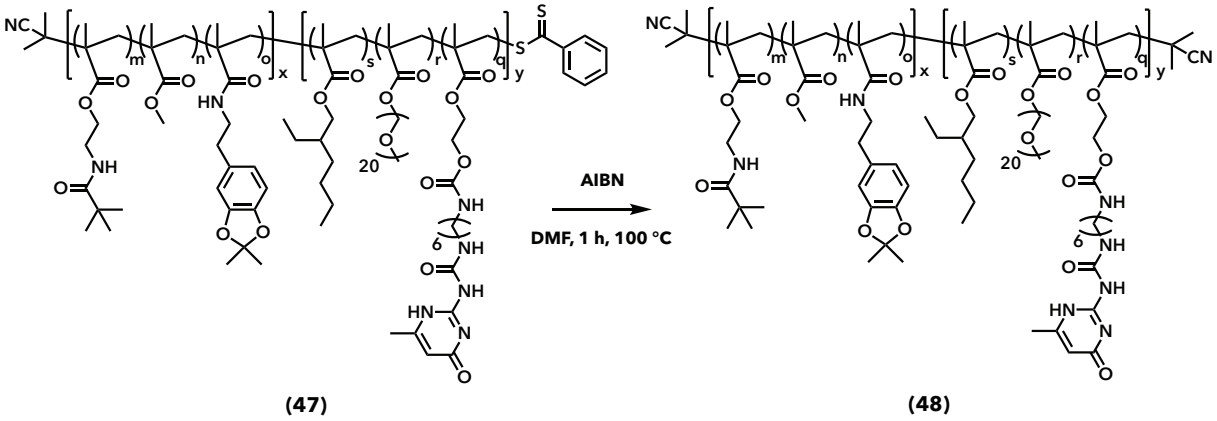

Figure 8.16

Entry	
p(AcDMA-bocAEMA-MMA)-b-(UPyHEMA-EHMA-PEG20MA)-benzodithioate	1.0 eq.
AIBN	20.0 eq.

The reaction solution obtained from the synthesis of p(AcDMA-bocAEMA-MMA)-b-(UPyHEMA-EHMA-PEG20MA)-benzodithioate was used without further precipitation steps. The Schlenk flask containing the solution was charged with AIBN and a constant flow of nitrogen was induced. The reaction was heated to 100 °C in an oil bath and stirred for 1 h. The reaction was quenched with liquid nitrogen and air. The solution was precipitated into a 10-fold amount of ice/salt bath cooled Et_2O with 10 % Hex. After redissolving in $CHCl_3$ with 10 % MeOH, two more precipitation steps were performed. The product was dried on high vacuum.

yield: 78.5 % of theory, translucent polymer with yellow hue.

Deprotection of p(AcDMA-bocAEMA-MMA)-b-(UPyHEMA-EHMA-PEG20MA)

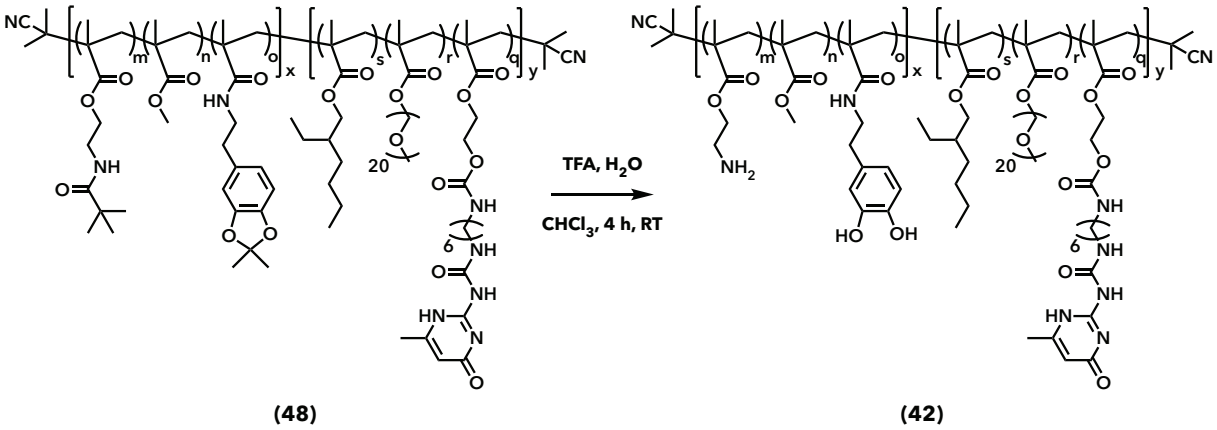

(48) (42)

Figure 8.17

Entry	
p(p(AcDMA-bocAEMA-MMA)-UPyHEMA-EHMA-PEG20MA)	1.0 eq.
TFA	0.018 M
H_2O	5 drops
$CHCl_3$	0.006 M

A single neck flask equipped with a stir bar was charged with the polymer p(AcDMA-bocAEMA-MMA)-b-(UPyHEMA-EHMA-PEG20MA), $CHCl_3$ and TFA. The flask was closed with a septum and the mixture was stirred until completely dissolved. Two needles were inserted through the septum and a constant stream of nitrogen for degassing the solution was induced. Five drops of H_2O were added with a syringe and the solution was stirred at RT for 4 h. The solution was then precipitated into a 10-fold amount of ice/salt bath cooled Et_2O with 10 % Hex. After redissolving in $CHCl_3$ with 10 % of MeOH, four more precipitation steps were performed. The product was dried on high vacuum.

yield: 80.7 % of theory, translucent polymer with yellow hue.

9 General Methods

Polymer films were prepared by **compression molding** the desired amount of polymer between two sheets of PTFE film with a spacer of 0.13 mm thickness on a Grizzly Industrial 10-ton benchtop shop press with heated plates. The press was operated at 200 bar and 65 °C and films were pressed multiple times for 30 sec each.

Cytocompatibility studies were carried out by Sally Winkler of the Messersmith lab. Cell viability was tested *via* a conditioned media test according to the standard ISO 10993-5 with NIH 3T3 (mouse

fibroblast) and CCD-32sk (human fibroblast) cells. Media (DMEM, FBS, pen/strep) was conditioned with 20 mg/mL polymer patch for 24 h at 27 °C and stored at -80 °C. Thawed, diluted media was put on cells and incubated for at least 24 h. Absorption measurements were performed on a Tecan Infinite 200 Plate Reader at 540 nm.

Differential scanning calorimetry (DSC) was performed on a Mettler Toledo DSC 1 STARe System with liquid nitrogen cooling with heating/cooling rates of of 10 °C/minute, unless otherwise indicated. Temperature ranges were within -100 to 200 °C with typical measurements consisting of three cycles of heating and cooling.

The **failure mode** was assessed visually with the help of the Arnow stain. Bovine pericardium tissue specimens and polymer specimens after tissue shear adhesion testing were immersed in 0.5 N HCl, a salt solution (100 g/L $NaNO_2$, 100 g/L Na_2MoO_4) and 1 N NaOH consecutively for 5 min each and their discoloration was assessed visually.

FT-IR spectra were recorded on a Bruker Vertex80 Time-resolved FTIR, using OPUS software for data analysis. Spectra were recorded from 4000 to 400 cm^{-1}.

Gel Permeation Chromatography (GPC) was performed on an Agilent 1260 Infinity II system with DMF with 0.02 M LiBr mobile phase (flow rate 0.6 mL/min) equipped with one Guard and two Polypore Columns (PS-DVB Column Material, 5 μm particle size, 200-2 MM g/mol range) and an RI and UV detector, calibrated with PMMA standards. Samples were prepared in 2 mg/mL concentration, stored in THF for 24 h and filtered with a 0.2 μm PTFE syringe filter before injection into the instrument. Chromatograms were processed with Agilent SEC Software 2.1.9.

^{1}H NMR spectra were recorded on a Bruker AVB-400 (400.13 MHz) spectrometer equipped with a 5 mm Z-gradient broad band probe, a Bruker AVQ-400 (400.13 MHz) spectrometer equipped with a 5 mm Quad Nucleus probe and a Bruker AV-500 (500.23 MHz) spectrometer equipped with a 5 mm Z-gradient Triple Broad Band Inverse detection probe in deuterated solvents. Spectra were processed in MestReNova 14.1.0 (Mestrelab Research).

Tensile testing was carried out on an Instron universal materials tester equipped with a 5 kN load cell with a rate of tensile strain of 0.25 %/min. Specimens were cut out dog bone shaped. Specimens were attached to the clamps with handles of sand paper to facilitate clamping. Elastic moduli were determined from the initial 5 % strain of the stress strain curves.

Tissue shear adhesion testing was carried out using a procedure described in ASTM-2255-05 on an Instron universal materials tester equipped with a 5 kN load cell with a rate of shear of 5 mm/min. The specimen width and length was 10 mm and the bonded overlap thickness was measured with a digital caliper prior to testing. Adhesion strength was determined by the maximum load divided by the bonded overlap area. Typically, specimens were prepared by attaching a polymer film piece of 1 x 1 cm

to a stripe of polycarbonate (PC) with cyanoacrylate glue. PC stripes with bovine pericardium tissue were prepared by defrosting the tissue in PBS and attaching stripes of 1 x 1.5 - 3 cm to the PC substrate with cyanoacrylate glue. Polymer and bovine pericardium surfaces were gently pressed together and incubated in PBS at 37 °C under a force of 2 N for 20 to 120 min.

Statistical analysis was performed using a Mann-Whitney-U-test and a p-value of <0.05 was considered to be significant if not indicated otherwise.

Swelling Properties were assessed by swelling polymer film specimens in PBS and tracking their weight change over a range of 0 to 20 h. Caution was taken to carefully pad the specimens dry before weighing.

Appendix A List of Structures

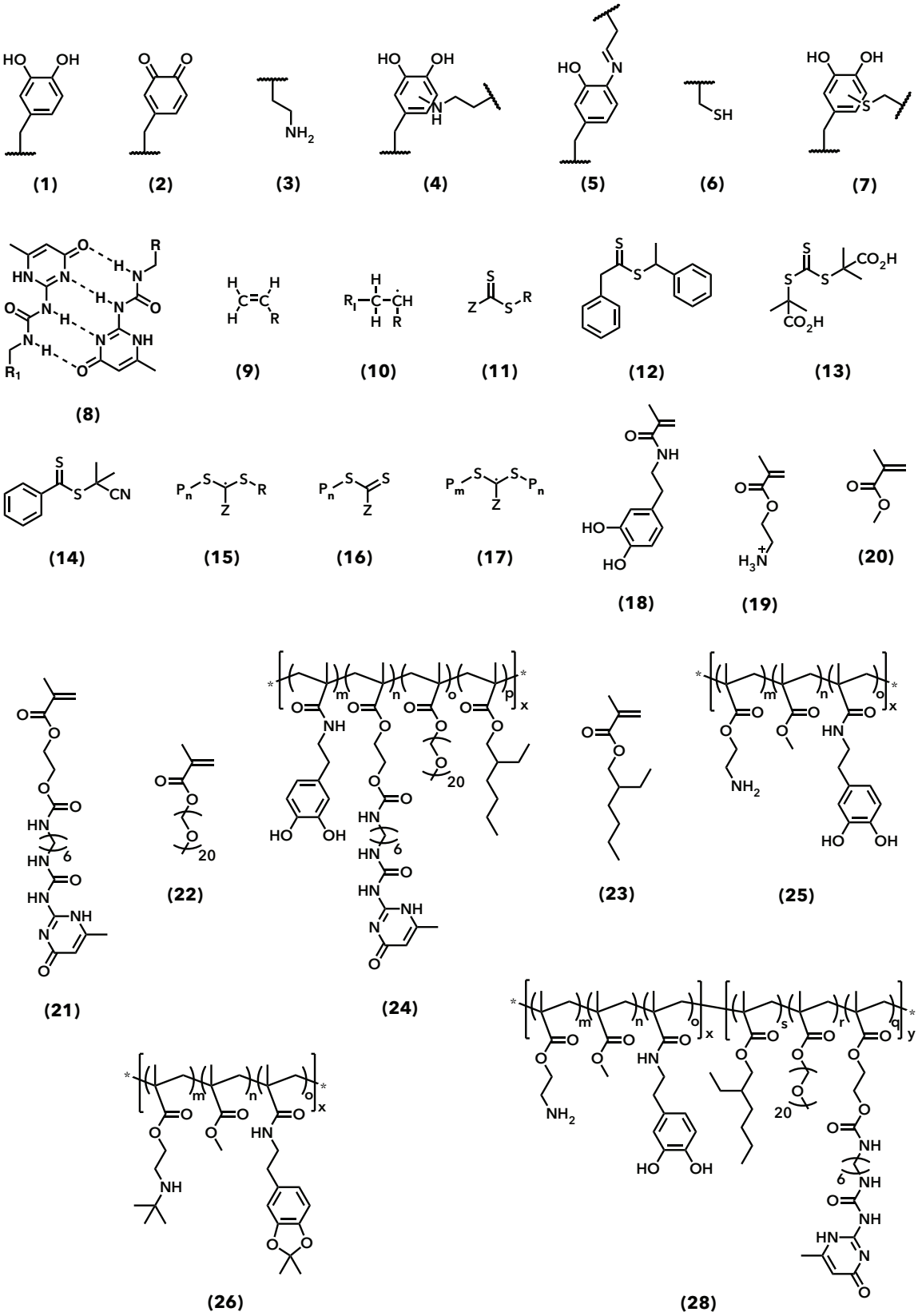

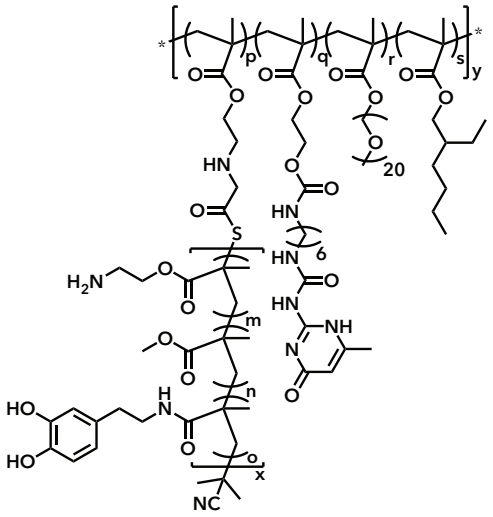

(27)

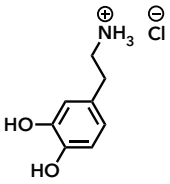

(29)

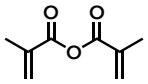

(30)

(31)

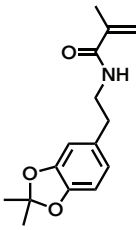

(32)

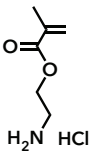

(33)

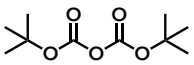

(34)

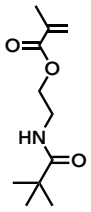

(35)

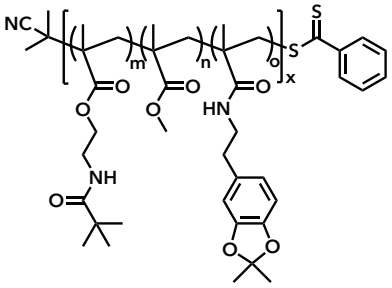

(36)

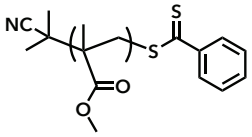

(37)

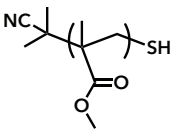

(38)

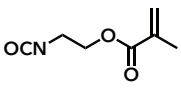

(39)

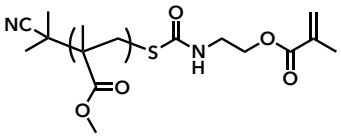

(40)

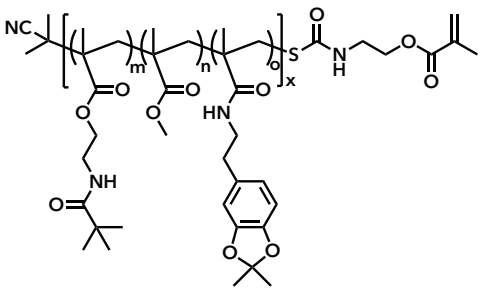

(41)

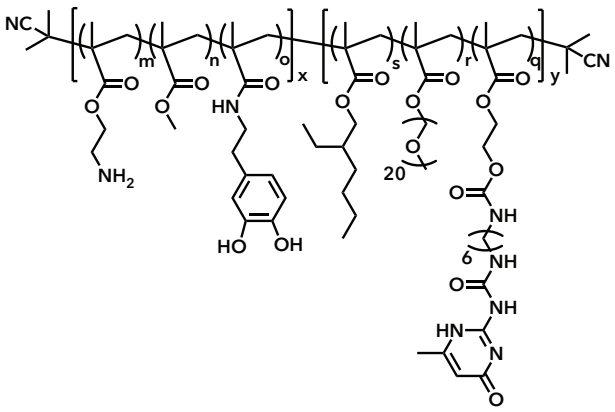

(42)

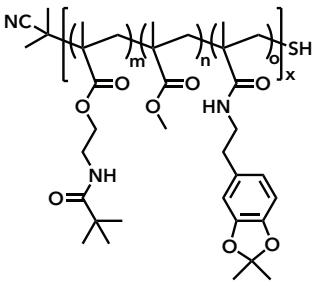

(43)

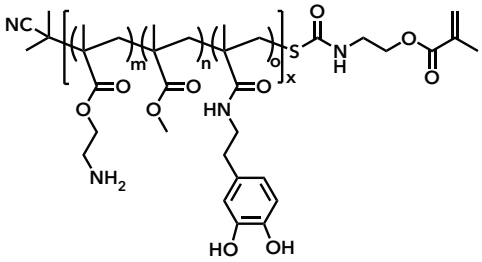

(44)

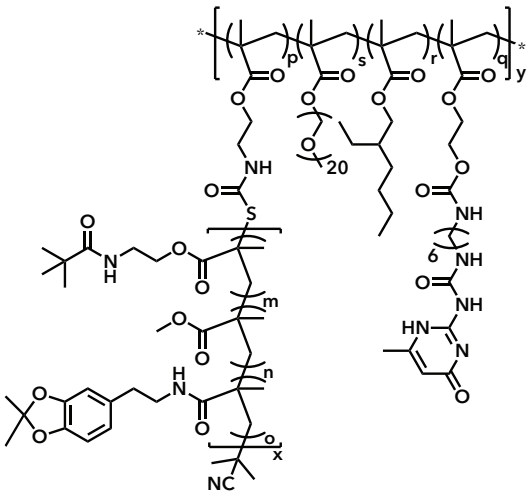

(45)

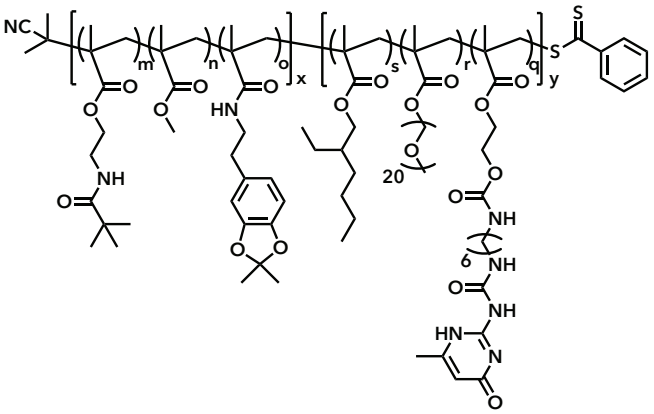

(47)

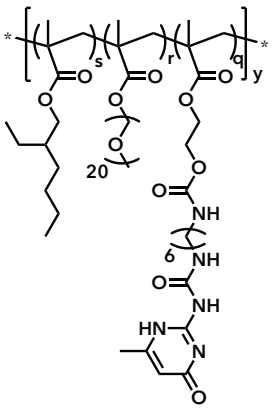

(46)

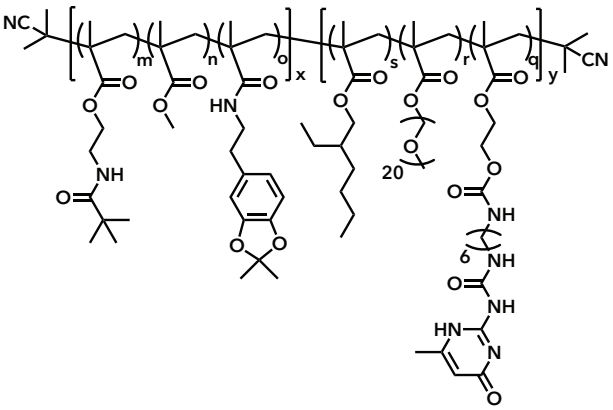

(48)

Appendix B

B.1 Sequence macromonomer p(AcDMA-bocAEMA-MMA)

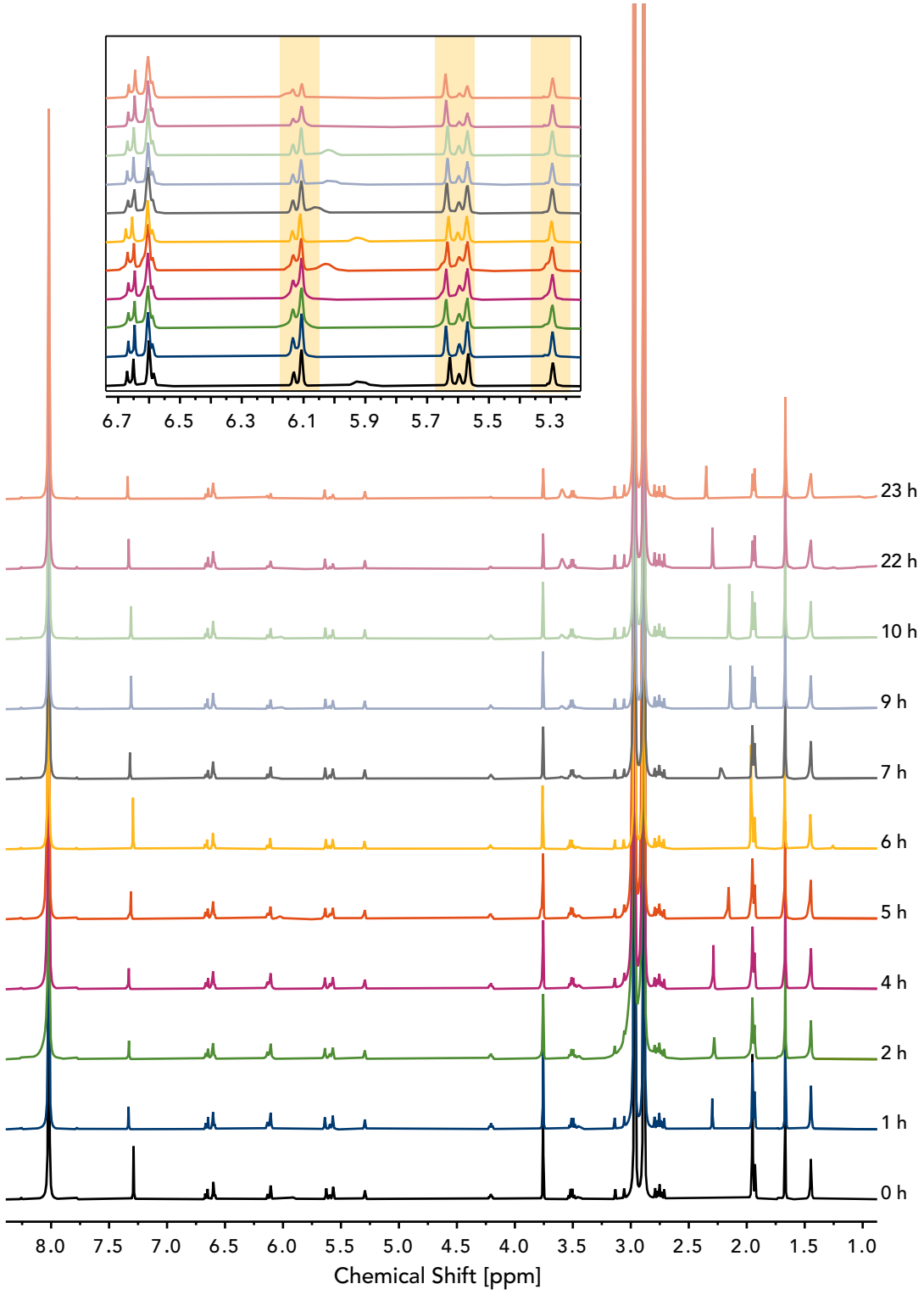

Figure B.1: Stacked ^{1}H NMR spectra of the progressing RAFT polymerization of the SMM from t = 0 h to t = 23 h.

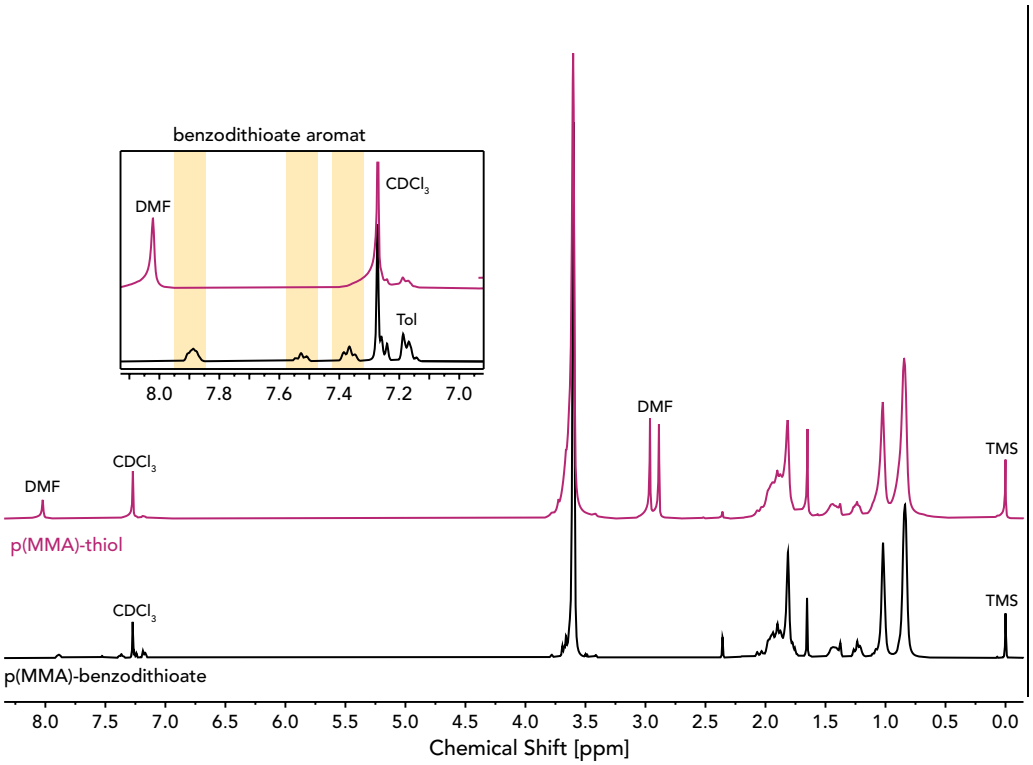

Figure B.2: ^{1}H NMR spectra of p(MMA)-benzodithioate (black) and p(MMA)-thiol (pink). The aromatic benzodithioate peaks are highlighted to show full conversion to the thiol.

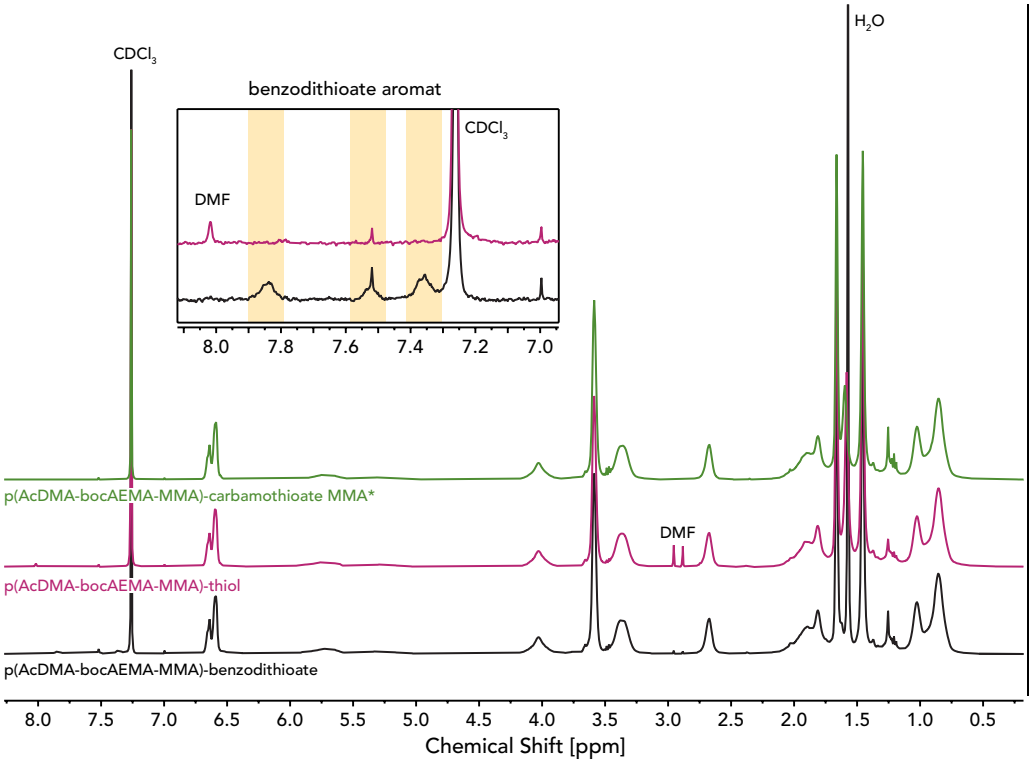

Figure B.3: ^{1}H NMR spectra of a second batch of p(AcDMA-bocAEMA-MMA) with the end group benzodithioate (black), thiol (pink) and after the attempted click reaction towards carbamothioate MMA (green). Signals for the latter were expected at 6.05-5.67 ppm. The aromatic benzodithioate peaks are highlighted to show full conversion to the thiol. *Reaction did not work and the product is not p(AcDMA-bocAEMA-MMA)-carbamothioate MMA.

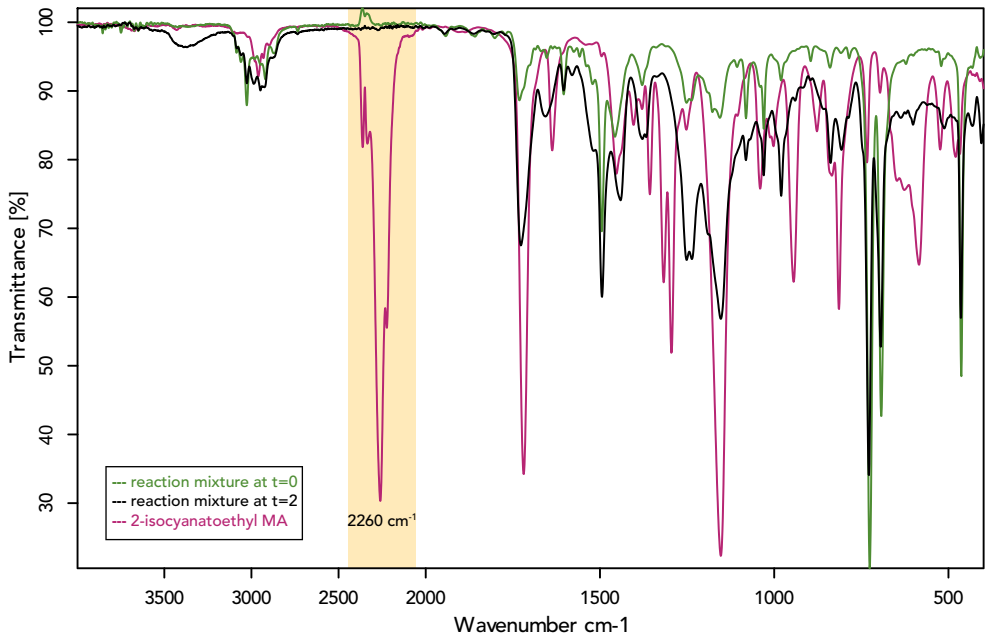

Figure B.4: IR spectrum of 2-isocyanatoethyl MA (pink) and the reaction mixture of the SMM end group functionalization from SMM-thiol to SMM-carbamothioate MMA at t = 0 h (green) and t = 2 h (black). The band caused by the isocyanate at 2260 cm^{-1} is highlighted in yellow.

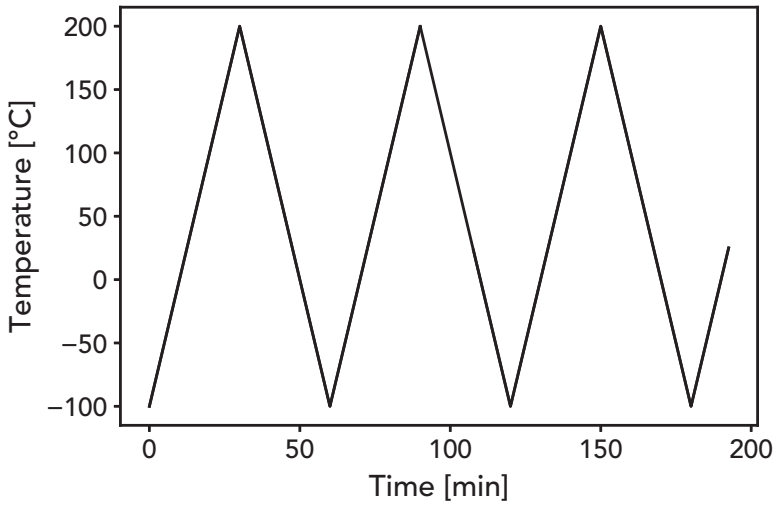

Figure B.5: DSC heating curve applied in measurements of the SMM, dry patches of random co-polymer and dry patches of block-co-polymer.

Table B.1: Calculations of M_W, conversion and monomer ratios of the SMM from ^{1}H NMR for all batches.

SMM batch		1	2	3	4	5	6	7	8
Mw [g/mol]		15193	10876	14341	21680	13064	38256*	14333	12472
M [mol/L]		0.95	2	2	2	2	2	2	2
conversion [%]		62	81	84	59	83	74	80	95
monomer entry [g]		1.01	5.04	6.72	1.68	6.72	1.68	4.24	1.68
monomer ratio [%mol]	MMA	56.8	51.7	51.3	55.2	53	57.2	53.1	54
	AcDMA	23.1	25.4	27.2	24.2	26.4	24.7	25.5	26.3
	bocAEMA	20	22.9	21.6	20.7	20.6	18.1	21.5	19.7
difference to calculated ratio [%]	MMA	13.6	3.4	2.6	10.4	6	14.4	6.2	8
	AcDMA	-7.6	1.6	8.8	-3.2	5.6	-1.2	2	5.2
	bocAEMA	-20	-8.4	-13.6	-17.2	-17.6	-27.6	-14	-21.2

* A peak in the benzodithioate region was only visible upon changing exponential apodiziation along t1 to 5 Hz and no proper calculation of the M_W was possible.

B.2 Random Co-polymer and Block-co-polymer

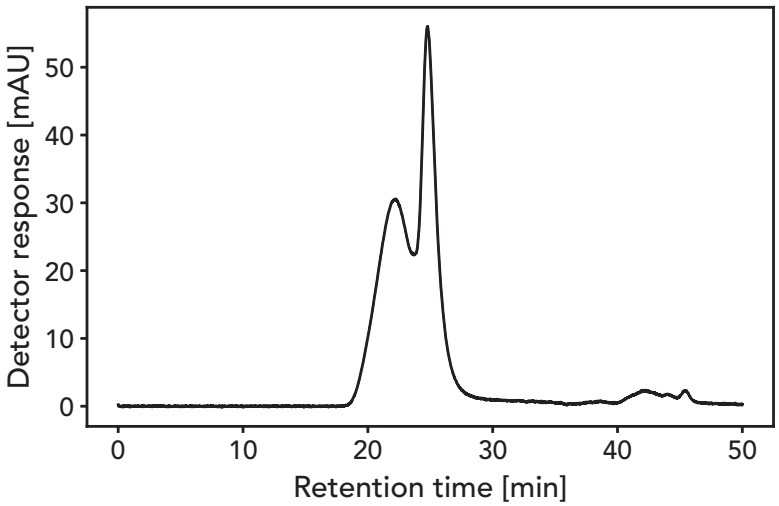

Figure B.6: GPC chromatogram of the second batch of random co-polymer in its protected state, showing a bimodal distribution.

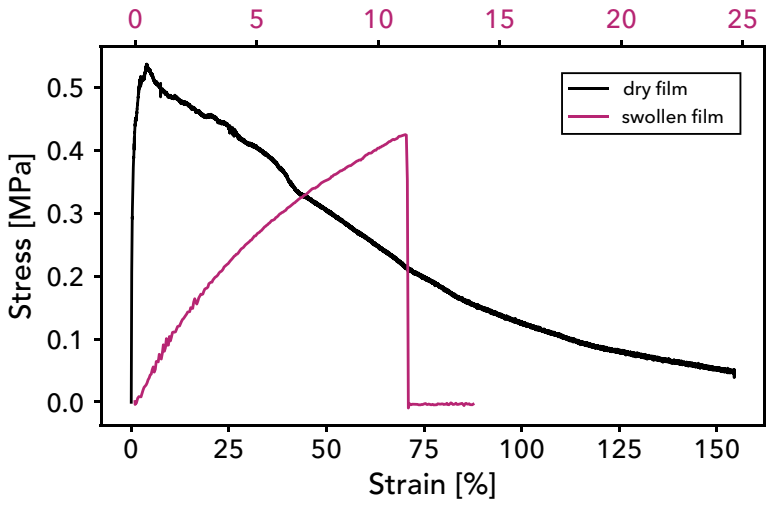

Figure B.7: Characteristic stress-strain curves of the block-co-polymer in its dry (black) and swollen (pink) state.

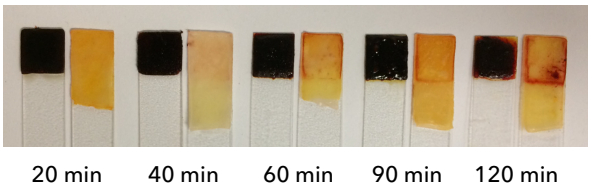

Figure B.8: Random co-polymer batch 2 tissue adhesion samples of different incubation times after shear adhesion testing. Samples were discolored with Arnow stain to determine the failure mode.

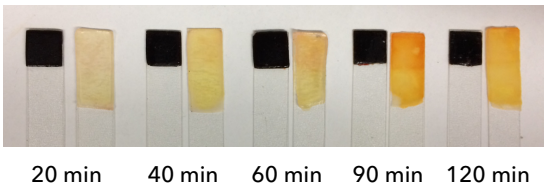

Figure B.9: Block-co-polymer batch 2 tissue adhesion samples of different incubation times after shear adhesion testing. Samples were discolored with Arnow stain to determine the failure mode.

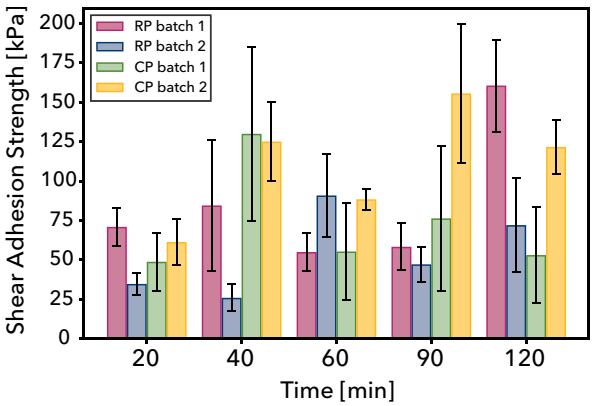

Figure B.10: Tissue adhesion strength as a function of time for both batches of random co-polymer (pink and blue) and block-co-polymer (green and yellow), depicted with standard deviations.

Table B.2: Weight uptake of PBS during swelling experiments for both batches of random co-polymer and block-co-polymer each.

	PBS intake [%w]			
	random co-polymer		block-co-polymer	
time [min]	batch 1	batch 2	batch 1	batch 2
0	0	0	0	0
10	192.9 ± 20.5	182.7 ± 13.5	106.7 ± 6.3	96.1 ± 8.9
20		219.8 ± 30	114.7 ± 4.2	112.5 ± 3.2
30	255.9 ± 44.6	245.7 ± 7.8	117.6 ± 4.4	118.6 ± 1
45		250.7 ± 32.7		119.9 ± 2.1
50	276.3 ± 50.8			
60		262.2 ± 28.8		121.3 ± 2.1
85	306.2 ± 10.4			
90		275.8 ± 29.1	126.8 ± 3.7	123.2 ± 4.1
120		282.2 ± 26.9		129.6 ± 7.5
140	301.7 ± 15.1			
180		311.3 ± 38.6		132.7 ± 6.8
200	306.2 ± 18.4			
370			137.9 ± 2.9	
425	314.2 ± 24.2			
1230		320.1 ± 28.6		141.1 ± 7.7
5760	282.7 ± 34.5		149.7 ± 2.9	

Table B.3: Shear adhesion strength to bovine pericardium tissue in dependence of incubation time for both batches of random co-polymer and block-co-polymer.

	shear adhesion strength [kPa]			
	random co-polymer		block-co-polymer	
time	batch 1	batch 2	batch 1	batch 2
20	71.01 ± 11.97[1]	34.80 ± 6.77	48.86 ± 18.30	61.35 ± 14.45
30	50.46 ± 13.69			
40	84.59 ± 41.83[2]	26.00 ± 8.61	130.06 ± 55.16[2]	125.11 ± 24.97
60	71.82 ± 29.64	90.93 ± 26.49	55.36 ± 30.69	88.49 ± 6.54
75	67.94 ± 25.96			
90	58.38 ± 14.94	47.23 ± 11.01	76.38 ± 45.91	155.67 ± 43.93
120	160.68 ± 29.17[3]	72.09 ± 29.97	53.10 ± 30.37	121.73 ± 17.23

[1] Incubation duration was 15 min.
[2] Incubation duration was 45 min.
[3] Incubation duration was 150 min.

Table B.4: Cytoviability data for the block-co-polymer at different concentrations with NIH 3T3 cells (mouse fibroblast) and CCD-32sk cells (human fibroblast), listed with positive and negative control group.

	cell type	
	NIH 3T3	CCD-32sk
positive control	100 ± 10.33	100 ± 7.2
negative control	1.41 ± 6.57	3.12 ± 4.5
5 mg/mL	104.84 ± 14.64	100.12 ± 9.65
10 mg/mL	90.84 ± 8.37	89.12 ± 6.21
20 mg/mL	85.4 ± 8.37	91.65 ± 6.21

Bibliography

[1] K. M. Maselli, A. Badillo, *Ann Transl Med* **2016**, *4*, 394.

[2] C. E. Graves, M. R. Harrison, B. E. Padilla, *Clin Perinatol* **2017**, *44*, 729–751.

[3] J. M. Estes, T. E. MacGillivray, M. H. Hedrick, N. S. Adzick, M. R. Harrison, *J Pediatr Surg* **1992**, *27*, 950–4.

[4] S. M. Winkler, M. R. Harrison, P. B. Messersmith, *Biomater Sci* **2019**, *7*, 3092–3109.

[5] T. Jancelewicz, M. R. Harrison, *Clin Perinatol* **2009**, *36*, 227–36, vii.

[6] P. Y. Ancel, F. Goffinet, E.-. W. Group, P. Kuhn, B. Langer, J. Matis, X. Hernandorena, P. Chabanier, L. Joly-Pedespan, B. Lecomte, F. Vendittelli, M. Dreyfus, B. Guillois, A. Burguet, P. Sagot, J. Sizun, A. Beuchee, F. Rouget, A. Favreau, E. Saliba, N. Bednarek, P. Morville, G. Thiriez, L. Marpeau, S. Marret, G. Kayem, X. Durrmeyer, M. Granier, O. Baud, P. H. Jarreau, D. Mitanchez, P. Boileau, P. Boulot, G. Cambonie, H. Daude, A. Bedu, F. Mons, J. Fresson, R. Vieux, C. Alberge, C. Arnaud, C. Vayssiere, P. Truffert, V. Pierrat, D. Subtil, C. D'Ercole, C. Gire, U. Simeoni, A. Bongain, L. Sentilhes, J. C. Roze, J. Gondry, A. Leke, M. Deiber, O. Claris, J. C. Picaud, A. Ego, T. Debillon, A. Poulichet, E. Coline, A. Favre, O. Flechelles, S. Samperiz, D. Ramful, B. Branger, V. Benhammou, L. Foix-L'Helias, L. Marchand-Martin, M. Kaminski, *JAMA Pediatr* **2015**, *169*, 230–8.

[7] A. Kivelio, N. Ochsenbein-Koelble, R. Zimmermann, M. Ehrbar, *Acta Biomater* **2015**, *15*, 1–10.

[8] F. Breathnach, S. Daly, E. Griffin, N. Gleeson, *J Perinat Med* **2005**, *33*, 458–60.

[9] B. K. Young, A. S. Roman, A. P. MacKenzie, C. D. Stephenson, V. Minior, A. Rebarber, I. Timor-Tritsch, *Fetal Diagnosis and Therapy* **2004**, *19*, 296–300.

[10] L. K. Mann, R. Papanna, K. J. Moise, R. H. Byrd, E. J. Popek, S. Kaur, S. C. G. Tseng, R. J. Stewart, *Acta Biomaterialia* **2012**, *8*, 2160–2165.

[11] D. W. R. Balkenende, Y. Li, B. Estipona, P. B. Messersmith, "Orthogonal supramolecular polymers as surgical adhesives", Unpublished Work.

[12] G. Hanks, T.W.; Swiegers in *Bioinspiration and Biomimicry in Chemistry*, **2012**, pp. 1–15.

[13] B. A. Armitage, *Annual Reports Section "B" (Organic Chemistry)* **2000**, *96*, 187–229.

[14] W. H. Binder, M. Schunack, F. Herbst, B. Pulamagatta in *Bioinspiration and Biomimicry in Chemistry*, **2012**, pp. 323–366.

[15] G. F. Swiegers, J. Chen, P. Wagner in *Bioinspiration and Biomimicry in Chemistry*, **2012**, pp. 165–208.

[16] P. Aranda, F. M. Fernandes, B. Wicklein, E. Ruiz-Hitzky, H. J. P., K. Ariga in *Bioinspiration and Biomimicry in Chemistry*, **2012**, pp. 121–138.

[17] R. W. Hoffmann in *Bioinspiration and Biomimicry in Chemistry*, **2012**, pp. 419–453.

[18] Z. Zhu, C.; Gu in *Bioinspiration and Biomimicry in Chemistry*, **2012**, pp. 293–322.

[19] G. D. Bixler, B. Bhushan, *Soft Matter* **2012**, *8*, 11271–11284.

[20] M. Zhang, S. Feng, L. Wang, Y. Zheng, *Biotribology* **2016**, *5*, 31–43.

[21] I. P. Parkin, R. G. Palgrave, *Journal of Materials Chemistry* **2005**, *15*, 1689–1695.

[22] M. Heim, D. Keerl, T. Scheibel, *Angewandte Chemie International Edition* **2009**, *48*, 3584–3596.

[23] Y. Zhao, Z. Xie, H. Gu, C. Zhu, Z. Gu, *Chemical Society Reviews* **2012**, *41*, 3297–3317.

[24] L. Lindoy, C. Richardson, J. Clegg in *Bioinspiration and Biomimicry in Chemistry*, **2012**, pp. 17–46.

[25] M. Nakano, J. R. Shen, K. Kamino, *Biomacromolecules* **2007**, *8*, 1830–5.

[26] J. H. Waite, *J Exp Biol* **2017**, *220*, 517–530.

[27] D. W. R. Balkenende, S. M. Winkler, P. B. Messersmith, *European Polymer Journal* **2019**, *116*, 134–143.

[28] S. Baik, D. W. Kim, Y. Park, T. J. Lee, S. Ho Bhang, C. Pang, *Nature* **2017**, *546*, 396–400.

[29] H. Shao, K. N. Bachus, R. J. Stewart, *Macromol Biosci* **2009**, *9*, 464–71.

[30] C. Liang, J. Strickland, Z. Ye, W. Wu, B. Hu, D. Rittschof, *Frontiers in Marine Science* **2019**, *6*.

[31] A. P. Duarte, J. F. Coelho, J. C. Bordado, M. T. Cidade, M. H. Gil, *Progress in Polymer Science* **2012**, *37*, 1031–1050.

[32] P. Kord Forooshani, B. P. Lee, *J Polym Sci A Polym Chem* **2017**, *55*, 9–33.

[33] J. H. Waite, N. H. Andersen, S. Jewhurst, C. Sun, *The Journal of Adhesion* **2005**, *81*, 297–317.

[34] J. H. Waite, M. L. Tanzer, *Science* **1981**, *212*, 1038–40.

[35] H. Lee, N. F. Scherer, P. B. Messersmith, *Proc Natl Acad Sci U S A* **2006**, *103*, 12999–3003.

[36] H. Zhao, C. Sun, R. J. Stewart, J. H. Waite, *J Biol Chem* **2005**, *280*, 42938–44.

[37] J. H. Waite, *Comp Biochem Physiol B* **1990**, *97*, 19–29.

[38] M. V. Rapp, G. P. Maier, H. A. Dobbs, N. J. Higdon, J. H. Waite, A. Butler, J. N. Israelachvili, *J Am Chem Soc* **2016**, *138*, 9013–6.

[39] A. D. Jenkins, P. Kratochvíl, R. F. T. Stepto, U. W. Suter, Glossary of basic terms in polymer science (IUPAC Recommendations 1996), **1996**.

[40] H. P. Latscha, U. Kazmaier, H. Klein, *Springer-Lehrbuch* **2016**, XXIV, 629.

[41] P. C. Nicolson, J. Vogt, *Biomaterials* **2001**, *22*, 3273–83.

[42] S. Koltzenburg, M. Maskos, O. Nuyken, **2014**.

[43] R. Jain, S. Wairkar, *Int J Biol Macromol* **2019**, *137*, 95–106.

[44] M. Perrini, D. Barrett, N. Ochsenbein-Koelble, R. Zimmermann, P. Messersmith, M. Ehrbar, *Journal of the Mechanical Behavior of Biomedical Materials* **2016**, *58*, 57–64.

[45] T. Aida, E. W. Meijer, S. I. Stupp, *Science* **2012**, *335*, 813.

[46] V. I. Minkin, Glossary of terms used in theoretical organic chemistry, **1999**.

[47] L. M. de Espinosa, G. L. Fiore, C. Weder, E. Johan Foster, Y. C. Simon, *Progress in Polymer Science* **2015**, *49-50*, 60–78.

[48] R. E. Kieltyka, A. C. Pape, L. Albertazzi, Y. Nakano, M. M. Bastings, I. K. Voets, P. Y. Dankers, E. W. Meijer, *J Am Chem Soc* **2013**, *135*, 11159–64.

[49] L. Brunsveld, J. A. Vekemans, J. H. Hirschberg, R. P. Sijbesma, E. W. Meijer, *Proc Natl Acad Sci U S A* **2002**, *99*, 4977–82.

[50] J. L. Mann, A. C. Yu, G. Agmon, E. A. Appel, *Biomaterials Science* **2018**, *6*, 10–37.

[51] M. J. Webber, E. A. Appel, E. W. Meijer, R. Langer, *Nat Mater* **2016**, *15*, 13–26.

[52] R. P. Sijbesma, F. H. Beijer, L. Brunsveld, B. J. B. Folmer, J. H. K. K. Hirschberg, R. F. M. Lange, J. K. L. Lowe, E. W. Meijer, *Science* **1997**, *278*, 1601.

[53] E. Krieg, M. M. C. Bastings, P. Besenius, B. Rybtchinski, *Chemical Reviews* **2016**, *116*, 2414–2477.

[54] P. Y. W. Dankers, T. M. Hermans, T. W. Baughman, Y. Kamikawa, R. E. Kieltyka, M. M. C. Bastings, H. M. Janssen, N. A. J. M. Sommerdijk, A. Larsen, M. J. A. van Luyn, A. W. Bosman, E. R. Popa, G. Fytas, E. W. Meijer, *Advanced Materials* **2012**, *24*, 2703–2709.

[55] P. Y. W. Dankers, M. C. Harmsen, L. A. Brouwer, M. J. A. Van Luyn, E. W. Meijer, *Nature Materials* **2005**, *4*, 568–574.

[56] H. Elias in *Makromoleküle, Vol. 3*, **2001**, pp. 82–142.

[57] J. Chiefari, Y. K. Chong, F. Ercole, J. Krstina, J. Jeffery, T. P. T. Le, R. T. A. Mayadunne, G. F. Meijs, C. L. Moad, G. Moad, E. Rizzardo, S. H. Thang, *Macromolecules* **1998**, *31*, 5559–5562.

[58] G. Moad, E. Rizzardo, S. Thang, *Australian Journal of Chemistry - AUST J CHEM* **2006**, *59*.

[59] H. Tobita in *Ullmann's Encyclopedia of Industrial Chemistry*, **2015**, pp. 1–50.

[60] M. R. Hill, R. N. Carmean, B. S. Sumerlin, *Macromolecules* **2015**, *48*, 5459–5469.

[61] G. Moad, E. Rizzardo, S. H. Thang, *Australian Journal of Chemistry* **2009**, *62*, 1402–1472.

[62] C. M. Haller, W. Buerzle, C. E. Brubaker, P. B. Messersmith, E. Mazza, N. Ochsenbein-Koelble, R. Zimmermann, M. Ehrbar, *Prenat Diagn* **2011**, *31*, 654–60.

[63] A. Stepuk, J. G. Halter, A. Schaetz, R. N. Grass, W. J. Stark, *Chemical Communications* **2012**, *48*.

[64] G. P. Maier, M. V. Rapp, J. H. Waite, J. N. Israelachvili, A. Butler, *Science* **2015**, *349*, 628–32.

[65] R. Wang, J. Li, W. Chen, T. Xu, S. Yun, Z. Xu, Z. Xu, T. Sato, B. Chi, H. Xu, *Advanced Functional Materials* **2017**, *27*.

[66] C. Heinzmann, U. Salz, N. Moszner, G. L. Fiore, C. Weder, *ACS Appl Mater Interfaces* **2015**, *7*, 13395–404.

[67] C. Freij-Larsson, T. Nylander, P. Jannasch, B. Wesslen, *Biomaterials* **1996**, *17*, 2199–207.

[68] B. P. Lee, J. L. Dalsin, P. B. Messersmith, *Biomacromolecules* **2002**, *3*, 1038–47.

[69] M. Gerst, B. B. Tiu, P. B. Messersmith, P. A. Delparastan, Acrylic copolymers for wet pressure-sensitive adhesives, **2019**.

[70] H. Lee, B. P. Lee, P. B. Messersmith, *Nature* **2007**, *448*, 338–41.

[71] Z. Liu, B. H. Hu, P. B. Messersmith, *Tetrahedron Lett* **2010**, *51*, 2403–2405.

[72] P. G. M. Wuts in *Greene's Protective Groups in Organic Synthesis*, **2014**, Chapter 7, pp. 895–1193.

[73] M.-H. Dufresne, J.-C. Leroux, *Pharmaceutical Research* **2004**, *21*, 160–169.

[74] P. Dubruel, B. Christiaens, M. Rosseneu, J. Vandekerckhove, J. Grooten, V. Goossens, E. Schacht, *Biomacromolecules* **2004**, *5*, 379–388.

[75] H. Ceylan, A. B. Tekinay, M. O. Guler in *Biological and Biomimetic Adhesives: Challenges and Opportunities*, The Royal Society of Chemistry, **2013**, pp. 103–116.

[76] M. Wolman, *Journal of Supramolecular Structure* **1975**, *3*, 80–89.

[77] B. P. Lee, K. Huang, F. N. Nunalee, K. R. Shull, P. B. Messersmith, *Journal of Biomaterials Science Polymer Edition* **2004**, *15*, 449–464.

[78] C. Barner-Kowollik, P. Vana, T. Davis in *Handbook of Radical Polymerization*, (Eds.: K. Matyjazewski, T. Davis), **2002**, pp. 187–261.

[79] S. Perrier, *Macromolecules* **2017**, *50*, 7433–7447.

[80] A. Favier, M.-T. Charreyre, C. Pichot, *Polymer* **2004**, *45*, 8661–8674.

[81] G. Moad in *Reference Module in Materials Science and Materials Engineering*, Elsevier, **2016**.

[82] H. Li, B. Yu, H. Matsushima, C. E. Hoyle, A. B. Lowe, *Macromolecules* **2009**, *42*, 6537–6542.

[83] C. Lü, Z. Cui, Z. Li, B. Yang, J. Shen, *Journal of Materials Chemistry* **2003**, *13*, 526–530.

[84] M. Benaglia, E. Rizzardo, A. Alberti, M. Guerra, *Macromolecules* **2005**, *38*, 3129–3140.

[85] B. Chong, G. Moad, E. Rizzardo, M. Skidmore, S. Thang, *Australian Journal of Chemistry - AUST J CHEM* **2006**, *59*.

[86] W. Shen, Q. Qiu, Y. Wang, M. Miao, B. Li, T. Zhang, A. Cao, Z. An, *Macromol Rapid Commun* **2010**, *31*, 1444–8.

[87] G. Moad, E. Rizzardo, S. H. Thang, *Polymer International* **2011**, *60*, 9–25.

[88] A. L. Silva, J. C. Bordado, *Catalysis Reviews* **2004**, *46*, 31–51.

[89] F. Gamardella, X. Ramis, S. De la Flor, À. Serra, *Reactive and Functional Polymers* **2019**, *134*, 174–182.

[90] E. B. Berda, E. J. Foster, E. W. Meijer, *Macromolecules* **2010**, *43*, 1430–1437.

[91] L. Arnow, *J. Biol. Chem.* **1937**, 531–537.

[92] S. E. Calvin, M. L. Oyen, *Annals of the New York Academy of Sciences* **2007**, *1101*, 166–185.

[93] C. M. Haller, W. Buerzle, A. Kivelio, M. Perrini, C. E. Brubaker, R. J. Gubeli, A. S. Mallik, W. Weber, P. B. Messersmith, E. Mazza, N. Ochsenbein-Koelble, R. Zimmermann, M. Ehrbar, *Acta Biomaterialia* **2012**, *8*, 4365–4370.

[94] *International Organization for Standardization* **2009**, *ISO/TC 194 Biological and clinical evaluation of medical devices*.

[95] A. Kivelio, P. Dekoninck, M. Perrini, C. E. Brubaker, P. B. Messersmith, E. Mazza, J. Deprest, R. Zimmermann, M. Ehrbar, N. Ochsenbein-Koelble, *European Journal of Obstetrics and Gynecology and Reproductive Biology* **2013**, *171*, 240–245.

[96] S. Kull, I. Martinelli, E. Briganti, P. Losi, D. Spiller, S. Tonlorenzi, G. Soldani, *J Surg Res* **2009**, *157*, e15–21.

[97] J. Simson, J. Crist, I. Strehin, Q. Lu, J. H. Elisseeff, *Journal of Orthopaedic Research* **2013**, *31*, 392–400.

[98] R. A. Chivers, R. G. Wolowacz, *International Journal of Adhesion and Adhesives* **1997**, *17*, 127–132.

[99] M. S. Ltd, MedCalc, **2020**.